NASA/CR—2009-214831

Experimental Study of the Effects of Periodic Unsteady Wakes on Flow Separation in Low Pressure Turbines

Burak Ozturk and Meinhard T. Schobeiri
Texas A&M University, College Station, Texas

March 2009

NASA STI Program . . . in Profile

Since its founding, NASA has been dedicated to the advancement of aeronautics and space science. The NASA Scientific and Technical Information (STI) program plays a key part in helping NASA maintain this important role.

The NASA STI Program operates under the auspices of the Agency Chief Information Officer. It collects, organizes, provides for archiving, and disseminates NASA's STI. The NASA STI program provides access to the NASA Aeronautics and Space Database and its public interface, the NASA Technical Reports Server, thus providing one of the largest collections of aeronautical and space science STI in the world. Results are published in both non-NASA channels and by NASA in the NASA STI Report Series, which includes the following report types:

- TECHNICAL PUBLICATION. Reports of completed research or a major significant phase of research that present the results of NASA programs and include extensive data or theoretical analysis. Includes compilations of significant scientific and technical data and information deemed to be of continuing reference value. NASA counterpart of peer-reviewed formal professional papers but has less stringent limitations on manuscript length and extent of graphic presentations.

- TECHNICAL MEMORANDUM. Scientific and technical findings that are preliminary or of specialized interest, e.g., quick release reports, working papers, and bibliographies that contain minimal annotation. Does not contain extensive analysis.

- CONTRACTOR REPORT. Scientific and technical findings by NASA-sponsored contractors and grantees.

- CONFERENCE PUBLICATION. Collected papers from scientific and technical conferences, symposia, seminars, or other meetings sponsored or cosponsored by NASA.

- SPECIAL PUBLICATION. Scientific, technical, or historical information from NASA programs, projects, and missions, often concerned with subjects having substantial public interest.

- TECHNICAL TRANSLATION. English-language translations of foreign scientific and technical material pertinent to NASA's mission.

Specialized services also include creating custom thesauri, building customized databases, organizing and publishing research results.

For more information about the NASA STI program, see the following:

- Access the NASA STI program home page at *http://www.sti.nasa.gov*

- E-mail your question via the Internet to *help@sti.nasa.gov*

- Fax your question to the NASA STI Help Desk at 301–621–0134

- Telephone the NASA STI Help Desk at 301–621–0390

- Write to:
  NASA Center for AeroSpace Information (CASI)
  7115 Standard Drive
  Hanover, MD 21076–1320

NASA/CR—2009-214831

Experimental Study of the Effects of Periodic Unsteady Wakes on Flow Separation in Low Pressure Turbines

Burak Ozturk and Meinhard T. Schobeiri
Texas A&M University, College Station, Texas

Prepared under Cooperative Agreement NCC3–793

National Aeronautics and
Space Administration

Glenn Research Center
Cleveland, Ohio 44135

March 2009

Acknowledgments

This project was supported by NASA Glenn Research Center (GRC), as part of the Low Pressure Turbine (LPT) Flow Physics Program. The Technical Monitor was Dr. David E. Ashpis. His participation in the research via guidance, technical advice, leadership, and coordination of the LPT Program, are greatly appreciated. The authors also acknowledge Om Sharma, Dick Price, and Gary Stetson of Pratt & Whitney for providing the research community with the blade "PAK B" coordinates. In addition, the authors also acknowledge Jim Bartlett, Rick Hobson, and Arild Bertelrud from NASA Langley Research Center (LaRC), and David Ashpis from NASA Glenn for providing sensor fabrication support and components for hot-wire anemometry instrumentation.

This work was sponsored by the Fundamental Aeronautics Program at the NASA Glenn Research Center.

Level of Review: This material has been technically reviewed by NASA technical management.

Available from

NASA Center for Aerospace Information
7115 Standard Drive
Hanover, MD 21076–1320

National Technical Information Service
5285 Port Royal Road
Springfield, VA 22161

Available electronically at http://gltrs.grc.nasa.gov

Experimental Study of the Effects of Periodic Unsteady Wakes on Flow Separation in Low Pressure Turbines

Burak Ozturk and Meinhard T. Schobeiri
Texas A&M University
College Station, Texas 77843

EXECUTIVE SUMMARY

The present study, which is the first of a series of investigations dedicated to specific issues of low pressure turbine (LPT) boundary layer aerodynamics, is aimed at providing detailed unsteady boundary layer flow information to understand the underlying physics of the inception, onset, and extent of the separation zone. A detailed experimental study on the behavior of the separation zone on the suction surface of a highly loaded LPT-blade under periodic unsteady wake flow is presented. Experimental investigations were performed on a large-scale, high-subsonic unsteady turbine cascade research facility with an integrated wake generator and test section unit. Blade Pak B geometry was used in the cascade. The wakes were generated by continuously moving cylindrical bars device. To account for a high flow deflection of LPT-cascades at design and off-design operating points, the entire wake generator and test section unit including the traversing system is designed to allow a precise angle adjustment of the cascade relative to the incoming flow. This is done by a hydraulic platform, which simultaneously lifts and rotates the wake generator and test section unit. The unit is then attached to the tunnel exit nozzle with an angular accuracy less than 0.05°, which is measured electronically. Utilizing a Reynolds number of 110,000, based on the blade suction surface length and the exit velocity, one steady and two different unsteady inlet flow conditions with the corresponding passing frequencies, wake velocities, and turbulence intensities are investigated. The reduced frequencies cover the entire operation of LP-turbines. The measurements were made using hot-wire anemometry. In addition to the unsteady boundary layer measurements, blade surface pressure measurements were performed at Re = 50,000, 75,000, 100,000, 110,000, and 125,000. For each Reynolds number, surface pressure measurements are carried out at one steady and

two periodic unsteady inlet flow conditions. Detailed unsteady boundary layer measurement identifies the onset and extension of the separation zone as well as its behavior under unsteady wake flow. The results presented in ensemble-averaged and contour plot forms help to understand the physics of the separation phenomenon under periodic unsteady wake flow.

CONTENTS

LIST OF FIGURES

LIST OF TABLES

1. INTRODUCTION

In recent years gas turbine engine aerodynamicists have focused their attention on improving the efficiency and performance of the low pressure turbine (LPT) component. Research works from industry, research centers, and academia have shown that reduction in blade number can be achieved without substantially sacrificing the efficiency of the LPT-blading. This reduction contributes to an increase in thrust/weight ratio, thus reducing the fuel consumption. Contrary to the high pressure turbine (HPT) stage group that operates in a relatively high Reynolds number environment, based on the operating conditions, the LPT experiences an adverse change in Reynolds number ranging from 50,000 to 250,000. Since the major portion of the boundary layer, particularly along the suction surface is laminar, the low Reynolds number in conjunction with the local adverse pressure gradient makes it susceptible to flow separation, thus increasing the complexity of the LPT- boundary layer aerodynamics. The periodic unsteady nature of the incoming flow associated with wakes, that originate from upstream blades, substantially influences the boundary layer development including the onset of the laminar separation, the extent of the separation zone, and its turbulent re-attachment. Of particular relevance in context of LPT-aerodynamics is the interaction of the wake flow with the suction surface separation zone. While the phenomenon of the unsteady boundary layer development and transition in the absence of separation zones has been the subject of intensive research, that has led to better understanding the transition phenomenon, comprehending the multiple effect of mutually interacting parameters on the LPT-boundary layer separation and their physics still requires more research.

The objective of this present investigation under the supervision is to better understand the effect of the unsteady wake flow on the boundary layer behavior and the underlying physics of the inception, onset, and extent of the separation zone. Boundary layer measurements are taken on a LP turbine blade designed by Pratt &Whitney in a linear turbine cascade as described by Schobeiri et al.(1995) and (1997).

NOMENCLATURE

D_{in}	inside diameter of calibration nozzle (mm)
D_{out}	outside diameter of calibration nozzle (mm)
E	anemometer voltage (V)
m	number of hot-wire samples taken per revolution of the wake generator
N	total number of samples of hot-wire data for time-averaging
c	blade chord length
C_p	pressure coefficient, $C_p = \frac{P_i - P_{ref}}{\frac{1}{2}\rho V_{ref}^2}$
P_i	static pressure taps, i=1..48
P_{ref}	static pressure
U	rotor circumferential velocity, belt translational velocity(m/s)
V_∞	free-stream velocity (m/s)-
V_{in}	test section inlet velocity (m/s)
V	instantaneous velocity (m/s)
$\overline{V}$	time-averaged velocity (m/s)
v	turbulent fluctuation velocity (m/s)
s	streamwise distance from the leading edge of the blade
s_{md}	maximum separation bubble height at a streamwise distance from the leading edge of the blade
s_s	starting point of the separation zone at a streamwise distance from the leading edge of the blade
s_o	streamwise distance from the leading edge to the trailing edge of the blade
S_R	rod spacing

S_B	blade spacing
t	time (s) $Tu = \frac{v}{\bar{V}} \times 100$
Tu	turbulence intensity,
<Tu>	ensemble-averaged turbulence intensity
<V>	ensemble-averaged mean velocity
<v>	ensemble-averaged turbulent fluctuation velocity
y	lateral distance from plate surface (mm)
ν	kinematic viscosity of air (m^2/s)
ρ	density of air (kg/m^3)
σ	cascade solidity, $\sigma = c/S_B$
τ	one wake passing period
ϕ	velocity ratio, V_{ax}/U
λ	load coefficient of a constant mean diameter turbine stage, $\lambda=(V_{u2}+V_{u3})/U$
Ω	non-dimensionalized unsteady parameter, $\Omega = \frac{\sigma S_B}{\varphi S_R}$
Re_s	local Reynolds number based on longitudinal distance, $Re_s=(\bar{U}s)/\nu$
Re_{smd}	Reynolds number based on the conditions at separation
H_{12}	shape factor, $H_{12}=\delta_1/\delta_2$
δ	boundary layer thickness
δ_1	displacement thickness
δ_2	momentum thickness
δ_3	energy thickness
ω	data uncertainty

2. LITERATURE REVIEW

2.1 Flow Through a Multi-Stage Turbine

In turbomachinery aerodynamics the motion of neighboring blade rows generates the periodic unsteady wakes. Several factors such as wake interaction, endwall region, and secondary losses affect the flow behavior and thus the performance of the turbine blades and turbomachine. Therefore, wake induced unsteady flow has a profound affect upon the overall aerodynamic behavior of blade rows. This unsteady flow influences the individual boundary layer of each blade and is investigated in detail by Arndt (1993) where he concluded that there are significant changes in the free stream turbulence levels and wake structures at each row location.

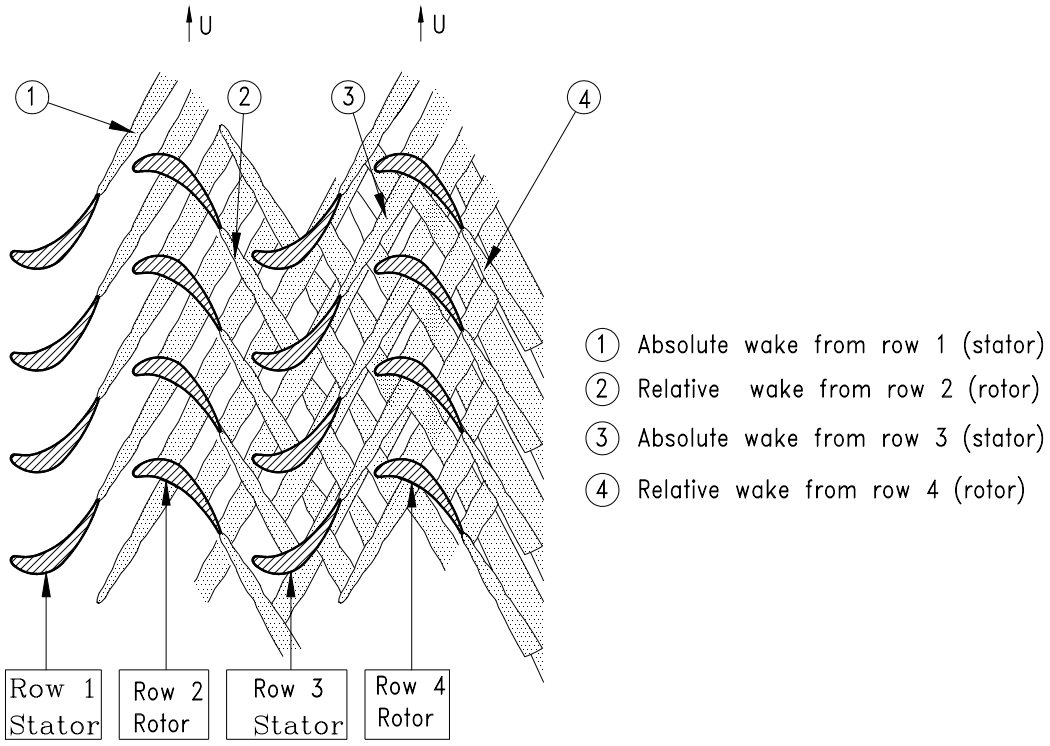

Figure 2.1: Schematic of the stator-rotor unsteady wake flow propagation through a multi-stage environment from Schobeiri et al. (1995).

The schematic shown in Figure 2.1 illustrates the findings by Schobeiri et al. (1995).The flow leaving the first stator blade row impinges upon the second blade row with a spatial frequency that is related to the blade spacing of the preceding stator row. Due to the rotation of the second row and the frame of reference change, a periodic unsteady turbulent flow results thus affecting the boundary layer behavior.

As the flow leaves the first stage, two sets of wake structures are present which have been generated from the preceding rows. These wakes impinge upon the third row with different velocity defects, phase displacements, and turbulent structure. Once the flow leaves the third row, a new set of wakes are generated while the previous wakes have interacted through intensive mixing resulting in high background turbulence. The turbulence intensity increases for each proceeding row until some limit is reached somewhere downstream.

2.2 Boundary Layer Transition in Turbomachinery

Since the state of the boundary layer affects the loss production and the heat transfer characteristics, the turbine designer needs to know the information about the distribution of the laminar and turbulent flow regimes and where the transition starts and ends on the blade surfaces. While the transition to turbulent state has been extensively investigated, transition in highly disturbed environments such as turbomachinery flows are adequately documented. Boundary layer transition from laminar state to the turbulent state is a stochastical, three-dimensional, and unsteady process which occurs in a region where the flow is intermittently laminar and turbulent. In general, there are three significant modes of transition. The first is called “natural” transition, and this mode of transition starts with a weak instability in the laminar boundary layer and proceeds through a various stages of amplified perturbance to fully turbulent flow. Since this transition mode occurs only in low free-stream turbulence environments, it is of little importance in gas turbine flow fields. The second one is called “bypass” transition and is caused by a large disturbances in the external flow that directly produces a turbulent spot in the boundary layer. It has been the general perception that the presence of wakes causes the Tollmien-Schlichting waves to be bypassed (Mayle 1991). Extensive unsteady boundary layer investigations at Texas A&M University

Turbomachinery Performance and Research Laboratory (Schobeiri and Radke 1994, Schobeiri et al. 1995) showed that despite the presence of wakes Tollmien-Schlichting waves are present. The third one is called "separated-flow" transition and it occurs in a separated laminar boundary layer. When a laminar boundary layer separates, transition may occur in the free shear layer near the surface and separation bubble length strongly depends on the transition process in the shear layer. This mode of transition occurs in gas turbine engines, particularly in the compressors and low-pressure turbines.

A review of boundary layer development and the periodic unsteady flow studies are presented.

2.3 Periodic Unsteady Boundary Layer Research

One of the major effects of unsteady wake flow is on the boundary layer development and the transition from laminar to turbulent state. Realizing the importance of unsteady flow, there has been an extensive research on unsteady aerodynamics of turbomachines in the past two decades. Initial studies utilized simplified models to simulate the turbomachinery flow conditions. Precise knowledge on how the unsteady flow affects the distribution of the laminar boundary layer development is of great importance for the turbine designer and also to develop better transition correlations for use in computational fluid dynamic codes.

An extensive unsteady boundary layer research program was initiated mid sixties at the Technical University Darmstadt, Germany. Fundamental studies by Pfeil and Pache (1977), Pfeil and Herbst (1979), Schröder (1983) examined the boundary layer transition on a flat plate with the effect of unsteady wake flow. They used squirrel cage type of wake creator, with a series of cylindrical rods, which is connected on two parallel rotating disks. Their studies show that the unsteady wakes generated by the cylindrical rods caused the boundary layer to become turbulent during their impingement on the plate and affect the length of the boundary layer transition region. They also pointed out that, wake-induced transition zones, which propagated downstream of the plate at velocity less than the wake passing velocity.

Orth (1993) studied and quantified the effect of unsteady wake flow on the boundary layer transition along a flat plate. First, he observed an early onset of transition when the high turbulence level of the wake disturbs the boundary layer and leads to the formation of turbulent patches. Second, laminar becalmed regions are formed behind the turbulent patches so that brief periods of laminar flow are still observed beyond the location at which the steady flow boundary layer is fully turbulent.

Orth (1993) and Schobeiri and Radke (1994) experimentally investigated the effects of periodic unsteady wake flow and pressure gradient on the boundary layer transition and development along the concave surface of a constant curvature plate. The measurements were carried out under zero and negative pressure gradients utilizing an unsteady flow research facility with a rotating cascade of rods positioned upstream of the curved plate. Based on the comprehensive experimental investigations, Schobeiri and Radke concluded that the wake induced unsteady flow significantly affects the boundary layer transition behavior. The onset of primary boundary layer and the location of its high turbulence intensity core was shifted towards the plate leading edge when subjected to periodic unsteady wakes. Their results were similar to those found by Liu and Rodi (1989, 1991) stating that the wake passing does not significant effect for the boundary layer development, but it cause the transition to occur earlier than in natural transition. They found that, transition region shifted towards to the leading edge.

The effects of passing wakes have also been investigated by Dullenkopf et al. (1991), Liu and Rodi (1991). Their results showed that an increase in wake passing frequency caused the transition region to shift towards the leading edge for the suction surface. Higher frequencies were noted by all the investigators to significantly enhance the heat transfer on both surfaces due to the increased turbulence intensity.

Halstead et al. (1997), performed an experimental studies of boundary layer development on the suction surface of the low pressure turbine blade. They found a region of laminar and transitional flow on the suction surface without flow separation. They also showed that becalmed regions generated by the turbulent spots produced in the wake path, were effective in suppressing the flow separation.

Analyzing the velocity and turbulence structure of the impinging wakes and their interaction with the boundary layer, Chakka and Schobeiri (1999) developed an intermittency based unsteady boundary layer transition model by analyzing the velocity and the turbulence structure of the impinging wakes and their interaction with the boundary layer. The analysis revealed an universal pattern for the relative intermittency function for all frequencies and pressure gradient investigated. However, they considered the above investigations were not sufficient to draw a final conclusion with regard to an eventual universal character of the relative intermittency function. Further detailed investigations of the unsteady boundary layer on a high Reynolds number turbine cascade by Schobeiri et al. (1995) and its subsequent analysis (1997), (1998), and (2002) verified the universal character of the relative intermittency function. For this purpose, Schobeiri et al. (1995) utilized a conceptually different type wake generator. Fottner and his co-workers (2000), and Schulte and Hodson (1996) used the same wake generating concept for investigations on the influence of unsteady wake flow on the LPT-boundary layer.

Kaszeta, Simon, and Ashpis (2001) experimentally investigated the laminar-turbulent transition aspect within a channel with the side walls resembling the suction and pressure surfaces of a LPT-blade.

Fottner et al. (2000) performed an experimental studies using mounted hot film measurement technique. The results shows that the transition moves when it is subjected to wake along the LP turbine blade, which significantly influence the loss generation in the suction side boundary layer. Thus, laminar separation is suppressed or reduced whenever the wake is present.

Lou and Hourmouziadis (2000) investigated the mechanism of separation, transition, and reattachment, and the effect of main flow unsteadiness on a flat plate, contouring the opposite wall to create the appropriate pressure gradient on the test wall. By using a rotating flap which is mounted downstream of the test section, they were able to produce periodic oscillations of the main flow and identify the characteristic instability frequencies in the shear layer over a separation bubble. They show that free shear layer instability originates at the maximum vorticity and energy is transferred from the shear flow to the instability

waves where the instability waves are amplified downstream and trigger the transition. They also show that the momentum transfer from the shear flow is increased due to the turbulence fluctuations. This causes the reattachment of the flow. They investigated the Reynolds number effect on the transition region. They showed that for the higher Reynolds number results an earlier transition and reduction of the transition length, while the separation point does not change its location.

Recent work presented by Cardamone et al. (2000) captures a separation zone in the steady state case at Re= 60,000, however, in unsteady case, the separation zone is not reproduced. The few boundary layer measurements are not comprehensive enough to provide any conclusive evidence for the interpretation of the boundary layer transition and separation processes and their direct impact on the profile loss, which is a critical parameter for blade design.

Shyne et al. (2000) performed an experimental study at a Reynolds number of 100,000 with different levels of free-stream turbulence. They showed that transition onset location and the length is strongly dependent on the free-stream turbulence. As the free-stream turbulence increase, the onset location and the length of the transition is decreased.

Recently Schultz and Volino (2001) have shown that concave curvature has a significant effect on transition at high free-stream turbulence.

Volino and Hultgren (2001) performed an experimental study and measured the detailed velocity along a flat plate which is subjected to the same dimensionless pressure gradient as the suction side of the modern LP turbine blade. They showed that the location of the boundary layer separation does not strongly depend on the Reynolds number or free-stream turbulence level, as long as the boundary layer remains non-turbulent before separation occurs. But they also showed the extent of the transition are strongly dependent on the Reynolds number and turbulence intensity. With higher free-stream turbulence levels, transition appears to occur in a bypass mode, similar to the attached boundary layers. On the other hand, under low turbulence intensity, transition is induced by instability waves in the shear layer of the separation bubble.

Treuren et al.(2002) performed an experimental study at a very low Reynolds number of 25,000 and with different free-stream turbulence levels. They showed that a massive separation at very low Reynolds number of 25,000 is persistent, in spite of elevated free stream turbulence intensity. However, at a higher Reynolds number of 50,000, there is a strong separation on the downstream of the suction side for the low free-stream turbulence level. The separation zone eliminated for the higher free-stream turbulence level of 8-9%. And they also added vortex generators to provide mixing for the reattachment. At very low Reynolds number of 25,000, they showed a massive separation on the suction surface, in spite of elevated free-stream turbulence level and vortex generators. However, elevated free-stream turbulence and vortex generators helps the flow to reattach to the surface at higher Reynolds number.

To prevent the separation in LP turbine vortex generator jets and dimples can be used. Recently Lake et al. (2000) suggested to use dimples on the suction surface of a turbine blade to control separation for the low Reynolds number. Their research showed a decrease in loss coefficient at low Reynolds number with an aerodynamic penalty at higher Reynold number. Another method, suggested to control or prevent the separation is the use of vortex generator jets. This method produce no important adverse effects at higher Reynolds number. Recently Bons et al. (1999) applied this method to low pressure turbine. He showed that the separation region was almost eliminated and there is a significant reduction in momentum loss downstream of the blade. Both grooves and vortex generators has been applied to wind turbines. While energizing the boundary layer and preventing the separation at low Reynolds numbers, there is a penalty at high Reynolds number which is considered unacceptable. On the other hand, Lin (1999) showed that micro-vortex generators are effective reducing the separation zone with a little drag penalty.

Even though, the published studies helped in better understanding the wake development, unsteady transition and the boundary layer development including the onset and extent of the laminar separation and its turbulent reattachment, they are neither complete to be applicable to turbomachinery flow nor to develop a theoretical framework.

3. OBJECTIVES

The objective of this study is to understand the physical mechanisms associated with the effects of wakes on separated LP turbine flows along the blade surface and to create high fidelity data base suitable to be used for validation of transition, turbulence, separation models as well as CFD-codes. Measurements were performed in a single row cascade representative of LP turbine designs. A large-scale, high subsonic research facility has been used for the investigation. The wake passing frequency is varied from 0 to 120 Hz to simulate various turbomachinery-operating conditions.

Careful documentation was made of (1) the development of the boundary layer which approaches the separated flow region, (2) the free shear layer over the separation region and (3) the reattached flow downstream of the separation bubble.

Detailed steady and unsteady boundary layer velocity, turbulence intensity, and static pressure measurements have been performed along the suction and pressure surface of one blade. A single hot wire probe has been used for the velocity measurements. The results are presented in temporal-spatial domain for a detailed display of transition and further development of boundary layer.

In addition to unsteady boundary layer measurements, blade surface measurements were investigated at Re=50,000, 75,000, 100,000, 110,000 and 125,000. For each Reynolds number, surface pressure measurements are carried out at one steady and two different unsteady inlet conditions.

4. EXPERIMENTAL TEST FACILITY

For the detailed investigations on the varying wake passing frequencies, a large scale, high-subsonic research facility has been used. The facility in its original configuration is described by Schobeiri et al. (1995) and (1997). The facility is shown in Figure 4.1. The facility consists of a large centrifugal fan, straight pipe, diffuser, settling chamber, nozzle, cascade test section, motor driving the wake generator. A detailed description of the test facility is given below.

4.1 Air Supplier

Air is supplied from a large centrifugal fan, which is driven by 93 kW 3-phase AC electric motor running at a rated speed of 1760 rpm, with a volumetric flow rate of 15 m^3. The blower reduces the rotary speed to a fan speed of 1035 rpm by a belt-pulley transmission. The capacity of the fan is 100 m/s for the maximum mean velocity at the test section. It corresponds to a Mach number of M=0.6 for a turbine cascade with an acceleration ratio of V_2/V_1=2. Various inlet velocity can be obtained by changing the fan speed or the throttle which is located at the exit of the fan. For the present investigation, the throttle is adjusted to give a maximum Reynolds number 120,000 at the inlet of the test section. To protect the hot-wire system, a fiber-glass filter with a thickness of 50 mm and a pore size of 5μm is attached at the inlet of the fan.

Since the fan exit has a higher elevation than the test facility, a set of transition ducts followed by a straight pipe with a diameter of 600 mm are used for the smooth channeling of the flow from the fan exit to the diffuser inlet. A Prandtl probe is located at the inlet of the diffuser to get the variations in the mean velocity resulting from the voltage difference, fluctuations of the fan speed, or change of environmental temperature and pressure.

4.2 Diffuser, Settling Chamber, and Nozzle Assembly

The straight pipe leads to the diffuser with a length of 1500 mm and area ratio of

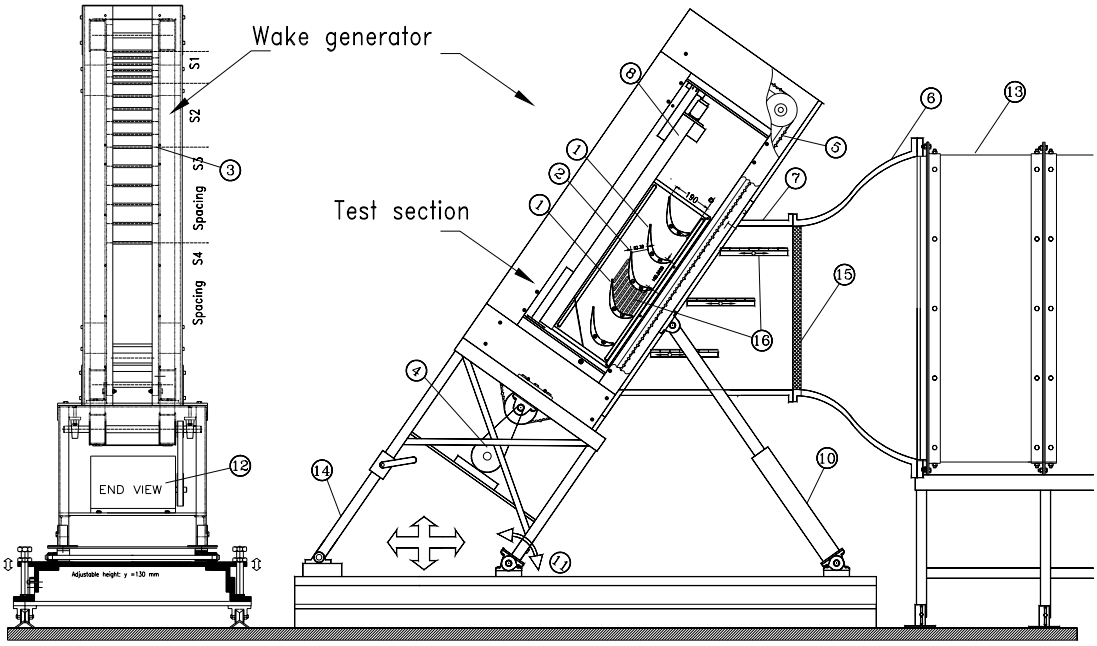

Figure 4.1: Turbine cascade research facility with the components and the adjustable test section.

1:4.75. The flow is decelerated before entering the settling chamber, which consists of four sections. Each section has a length of a 900 mm and cross section of 1500×900 mm. Five screens and one honeycomb flow straightener are used in the settling chamber to control the flow uniformity and turbulence intensity level. The screens are made of stainless steel and have different mesh sizes and wire diameters. The first screen is placed at the diffuser exit to reduce the scale of vortices generated by the diffuser vanes. The honeycomb flow straightener with a cell size of 6 mm is placed between the first two settling chamber. The second screen is located directly downstream of the honeycomb. The honeycomb and screen combination results in a much lower turbulence intensity than a honeycomb alone because the large eddies exiting from the honeycomb cells are broken into smaller eddies. The other screens are placed downstream of the second, third and fourth sections of the settling

chamber. The nozzle is located downstream of the settling chamber with an area ratio of 6.75:1. The flow accelerates before entering the wake generator and the nozzle provides a smooth transition of flow from the settling chamber to the wake generator. A straight channel transition piece is attached to the nozzle to accommodate the test section inclination.

4.3 Periodic Unsteady Inlet Wake Flow Generator

The translational motion of the wake generator generates the periodic unsteady wakes. It consists of a series of cylindrical rods that are placed on both side of the timing belt that is driven by an electric motor. The timing belts with a length of 5 m span over 10 pulleys arranged around the cascade test section. The drive pulleys also control the belt tension. For the present investigation, a certain number of cylindrical rods with a diameter of 2 mm are mounted between two timing belts. The purpose of the use of cylindrical rod is to get the similar rotor blade wakes. Attaching the rods to the belts or detaching the rods from the belt can change, the rod spacing, S_R. The wake flow generator system is driven by an electric motor with a maximum power of 7.5 kW (10hp). The controller allows the belt translational speed up to 25 m/s. For the present investigation, a belt speed of U=5 m/s is chosen. And also, a fiber optic system is used to monitor the wake passing frequency and it also serves as a trigger for the data acquisition.

4.4 Sequential Generation of Unsteady Wakes

With the special design of the test facility, it is possible to measure the velocities for different wake passing frequencies in one data set, when performing the boundary layer experiments. The wake passing frequency can be varied by changing the speed of the belt or the spacing of the rods on the belt, S_R, shown in the Figure 4.2. For the present study, the belt is subdivided into three different clusters of the same length. The first one with the spacing $S_R=\infty$, which is steady flow case with no rods. The second and the third part have the rod spacing of S_R=160mm and 80 mm respectively. Within each cluster the rods have the same spacings. The clusters are all arranged with a certain distance from each other. By

using the triggering system, a continuous data set is acquired and the buffer zones between the data clusters are visible. The data analysis program is able to cut the buffer zone and evaluates the data for each cluster.

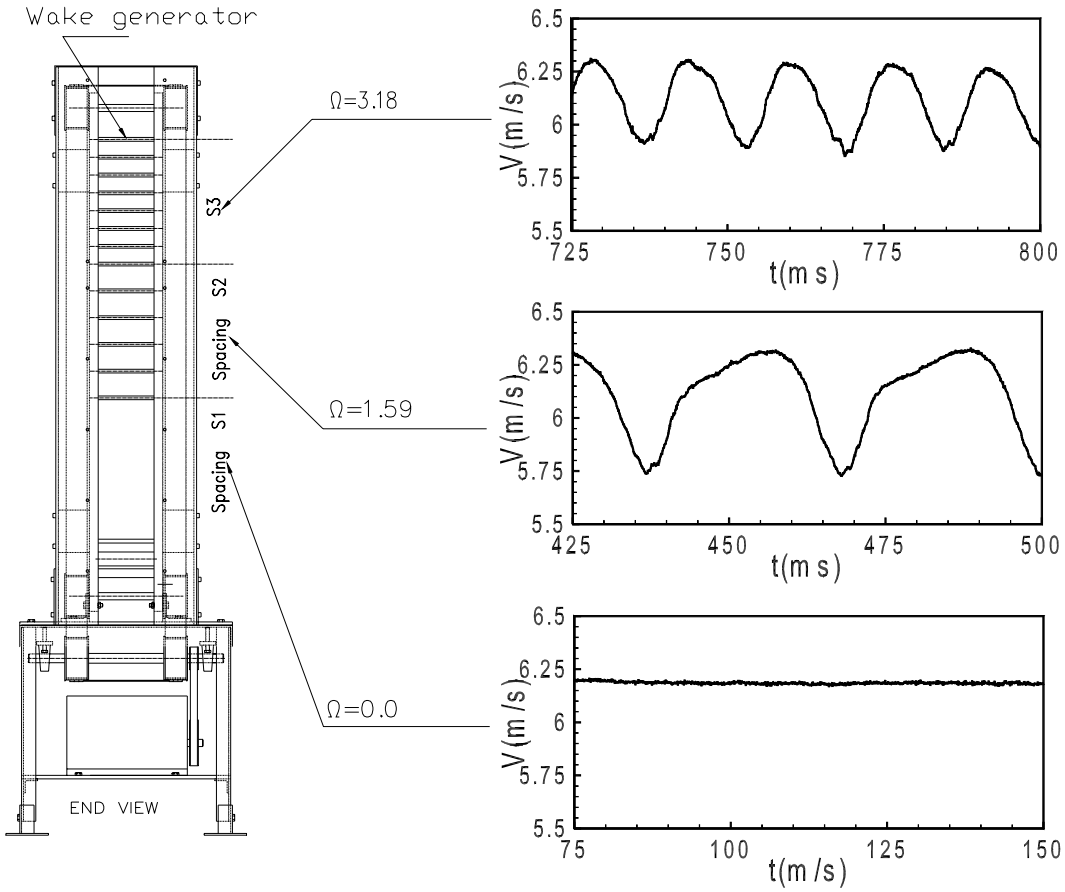

Fig. 4.2: (left)Wake generator with different rod spacing clusters, (right) velocities produced for rod spacing of S_R = 80 mm (top), 160 mm (middle), and ∞.

In order to account for the unsteadiness caused by the frequency of each individual wake generating cluster and its spacing, the flow velocity and the cascade parameters the unsteady flow parameter Ω is defined:

$$\Omega = \frac{c}{S_R}\frac{U}{V_{ax}} = \frac{\sigma}{\varphi}\frac{S_B}{S_R} \tag{4.1}$$

Many researchers have used Strouhal number as an unsteady flow parameter which includes the wake generator speed and the inlet flow velocity. However the unsteady flow parameter which is defined above and includes the cascade solidity, the flow coefficient, the blade spacing and the rod spacing, is an extension of Strouhal number in the sense that it additionally includes the rod spacing S_B and blade spacing S_R. The individual cluster configurations with the corresponding Ω parameter are specified in Table 4.1.

Table 4.1: Test section cascade parameters

Parameters	Values	Parameters	Values
Inlet velocity	V_{in} = 4 m/s	Inlet turbulence intensity	Tu_{in} = 1.0 %
Rod translational speed	U = 5.0 m/s	Blade Re-number	Re = 110,000
Nozzle width	W = 200.0 mm	Blade height	h_B = 200 mm
Blade chord	c = 203.44 mm	Blade stagger angle	$\gamma = 26^o$
Blade axial chord	c_{ax} = 182.85mm	Cascade solidity	σ = 1.248
Blade suction surface length	L_{SS} = 270.32 mm	Cascade angle	$\varphi = 55°$
Cascade flow coefficient	Φ = 0.80	Cascade spacing	S_B = 163 mm
Inlet air angle, Fig. 2	$\alpha_1 = 55.0°$	Exit air angle, Fig. 2	$\alpha_2 = 145.0°$
Rod diameter	D_R = 2.0 mm	Rod distance to lead. edge	L_R = 122 mm
Cluster 1 (no rod, steady)	$S_R = \infty$ mm	Ω - parameter steady case	Ω = 0.0
Cluster 2 rod spacing	S_R = 160.0 mm	Ω - parameter for cluster 1	Ω = 1.59
Cluster 3 rod spacing	S_R = 80.0 mm	Ω - parameter for cluster 2	Ω = 3.18

4.5 Cascade Test Section

The cascade test section shown in Figure 4.3 is located downstream of the wake generator and it has an inlet cross section of 1000 mm×200 mm. The test section can

incorporate to 5 blades with a blade height of 200 mm and a chord of 203.44 mm. For boundary layer investigations, five identical blades designed by Pratt&Whitley were implemented whose cascade geometry is given in Table 4.1. The blade resembles the essential feature such as the laminar boundary layer separation that is inherent to typical LPT-blades. This blade number is necessary and sufficient to secure a spatial periodicity for the cascade flow. It also consists of two plexiglas side walls. One of the side walls includes inlet, exit traversing slots and the slots for the boundary layer measurements which are placed between the second and the third blade from the bottom as shown in Figure 4.1 item 16.

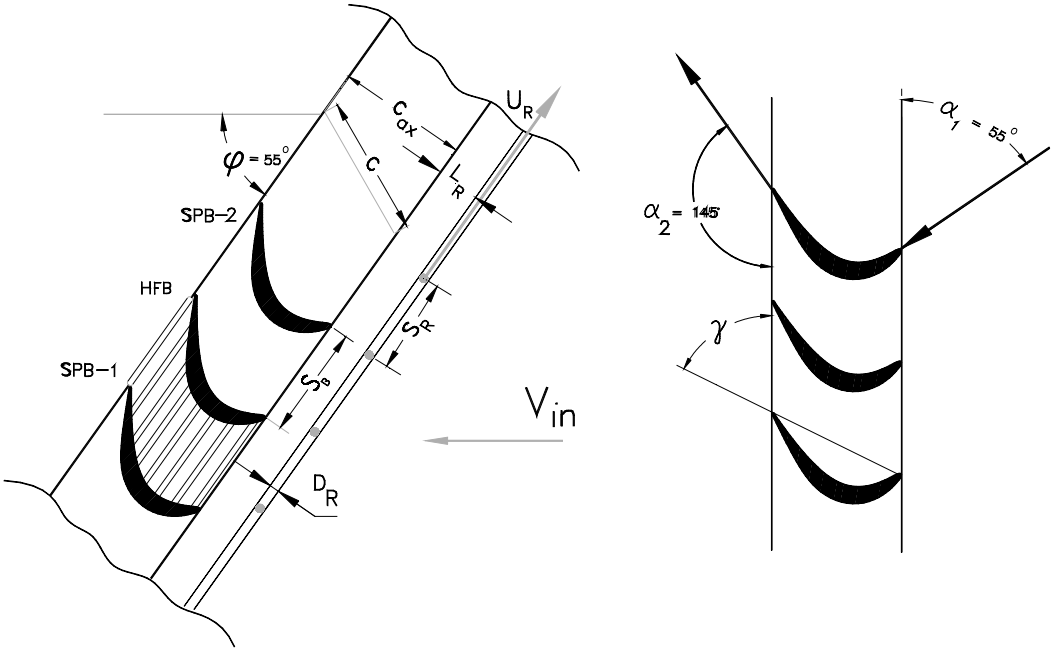

Figure 4.3: Cascade geometry, flow, and stagger angle are listed in Table 1. Number of blades=5, instrumented blades are: SPB-1 and SPB-2 with static pressure taps, HFB: Blade with surface mounted hot films to be used for future investigations

4.6 Probe Traversing System

A computer controlled traversing system is used for all the inlet, exit and boundary layer measurement at the cascade test section. The traversing system is mounted vertically on one of the plexiglas side walls. It consists of a power screw with a maximum traversing

length of 1200 mm which is connected to a stepper motor to provide the drive. It receives a signal from the LABVIEW program and turns the power screw by an exact number of pulses required. An optical encoder with 400 radial slots connected to the stepper motor provides a feedback to the stepper motor for accurate movement along the traversing system and the traversing system is capable to move in a small steps of 2.5 μm. The traversing system also includes a switch to prevent the probes movements beyond the desired limit.

4.7 Hydraulic Platform

To account for a high flow deflection of LPT-cascade, the entire wake generator and test section unit including the traversing system was modified to allow a precise angle adjustment of the cascade relative to the incoming flow. This is done by a hydraulic platform, which simultaneously lifts and rotates the wake generator and test section unit. The unit is then attached to the tunnel exit nozzle with an angular accuracy better than 0.05^{o}, which is measured electronically.

5. INSTRUMENTATION AND DATA ACQUISITION

The test facility is instrumented for fully automated data acquisition and is similar to the data acquisition system described in Schobeiri, et al. (1995).

5.1 Instrumentation of the Test Facility

The instrumentation and data acquisition concept has been further developed and applied to this research facility. The schematic layout of the test facility instrumentation is shown in Figure 5.1. For the aerodynamic investigations, the data acquisition and reduction system is controlled by a personal computer with a Pentium 3 processor. For the data acquisition and analysis, 16 channel 12-bit analog-digital (A/D) board (NI PCI-MIO 16-E1) is installed in the computer. The outputs from instruments are connected to the channels of the NI extension board from where the data are sampled by the computer. The NI board also has a separate DAC channel through which an analog voltage can be sent out. This DAC channel has been used in a sequential data acquisition from a 48-port scanivalve system for the pressure measurement.

Mean velocities and turbulent fluctuations are obtained using two existing commercial 3-channel (TSI, IFA-100), constant temperature hot-wire anemometer system. The systems have signal conditioner with an adjustable low pass filter, DC-offset, and adjustable gain. The offset and the gain can be adjusted to get the maximum resolution and signal noise ratio. The low pass filter of the signal conditioner has been set to the half of the sampling frequency of 20 kHz to avoid the aliasing effects. The hot wire has 250° C sensor operating temperature. All the hot wire sensors used are made of tungsten with a diameter of 4 μm. The first channel of the first anemometer is connected to a single hot-film probe for measuring the time-dependent velocity distributions within the blade channel. The second channel is used for calibration of the single hot-wire probe connected the second channel of the Ni extension board.

To measure the free-stream temperature, an OMEGA T-type thermocouple mounted

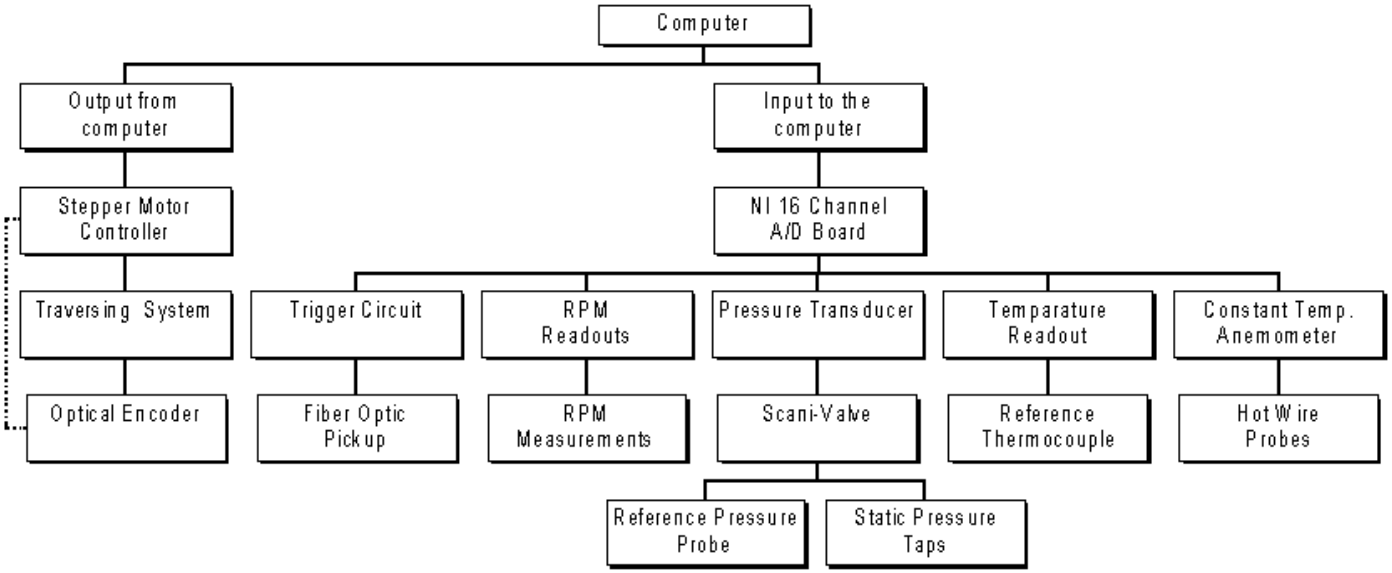

Figure 5.1: Schematic layout of the test facility instrumentation

at the top of the Plexiglas wall is connected to the third channel of the NI-board. Fourth channel of the NI-board is connected to a high precision capacitance type 0-10 mmHg differential pressure transducer (MKS) with a 0-10 Volt analog output. A Prandtl probe, placed upstream of the diffuser, monitors the reference velocity at a fixed location.

For the unsteady investigations, a trigger is required for phase-averaging the instantaneous data. A fiber optic proximity sensor placed close to the pulley of the wake is used. The passage signals of the rods are detected by the sensor using a silver-coated reflective paint on one side of the wake generating timing belts. This sensor gives an accurate readout of the speed of the wake generator and the passing frequency of the rods.

For static pressure measurement and also to make measurements with the five hole probe, it is necessarily to read from several ports. A 48-port scanivalve system has been used for this purpose. The output of the scanivalve system is connected to the MKS pressure transducer. By using the scanivalve system, it is possible to measure 48 pressures using the same pressure transducer.

5.2 Data Acquisition Procedure

The data acquisition system is computer controlled. The required code is written with LABVIEW. The computer acquires the data as a voltage from the differential pressure transducer, thermocouple, trigger circuit and from TSI IFA-100 flow analyzer.

For unsteady boundary layer investigations, 20,000 samples were taken at a rate of 20 kHz for each of the 100 revolutions of the wake generator. The low pass filter of the hot wire anemometer is set to 10 kHz to prevent the aliasing effect.

One of the blades was produced with 48 static pressure taps to obtain pressure distribution on the suction and the pressure surface of the blade. The 48 taps on the blade are connected with the 48 ports of the scanivalve and the output is connected to a high precision differential pressure transducer. When the data acquisition program is executed, the computer acquires 4096 samples at a rate of 4096 Hz from the first port and calculates the mean pressure. Then the program sends out a voltage pulse through DAC port and steps the scanivalve to the next port. The system waits until steady state is reached before sampling the data of the next port. The process is repeated until all the ports are scanned.

6. CALIBRATION PROCEDURE OF THE SINGLE HOT WIRE

Calibration of sensors is of great importance for accurate measurement of any physical quantity. The data acquisition procedures involve sampling of voltage signals from the NI board channels. These voltage signals have to be converted into real physical quantities by means of calibration. These quantities are temperature, pressure, flow velocity, flow angle etc. The pressure transducer is calibrated using a dead weight tester while the thermocouple is connected to the thermocouple calibrator. Least square polynomial fits are used to fit the averaged output voltages with the actual readings obtained from the dead weight tester and thermocouple calibrator. These coefficients are stored in separate data files. However, the calibration of five-hole probes and hot wire probes are more extensive and is performed in uniform flow open jet calibrating facility.

6.1 Description of the Calibration Facility

A schematic of the calibration facility is shown in Figure 6.1. This facility has been used to calibrate the hot wire and five-hole probes. Compressed air is drawn from a reservoir passes through a pressure regulator, filter and flow control valve before entering the calibration facility. It consists of settling chamber followed by a pipe with three axis-symmetric sections, each having a diameter of 150 mm. Screens are placed between flanges of the sections to reduce the turbulence level. The turbulence intensity level at the jet exit is approximately 0.35%. A nozzle with an exit diameter of 38.1 mm is attached at the end of the pipe. The inlet and outlet of the nozzle are parallel to the axis of the facility. A thermocouple is placed in the first section of the calibration facility to measure the air temperature. And a pressure tap is placed in the last section of the pipe to measure the pressure difference between static pressure inside the pipe and the atmospheric pressure with a differential pressure transducer. Two lynx stepper motor controllers are used to automatically change the pitch and yaw angle. The tip of the probes were placed about 0.4 diameters downstream of the nozzle exit plane and within the potential core of the jet. The

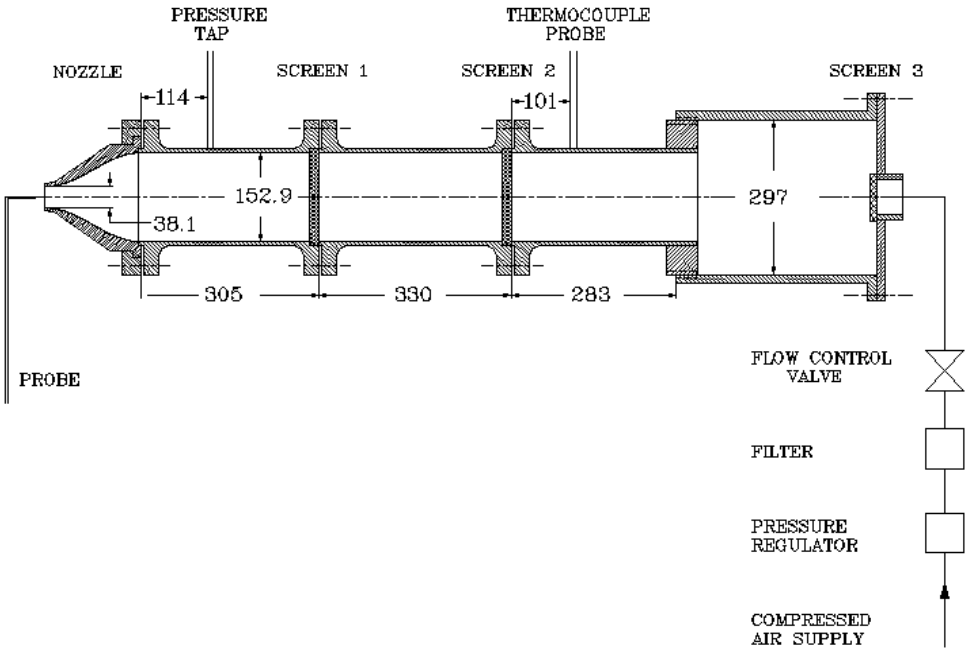

Figure 6.1: Test Facility for calibrating hot-wire and the five-hole probes

analog signal from the differential pressure transducer, thermocouple, stepper motor control and hot wire anemometer are transferred to the A/D board from where they are sampled.

6.2 Description of Calibration Technique for Single-Wire Probes

6.2.1.Single Sensor Hot -Wire Probe

To measure the unsteady velocity in the boundary layer, a single sensor hot wire probe is used which is shown in Figure 6.2. The wire is made of tungsten with a diameter of 4 μm. The wire temperature is constant, and the sensor temperature of the T_{probe}=250° C. The amount of electrical energy dissipated in the sensors is a measure of the cooling effect of the fluid past the heated sensor. The actual velocity is a function of the dissipated energy and the fluid temperature, assuming constant pressure and fluid properties.

A constant temperature anemometer is used to vary the electrical current through the hot wire in order to maintain a constant wire temperature T_{probe}. This is done by controlling the hot wire's resistance, which is a linear function of the temperature.

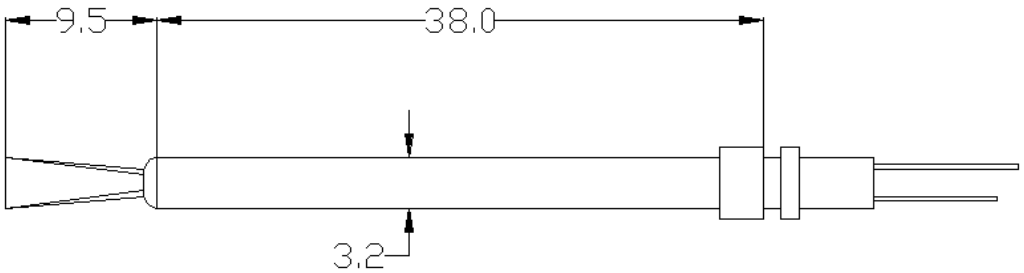

Figure 6.2: Single sensor hot-wire probe

6.2.2 Calibration Procedure

During the velocity calibration, single hot wire probe is kept normal to flow and the flow velocity is varied. The exit velocity is calculated by the differences between the static pressure at the inlet p_1 and the static pressure at the outlet of the nozzle p_2. From the Bernoulli-equation:

$$p_1 - p_2 = \frac{\rho}{2}(v_2^2 - v_1^2) \tag{6.1}$$

and the continuity equation for incompressible flow:

$$v_1 d_1^2 = v_2 d_2^2 \tag{6.2}$$

the formula for the exit velocity is:

$$v_2 = \sqrt{\frac{2\Delta p}{\rho}\frac{d_1^4}{d_1^4 - d_2^4}} \tag{6.3}$$

the density is calculated by the ideal gas equation:

$$\rho = \frac{p_1}{RT_1} \tag{6.4}$$

The temperature is measured by a thermocouple inside of the facility. All variables are displayed in Figure 6.3.

The exit velocity of the nozzle was varied from 0 to 12 m/s. For each velocity, a set

of data from constant temperature anemometry, thermocouple, pressure voltage signals were taken. The data are averaged for each channel. The correlation between the hot wire voltage (E) and the velocity (V) by a fourth-order polynomial:

$$V = a_0 + a_1 E + a_2 E^2 + a_3 E^3 + a_4 E^4 \tag{6.5}$$

The coefficients are calculated using the least-square method. The results of the calibration is shown in Figure 6.4.

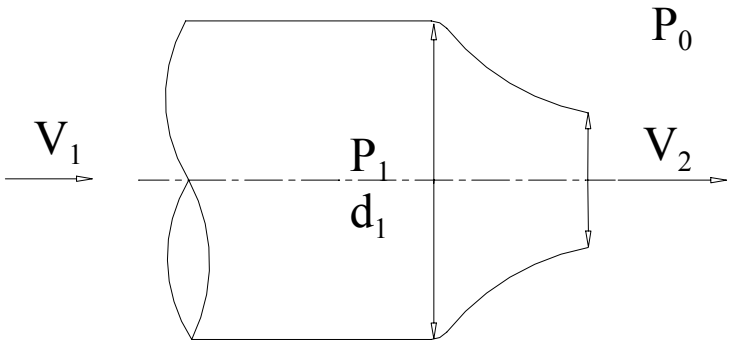

Figure 6.3: Nozzle of calibration test facility

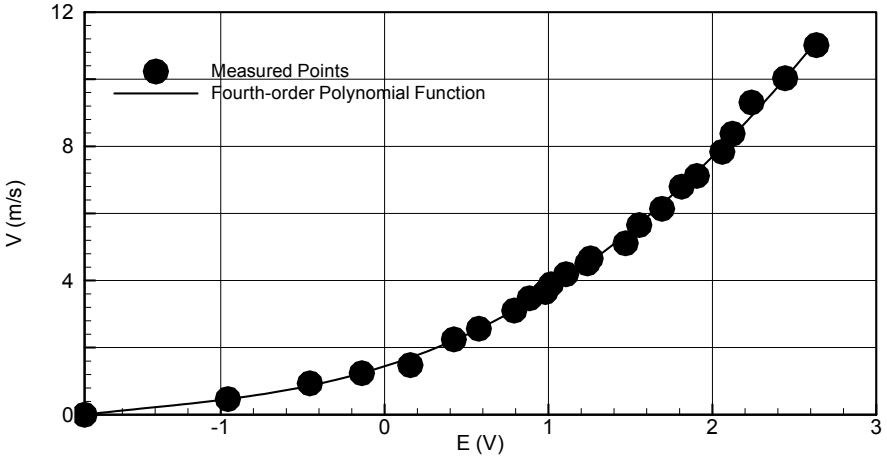

Figure 6.4: Calibration curve of single hot-wire probe

The temperature compensation of the velocity is made later, adjusting the anemometer output voltage according to the formula.

$$E_{adj} = E \frac{T_{probe} - T_{cal}}{T_{probe} - T} \tag{6.6}$$

where E is the sampled anemometer voltage, T is the actual temperature and T_{probe} is the operating temperature of the hot wire.

7. DATA REDUCTION

7.1 Data Reduction for Boundary Layer Measurement

7.1.1 Steady Flow

For data reduction and analysis, the characteristic response of the hot wire probe is stored in form of calibration constants. The instantaneous velocity component is calculated from the temperature compensated instantaneous voltages by using the calibration coefficients. The instantaneous velocity is represented in the following form:

$$V = \overline{V} + v \tag{7.1}$$

where $\overline{V}$ is the mean (time-averaged) velocity and v is the turbulent fluctuation component. The mean velocity, also known as the time-average, is given by:

$$\overline{V} = \frac{1}{N}\sum_{j=1}^{N} V_j \tag{7.2}$$

where N is the total number of samples taken at one boundary layer location. A sampling rate of 20kHz was used for investigating the steady flow (no wakes). The root mean square value of the turbulent velocity fluctuation is obtained from the instantaneous and mean velocities by:

$$v = \sqrt{\frac{1}{N}\sum_{j=1}^{N} (V_j - \overline{V})^2} \tag{7.3}$$

and the local turbulence intensity is defined as:

$$Tu_{loc} = \frac{v}{\overline{V}} \times 100 = \frac{1}{\overline{V}}\sqrt{\frac{1}{N}\sum_{j=1}^{N} (V_j - \overline{V})^2} \times 100 \tag{7.4}$$

7.1.2 Periodic Unsteady Flow

The unsteady data were reduced by ensemble-averaging method with respect to the rotation of the wake generator. At each boundary location, 20,000 samples were taken at a sampling rate of 20 kHz. The ensemble-averaged results were calculated for 100 rotation of the wake generator. For unsteady cases, the ensemble-averaged velocity, fluctuation velocity, and the turbulence intensity were calculated from the instantaneous velocity samples by:

$$V_i(t_i) \equiv < V_i(t_i) > \equiv \frac{1}{N}\sum_{j=1}^{N} V_{ij}(t_i) \tag{7.5}$$

$$v_i(t_i) \equiv < v_i(t_i) > = \sqrt{\frac{1}{N}\sum_{j=1}^{N} [V_{ij}(t_i) - < V_i(t_i) >]^2} \tag{7.6}$$

$$Tu_i(t_i) \equiv < Tu_i(t_i) > = \frac{< v_i(t_i) >}{< V_i(t_i) >} \times 100 \tag{7.7}$$

where N= 100 is the total number of wake generator cycles and M the number of samples taken per cycle. $<V_i(t_i)>$ is the ensemble averaged velocity for a particular spatial location. The ensemble-averaged boundary layer parameters such as displacement thickness $<\delta_1>$, momentum thickness $<\delta_2>$, and shape factor $<H_{12}>$ are calculated from:

$$\delta_1 \equiv < \delta_1 > = \int_0^{<\delta>} \left(1 - \frac{< V >}{< V >_e}\right) dy \tag{7.8}$$

$$\delta_2 \equiv < \delta_2 > = \int_0^{<\delta>} \frac{< V >}{< V >_e}\left(1 - \frac{< V >}{< V >_e}\right) dy \tag{7.9}$$

$$H_{12} \equiv < H_{12} > = \frac{< \delta_1 >}{< \delta_2 >} \tag{7.10}$$

7.1.3 Accurate Estimation of Boundary Layer Thickness

The accuracy of the boundary layer parameters such as displacement, momentum, and energy thickness depends primarily on an accurate estimation of the boundary layer thickness δ. Since in a turbine or compressor blade channel the velocity distribution outside the boundary layer is not constant as shown in Figure 7.1 (a). The estimation method used in conventional flat plate boundary layer calculation leads to incorrect results. In the following, a simple iterative method, developed by Schobeiri (2003), is presented that accurately determines the boundary layer thickness and thus the boundary layer parameters.

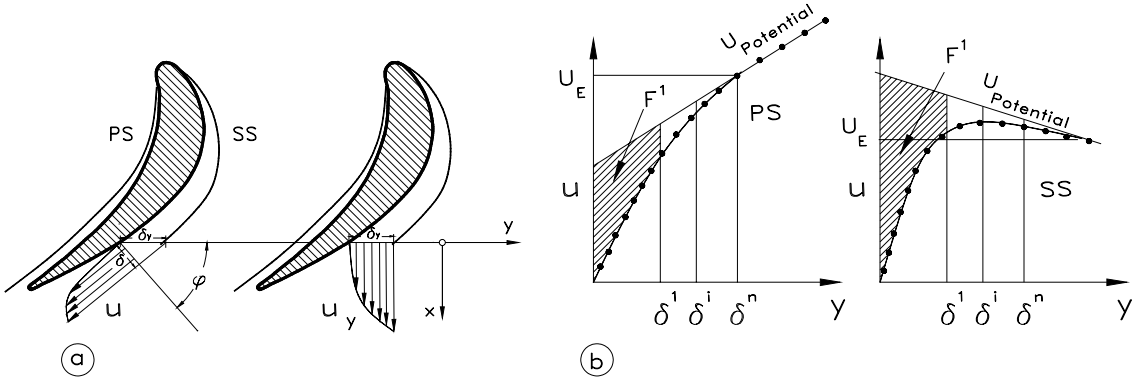

Figure 7.1: (a): Boundary layer velocity traverse, (b) Boundary layer edge velocity on pressure and suction side from Schobeiri (2003)

In Figure 7.1 the experimental velocity distribution on the pressure and suction surfaces are shown. To determine the boundary layer thickness, first a least square fit (LSQ) is performed and the velocity profile outside the boundary layer and its intersection with the u-axis is found. Starting from a first guessed value δ^1, the area F^1 is found using the relation:

$$F^1 = \int_0^{\delta^1} (U_{pot} - u)dy \tag{7.11}$$

In the next iteration step with δ^i the boundary of the integral in (7.11) is increased by a very small increment (for example 0.001mm) and the area F^i is calculated:

$$F^i = \int_0^{\delta^i} (U_{pot} - u)dy \tag{7.12}$$

We define the following ratio with the accuracy ϵ:

$$R = \frac{\left|F^i - F^{i+1}\right|}{F^i} \leq \varepsilon = 10^{-6} \tag{7.13}$$

and check if the ϵ has been reached. If the next iteration step with δ^{i+1} fulfils the above criterion, then the desired boundary layer thickness is δ^n, which can be used or the boundary layer thickness to be implemented into equations (7.8) to (7.10).

8.UNCERTAINTY ANALYSIS

Uncertainty analysis is performed on the single hot-wire measurements after calibration and data reduction utilizing the methods of Kline-McClintock (1956) and S. Yavuzkurt (1984). Kline and McClintock presented a technique to calculate how the uncertainty in individually measured values add together to result in an uncertainty for a quantity calculated from those values. However, it should be noted that the determined uncertainty may not be the actual uncertainty of the results because the Kline and McClintock method calculates the worst possible uncertainty. The main difference between these two uncertainty analysis method is coming from the way in which the actual uncertainty is calculated. The uncertainty for the Kline and McClintock method is a equivalent to the 95% confidence band that surrounds the single hot-wire curve fit. Since each point may have a different confidence interval, the uncertainty for each data point may be different. On the other hand, S. Yavuzkurt calculates the uncertainty by taking the square root sum of the squared errors divided by the number of data points. The results of the uncertainty analysis and the most significant equations used to determine the uncertainty for each case is presented below with the actual calculations documented in Appendix B.

8.1 Uncertainty Analysis for Single Hot-Wire Measurements

The uncertainty in velocity for the single hot-wire probe after calibration and data reduction is given in Table 8.1 for the Kline and McClintock and Table 8.2 for the S. Yavuzkurt method. The uncertainty in velocity during calibration increases when the flow velocity decreases. It is primarily due to large uncertainty in the pressure transducer that is used for calibration. As for the uncertainty in velocity after data reduction, the trend continues due to the fact that the calibration uncertainty is incorporated into the final velocity. For this case, the pneumatic velocity uncertainty and the total calibration uncertainty was determined using equations 8.1 and 8.3.

The uncertainty in the pneumatic velocity was found with the following equation;

$$\omega_v = \sqrt{\left[\left(\frac{\partial V}{\partial P}\right)\omega_p\right]^2 + \left[\left(\frac{\partial V}{\partial \rho}\right)\omega_\rho\right]^2 + \left[\left(\frac{\partial V}{\partial D_{ni}}\right)\omega_{D_{ni}}\right]^2 + \left[\left(\frac{\partial V}{\partial D_{no}}\right)\omega_{D_{no}}\right]^2} \quad (8.1)$$

In the above equation, ω_p is the uncertainty of pressure readings from pressure transducer, ω_ρ is the uncertainty during the calculation of density, $\omega_{Dno,}$ ω_{Dni} are respectively the uncertainty of the outer and inner diameter of calibration nozzle. The pneumatic velocity is calculated:

$$V = \sqrt{\frac{2P}{\rho\left[1 - \left(\frac{D_{no}}{D_{ni}}\right)^4\right]}} \quad (8.2)$$

In the above equation, P is the transducer pressure, D_{no} is the outside diameter of the calibration nozzle, D_{ni} is the inside diameter of the nozzle, ρ is the air density. The uncertainty in the effective velocity after the calibration for the Kline and McClintock method is:

$$\omega_{Ve_j} = \sqrt{\left(\frac{\partial Ve_j}{\partial e_j}\omega_{e_j}\right)^2 + \omega_{cf}{}^2 + \omega_V{}^2} \quad (8.3)$$

where ω_{Ve} is the effective velocity, ω_e is the uncertainty of the constant hot wire anemometry voltage readings, ω_V is the velocity and ω_{cf} is the uncertainty of the least square fit and equivalent to the 95% confidence interval which surrounds the curve fit. The effective velocity for any particular wire is represented by the following equation:

$$Ve_j = a_{0j} + a_{1j}E_j + a_{2j}E_j{}^2 + a_{3j}E_j{}^3 + a_{4j}E_j{}^4 \quad (8.4)$$

where a_{ij} are the coefficients determined by the least square fit.

As for the uncertainty in velocity after data reduction, it is given by the following equation;

$$\omega_{V_r} = \sqrt{\left(\frac{\partial V_r}{\partial e}\omega_e\right)^2 + \omega_{calib}{}^2} \tag{8.5}$$

where ω_{calib} is the uncertainty in the calibration.

The uncertainty in the curve fit from S. Yavuzkurt method is given by;

$$C_s = \frac{\sum_{i=1}^{n}\left[\left(\frac{\Delta V}{Ve}\right)^2 * i\right]^{\frac{1}{2}}}{n} \tag{8.6}$$

where n is the number of data points, and ΔV is the residual. This value is squared and added to the square of $\Delta V/V$, and raised to the one half power. This calculated value is the uncertainty of effective velocity.

The curve fit uncertainty for the S. Yavuzkurt method is much larger than the uncertainty determined from the 95% confidence interval.

Table 8.1: Uncertainty in velocity after calibration and data reduction

(Kline and McClintock Method)

V (m/s)	$\omega V/V$ (%)	$\omega V_e/V_e$ (%)$_{calib}$	$\omega V/V$ (%)$_{red}$
3	5.59	5.92	6.07
5	2.06	2.36	2.44
10	0.54	0.76	0.83

Table 8.2: Uncertainty in velocity after calibration and data reduction

(S. Yavuzkurt Method)

V (m/s)	$\omega V/V$ (%)	$\omega V_e/V_e$ (%)$_{calib}$	$\omega V/V$ (%)$_{red}$
3	5.59	5.71	5.72
5	2.06	2.30	2.35
10	0.54	1.28	1.37

9.RESULTS AND DISCUSSIONS

In this section, the experimental results from the steady and unsteady boundary layer development, periodic unsteady wake development, surface pressure measurements and the velocity distribution will be presented at different Re-numbers.

Detailed steady and steady boundary layer and surface pressure measurements were taken at four different Reynolds number to investigate the influence of periodic unsteady wake flow on the boundary layer development along the suction and the pressure surface of the LP turbine blade and the onset of the separation zone. For each Reynolds number three different frequencies were performed. For the generation of the unsteady wake flow along the pressure and the suction surfaces of the LP turbine blade, two clusters of cylindrical rods with the diameter d_R=2mm were attached to the two belts of the wake generator. The cylindrical rod diameter is chosen according to fulfill the generation of the drag coefficient C_D which is approximately equal to the drag coefficient of the turbine blade with the chord and spacing given in the Table 4.1.

To account for the unsteadiness caused by the frequency of the individual wakes, the flow velocity, the spacings and the cascade parameters, an unsteady flow parameter or reduced frequency Ω is defined which is including the cascade solidity σ, the flow coefficient ϕ, the blade spacing S_B, and the rod spacings S_R.

$$\Omega = \frac{c}{S_R}\frac{U}{V_{ax}} = \frac{\sigma}{\varphi}\frac{S_B}{S_R} \tag{9.1}$$

with $\sigma = \frac{c}{S_B}$ and $\varphi = \frac{V_{ax}}{U}$

Experimental investigations were performed for three different reduced frequencies Ω=0.0, 1.59, and 3.18 that correspond to the rod spacings S_R=∞ mm, 80 mm, and 160 mm.

9.1 Surface Pressure Distributions

Detailed pressure measurements were taken by a 48-port scanivalve at four different Re-numbers of 50,000, 75,000, 100,000, 110,000 and 125,000. For each Reynolds number three different reduced frequencies of Ω=0, 1.59, 3.18 were applied that correspond to rod spacings of S_R=∞,160 mm, and 80 mm. The pressure signals inherently signify the time-averaged pressure because of the internal pneumatic damping effect of the connecting pipes. The differences in pressure distributions between steady and unsteady cases, on the suction surface, are caused by the drag forces of the wake generated by moving rods. The drag forces cause a momentum deficiency that lead to a reduction of total and static pressure.

The time-averaged pressure coefficients along the pressure and suction surfaces are plotted in Figure 9.1 and 9.2. Starting from Re=50,000 and steady state with Ω=0, shown in Figure 9.1 (a), the suction surface (upper portion), exhibits a strong negative pressure gradient. The flow accelerates at a relatively steep rate and reaches its maximum surface velocity that corresponds to the minimum C_p=-4.0 at s/s_o=0.42. Passing through the minimum pressure, the fluid particle within the boundary layer encounter a positive pressure gradient that causes a sharp deceleration until s/s_o=0.55 has been reached. This point signifies the begin of the laminar boundary layer separation and the onset of a separation zone. As seen in the subsequent boundary layer discussion, the separation zone characterized by a constant c_p- plateau extends up to s/s_o=0.746, thus occupying more than 21% of the suction surface and constituting a massive separation. Passing the plateau, the flow first experiences a second sharp deceleration indicative of a process of re-attachment followed by a further deceleration at a moderate rate. On the pressure surface, the flow accelerates at a very slow rate, reaches a minimum pressure coefficient at s/s_o=0.42 and continues to accelerate until the trailing edge has been reached. Unlike the suction surface, the pressure surface boundary layer does not encounter any adverse positive pressure gradient, therefore it remains fully laminar.

Considering the unsteady case with the flow reduced frequency Ω=1.59 corresponding to a rod spacing of S_R=160 mm, Figure 9.1 (a) shows two important and different characteristics: (1) There is a significant difference in pressure distribution between

steady and unsteady cases. As mentioned above, this deviation is attributed to the

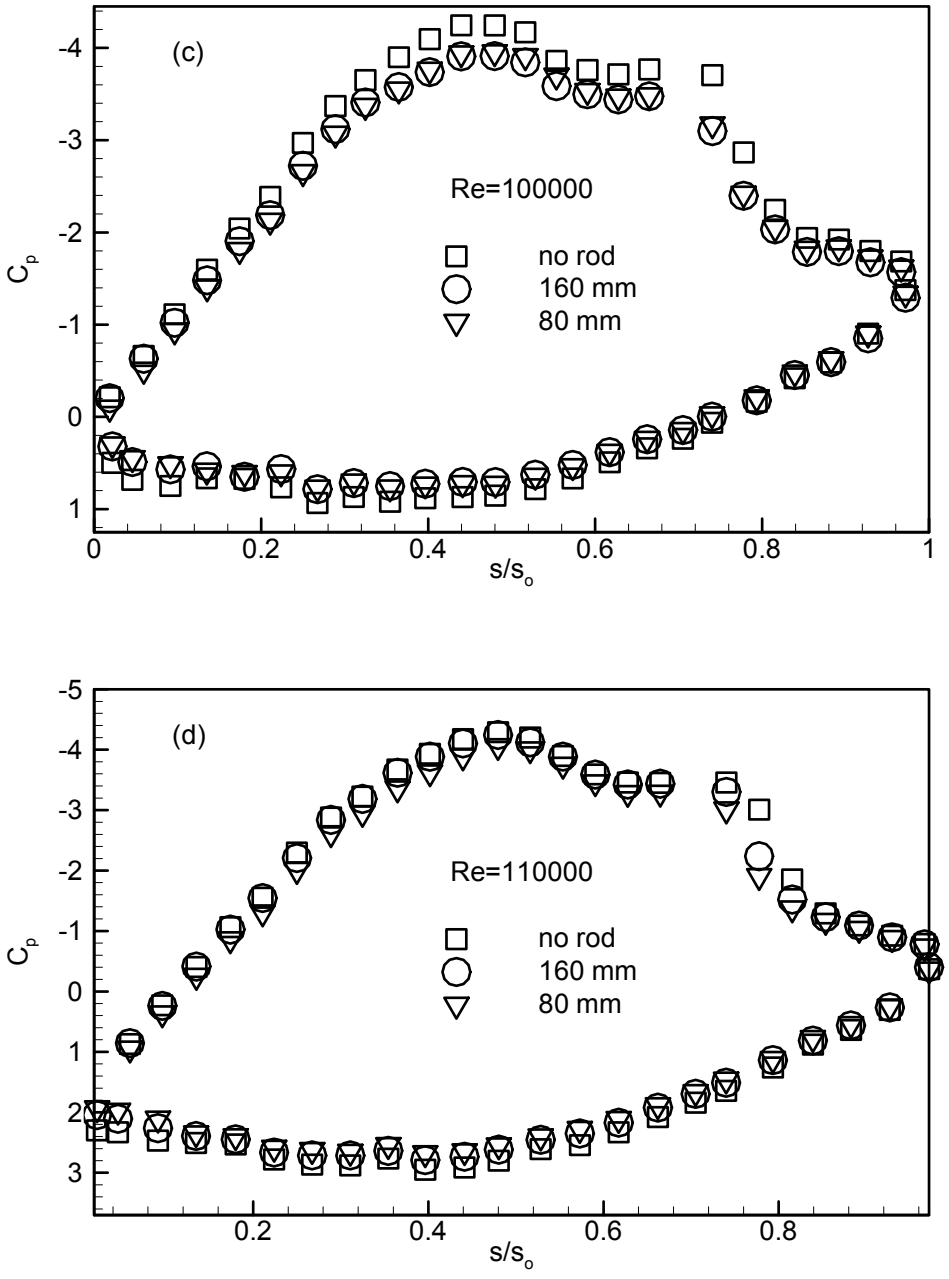

Figure 9.1: Static pressure distribution at (c) Re=100,000 and (d) Re=110,000 and reduced frequencies Ω=0 (S_R=∞), Ω=1.59 (S_R=160 mm), Ω=3.18 (S_R=80 mm)

momentum deficiency that leads to a reduction of total and static pressure. (2) For

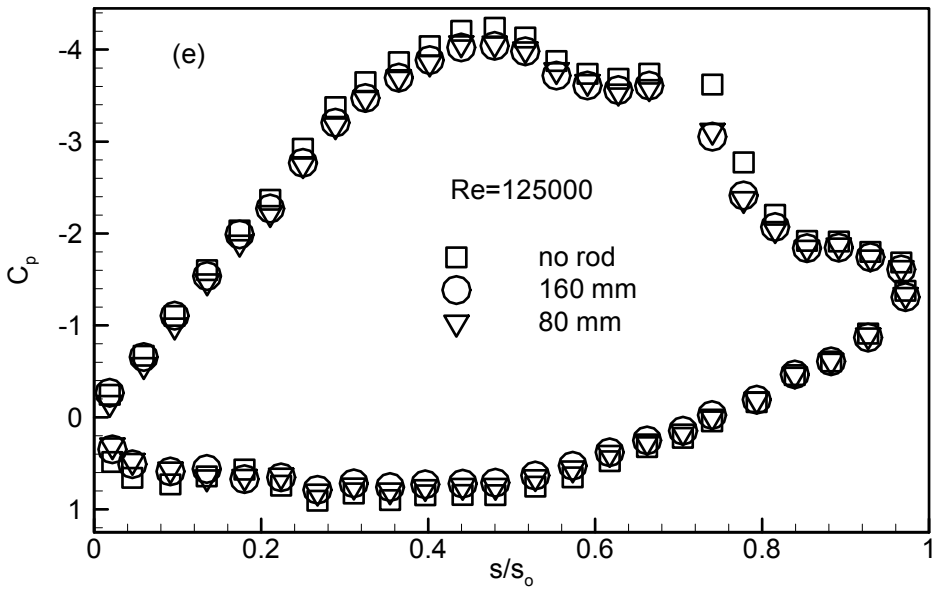

Figure 9.2: Static pressure distribution at (e) Re=125,000 and reduced frequencies Ω=0 (S_R=∞), Ω=1.59 (S_R=160 mm), Ω=3.18 (S_R=80 mm)

Re=50,000 and less than 125,000, the wakes have a substantial reducing impact of the separation zone. Increasing the reduced frequency to Ω=3.18 by reducing the rod spacing to S_R=80 mm causes a slight shift of the C_p-distribution compared with other frequencies.

Increasing the Reynolds number to Re=75,000, has not brought major changes in steady state C_p-distribution. This is also true for the subsequent higher Reynolds number cases at steady state Figure 9.1 and 9.2 (b,c,d,e). However, the higher Reynolds number with unsteady wakes reveals that the noticeable deviation in pressure distribution between the steady and unsteady cases discussed above is diminishing by increasing the Re-number as shown in Figure 9.1 and 9.2 (b,c,d,e). There is two factors which is contributing to this deviation: (1) As mentioned above, the momentum deficiency and the associated pressure losses caused by moving wakes. (2) The boundary layer energizing effect of the impinging wakes. Although the impinging wakes cause velocity and momentum deficits, their high turbulence intensity vortical cores provide an intensive exchange and transfer of mass, momentum, and energy to the blade surface, thus energizing the low energetic boundary layer. In conjunction with the surface pressure distribution, the kinetic energy of the lateral

velocity fluctuation plays a crucial role. In case of a low Re-number flow, the strong damping effect of the wall shear stress has the tendency to reduce the lateral turbulence kinetic energy, thereby diminishing its surface pressure augmenting effect. Increasing the Re-number results in a decrease of the damping effect of the wall shear stress, allowing the kinetic energy of the lateral velocity fluctuation component to be added integrally to the surface pressure, thus offsetting the wake deficit effects on the pressure distribution. This fact is clearly shown in Figure 9.1 and 9.2 (a,b,c,d,e), where the pressure distributions of unsteady flow cases at Ω=1.59 and Ω=3.18, with the exception of the separation zone, systematically approach the steady state cases at Re=75,000, 100,000 and very visibly at Re=125,000. It is worth noting that the impact of the unsteady wakes on the extent of the separation zone is preserved regardless of the Reynolds number variation performed in this study.

9.2 Ensemble-Averaged Boundary Layer Velocity Distributions

Boundary layer profiles were taken for one steady and two unsteady inlet flow conditions on the suction surface at 31 streamwise positions. Periodic unsteady flow was established by the wake generator, which included two clusters of cylindrical rods that were attached to the timing belts running with a translational speed of U = 5.0 m/s. To account for the unsteadiness caused by the frequency of the individual wake generating clusters and their spacing, the flow velocity, and the cascade parameters, the previously defined reduced frequency Ω is used. The individual cluster configurations with the corresponding Ω-parameter are specified in Table 4.1. Experimental investigations were performed for three different values of Ω = 0.0, 1.59, and 3.18. These values cover the entire reduced frequency range encountered in LPT-design and off-design operation conditions.

Figure 9.3 displays two representative temporal ensemble-averaged velocity distributions for steady and two unsteady flow conditions with their characteristic features. All these figures show the boundary layer development from the core flow region to the blade surface at different streamwise positions. Approaching the wall surface, all velocities experience a continuous deceleration. The velocity gradient in both cases causes generation

and formation of vortices that transform steady nature of steady case into an unsteady one as clearly demonstrated in Figure 9.3**.** The unsteady case displayed in Figure 9.3 is characterized by its deterministic temporal periodicity. Approaching the wall surface, the traveling wake experiences a phase shift, while maintaining its deterministic nature. However, by penetrating into the boundary layer, the interaction between wake and boundary layer causes the deterministic nature to degenerate into a stochastic one. As the flow continues downstream, continuous wake deformation occurs in large velocity peaks inside the boundary layer. Convecting downstream, passing the separation zone, the wake diminishes, while the turbulent boundary layer starting from s/s_o=0.766 dominates the flow picture.

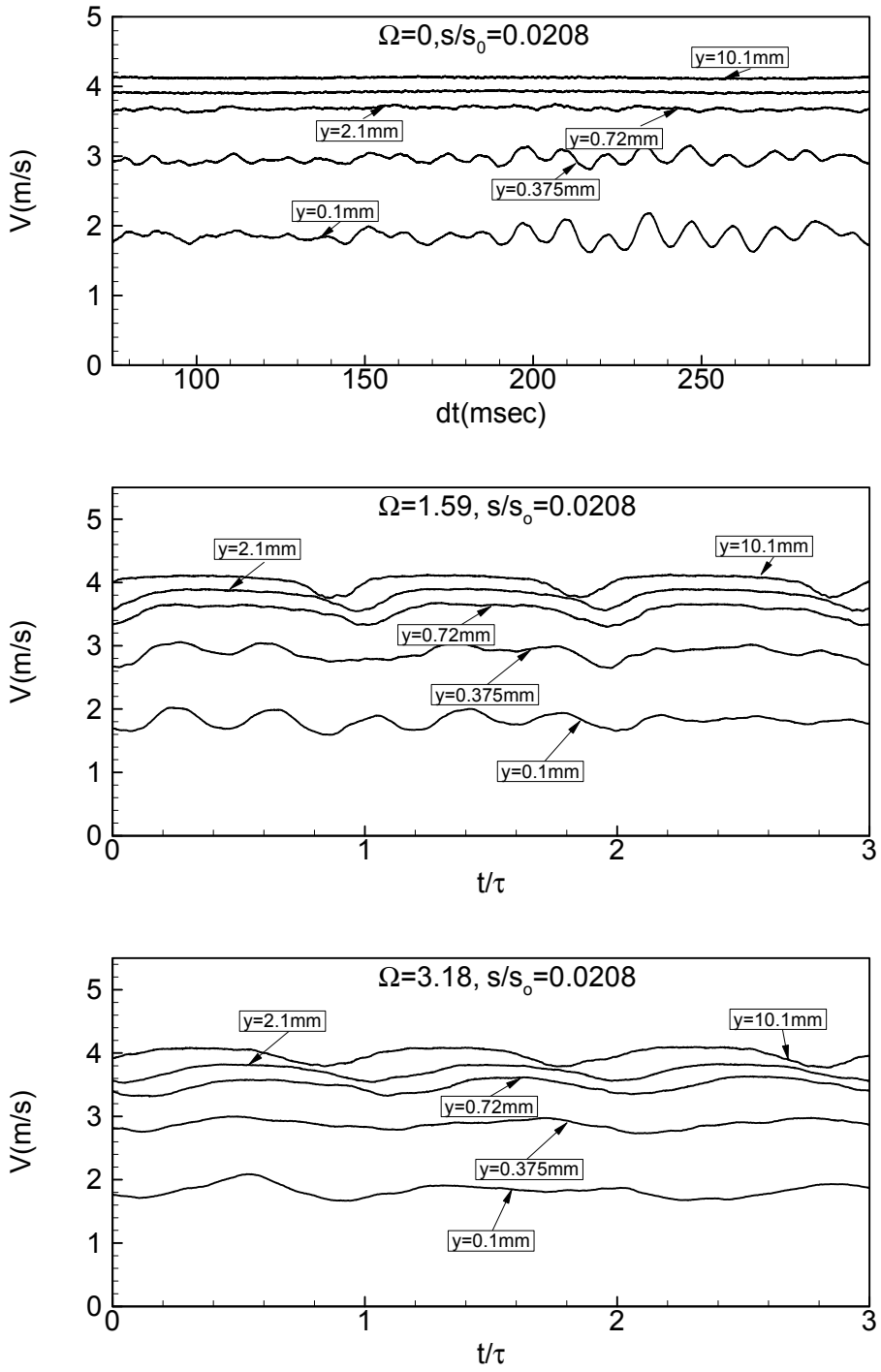

Figure 9.3: Ensemble-averaged velocity as a function of time for three different reduced frequency of Ω=0, 1.59, 3.18 at s/s_o=0.0208, Re=110,000

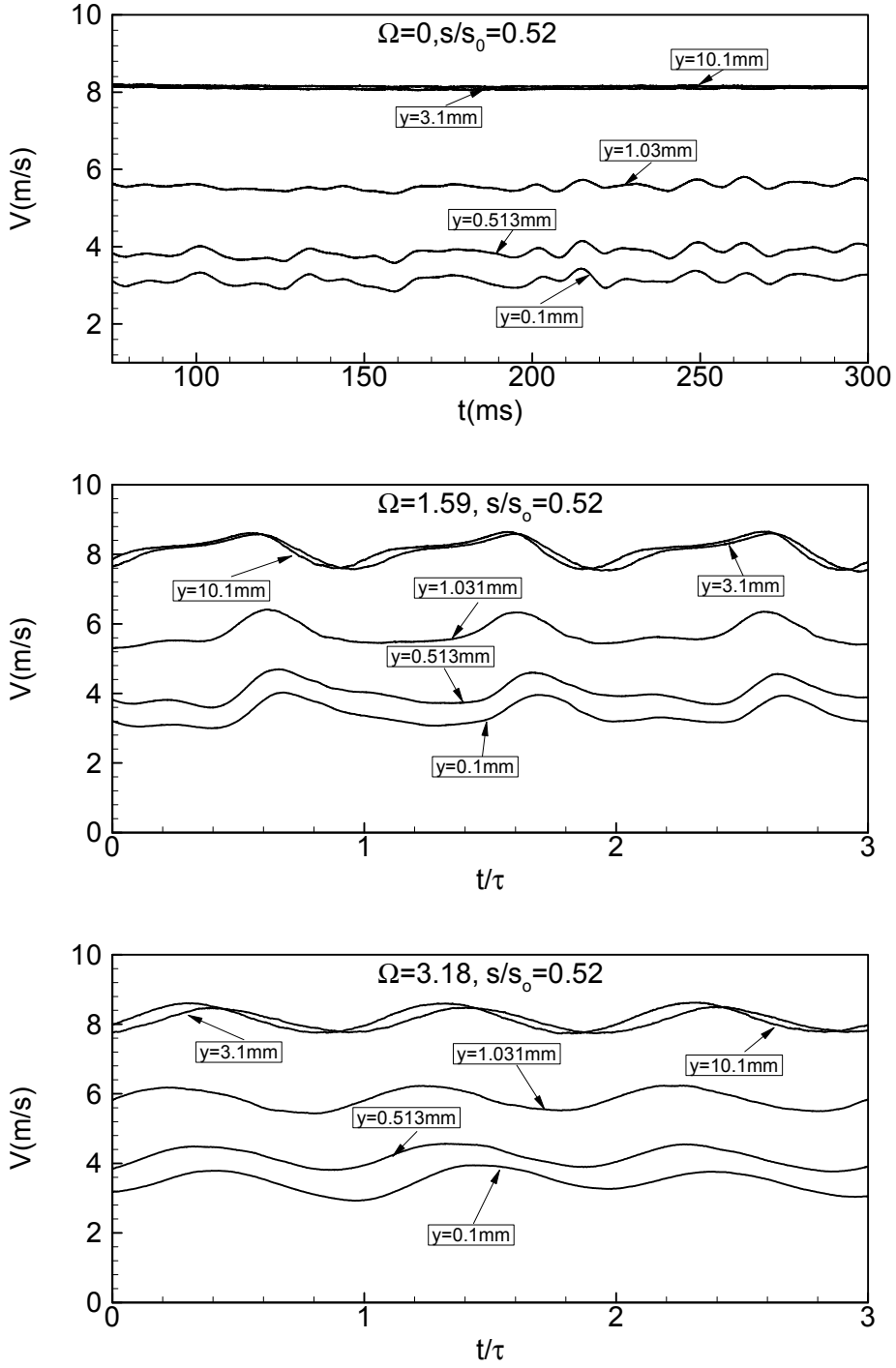

Figure 9.4: Ensemble-averaged velocity as a function of time for three different reduced frequency of Ω=0, 1.59, 3.18 at s/s_o=0.519, Re=110,000

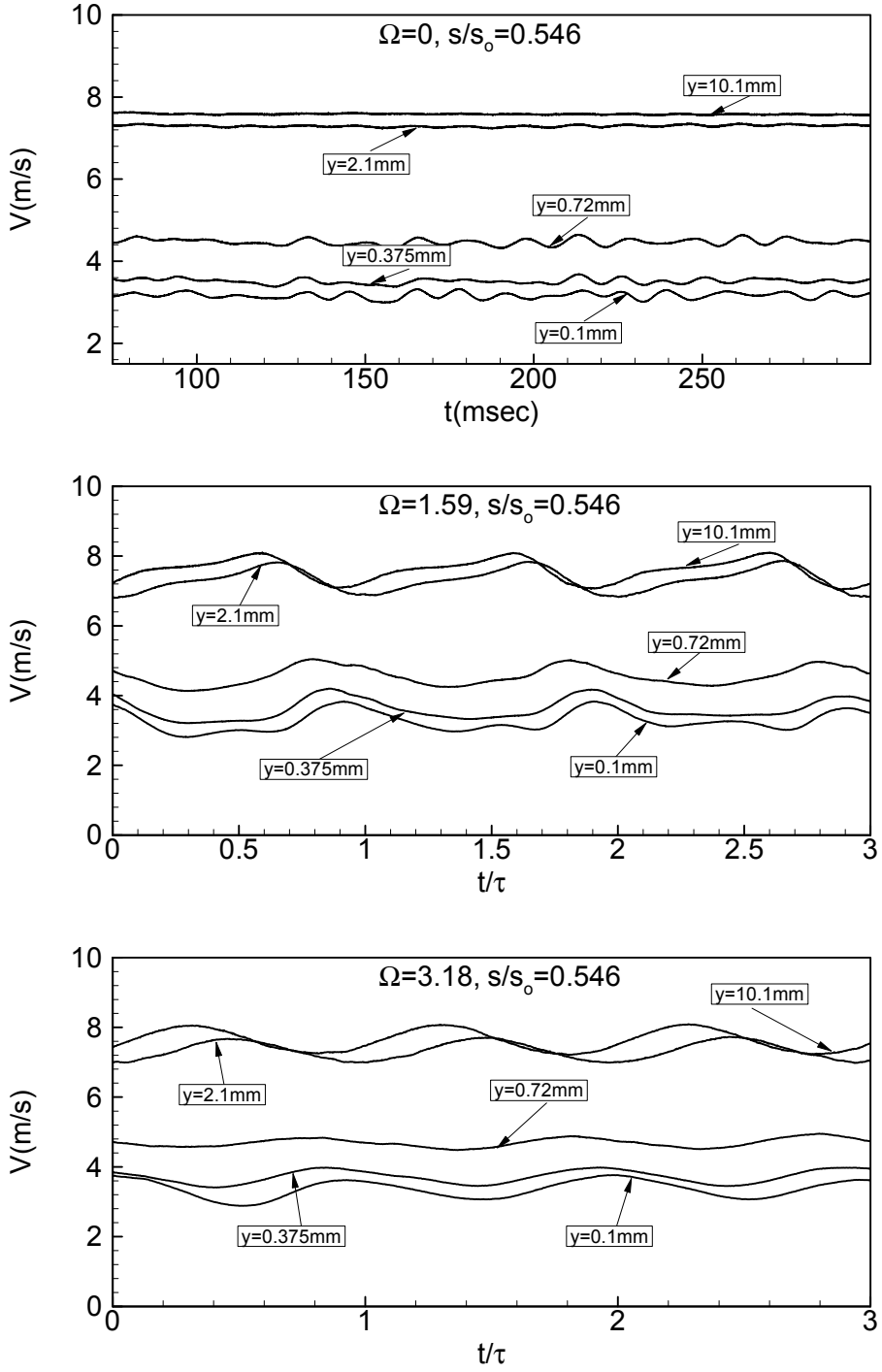

Figure 9.5: Ensemble-averaged velocity as a function of time for three different reduced frequency of Ω=0, 1.59, 3.18 at s/s_o=0.546, Re=110,000

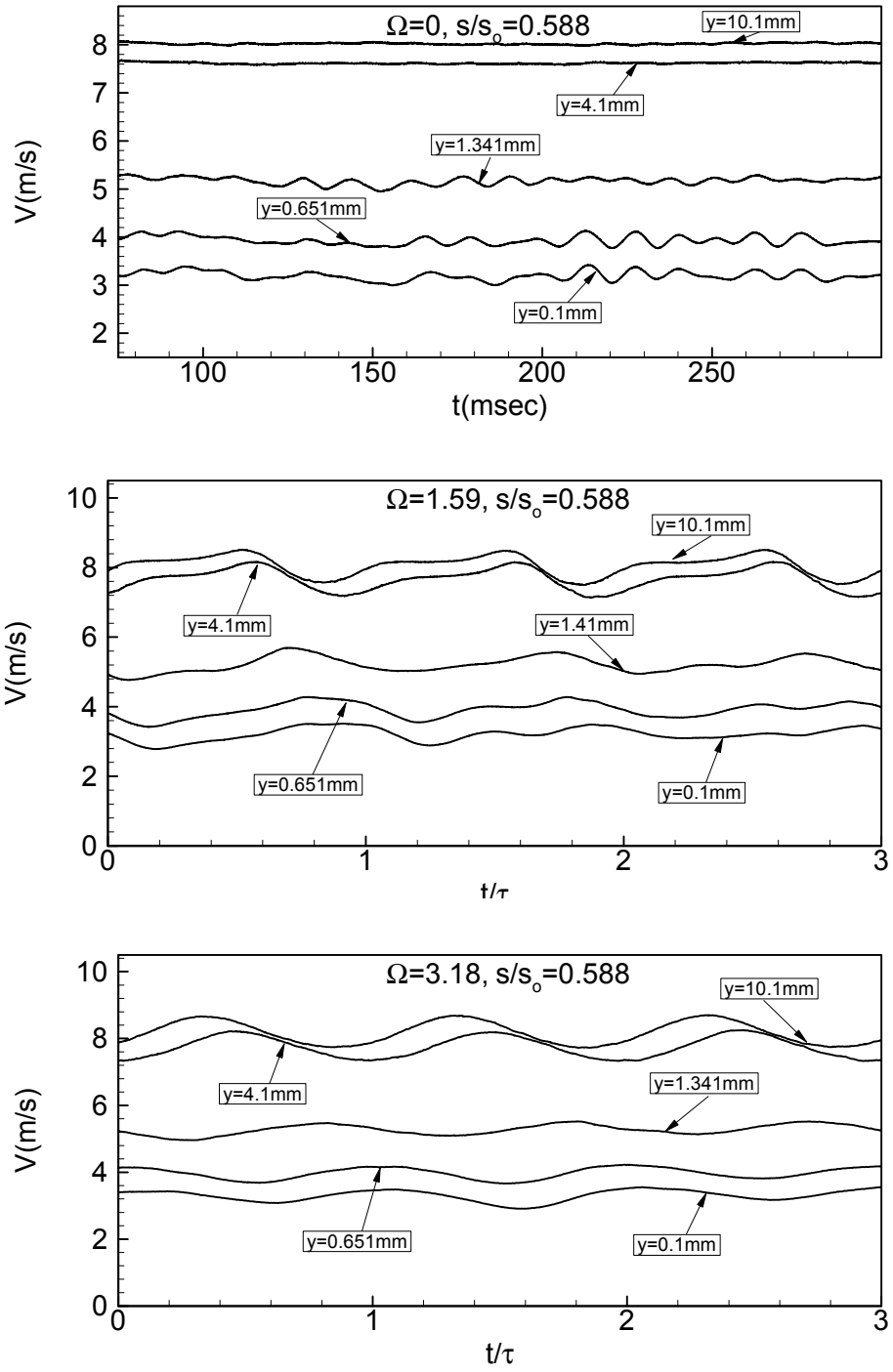

Figure 9.6: Ensemble-averaged velocity as a function of time for three different reduced frequency of Ω=0, 1.59, 3.18 at s/s_o=0.588, Re=110,000

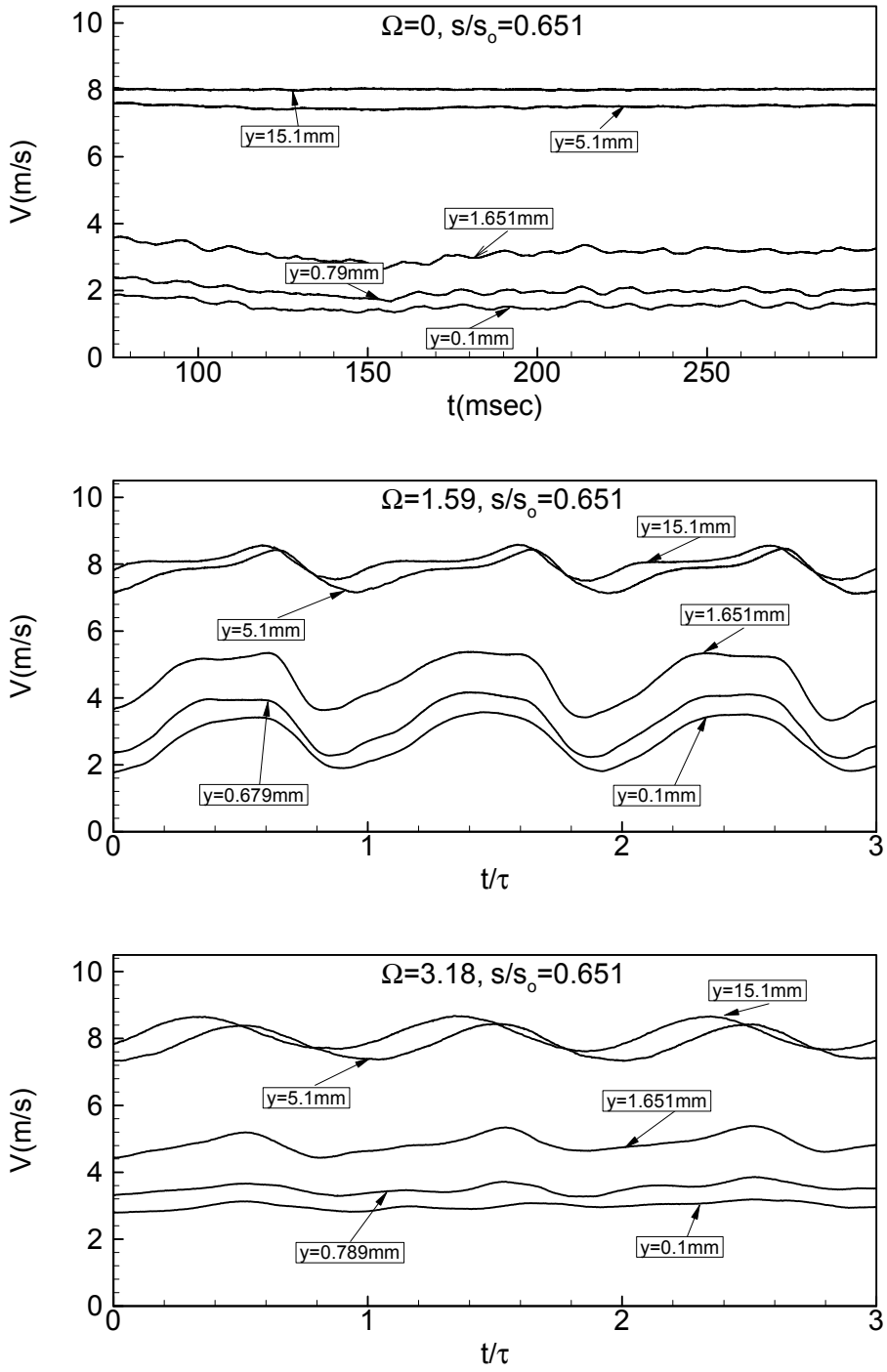

Figure 9.7: Ensemble-averaged velocity as a function of time for three different reduced frequency of Ω=0, 1.59, 3.18 at s/s_o=0.651, Re=110,000

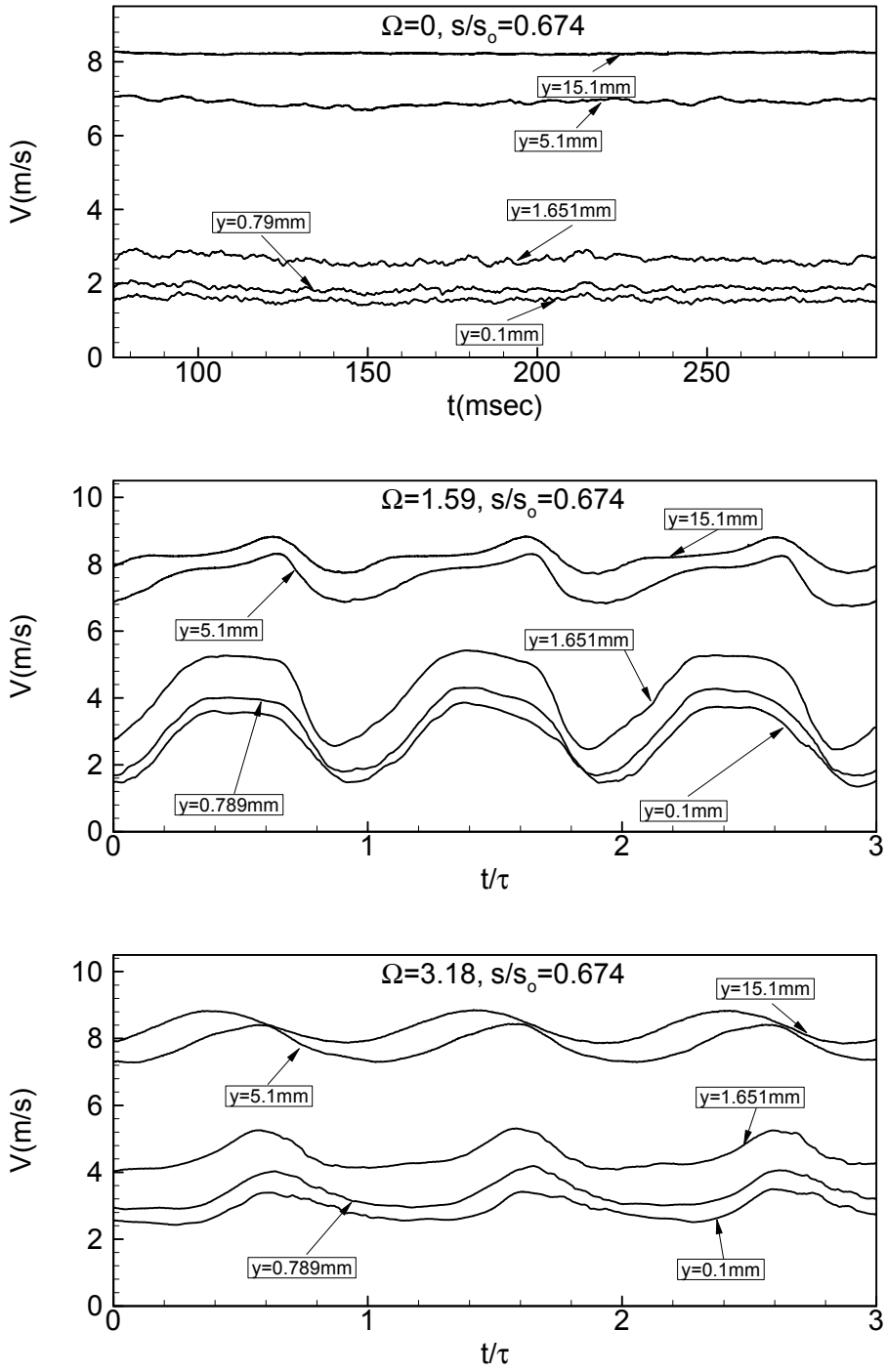

Figure 9.8: Ensemble-averaged velocity as a function of time for three different reduced frequency of Ω=0, 1.59, 3.18 at s/s_o=0.674, Re=110,000

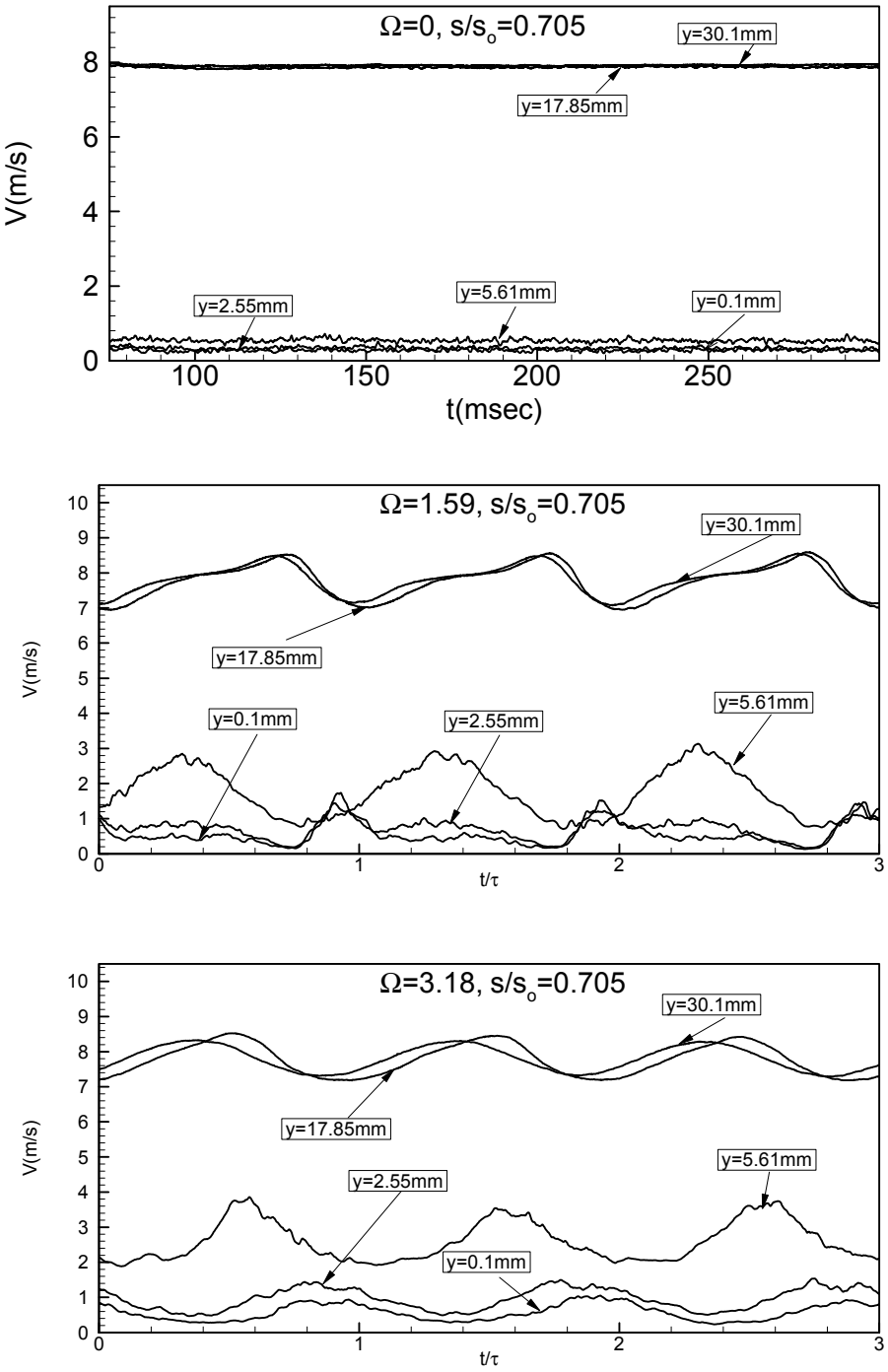

Figure 9.9: Ensemble-averaged velocity as a function of time for three different reduced frequency of Ω=0, 1.59, 3.18 at s/s_o=0.705, Re=110,000

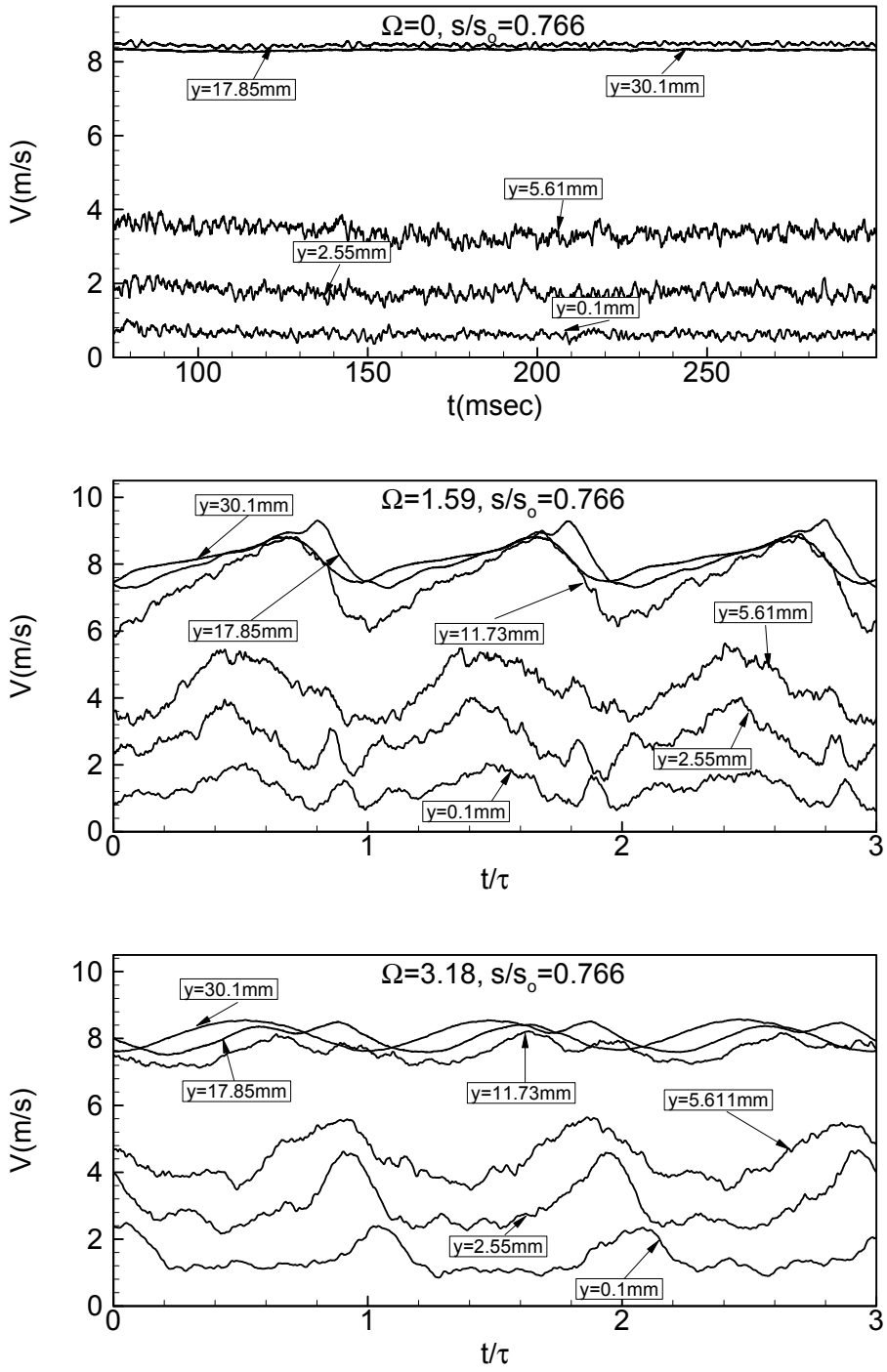

Figure 9.10: Ensemble-averaged velocity as a function of time for three different reduced frequency of Ω=0, 1.59, 3.18 at s/s_o=0.766, Re=110,000

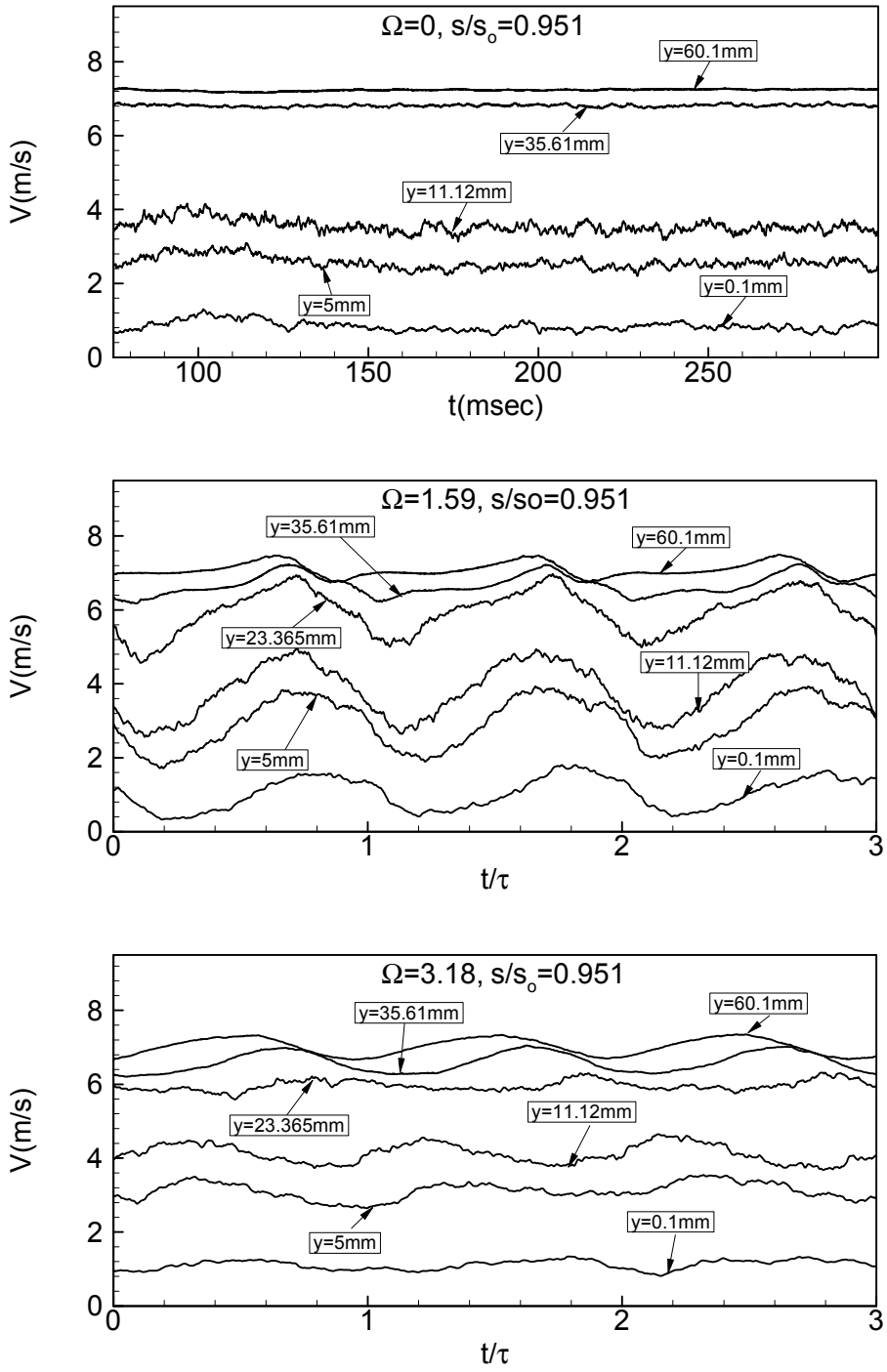

Figure 9.11: Ensemble-averaged velocity as a function of time for three different reduced frequency of Ω=0, 1.59, 3.18 at s/s_o=0.951, Re=110,000

9.3 Time Averaged Velocity Distributions

Consistent with the surface pressure distribution which is discussed above, the effect of the wake frequency on time-averaged velocity profiles and turbulence fluctuation distribution are presented for the corresponding rod spacings $S_R=\infty$ mm, 80 mm, and 160 mm at different longitudinal locations in Figures 9.12 to9.21. Upstream of the separation zone, the flow is attached to the blade, and the separation zone start at $s/s_o=0.52$. Upstream of the separation zone at $s/s_o=0.52$ and also at its immediate proximity $s/s_o=0.588$, the velocity distributions inside the boundary layer experience a moderate decrease with increasing the reduced frequency. Inside the separation zone at $s/s_o=0.705$, a substantial influence of the wake frequency is observed. Higher wake frequency introduces fluctuation kinetic energy into the boundary layer trying to reverse the separation tendency. And also, becalmed regions generated by the turbulent spots produced in the wake paths, were effective in suppressing or reducing the separation zone. As it can be seen from the velocity distribution profiles, the onset and the length of the separation zone is not changed. But, there is a slight change of the bubble height. This shows that flow does not have the capability to suppress the separation zone. It only reduces the separation bubble height.

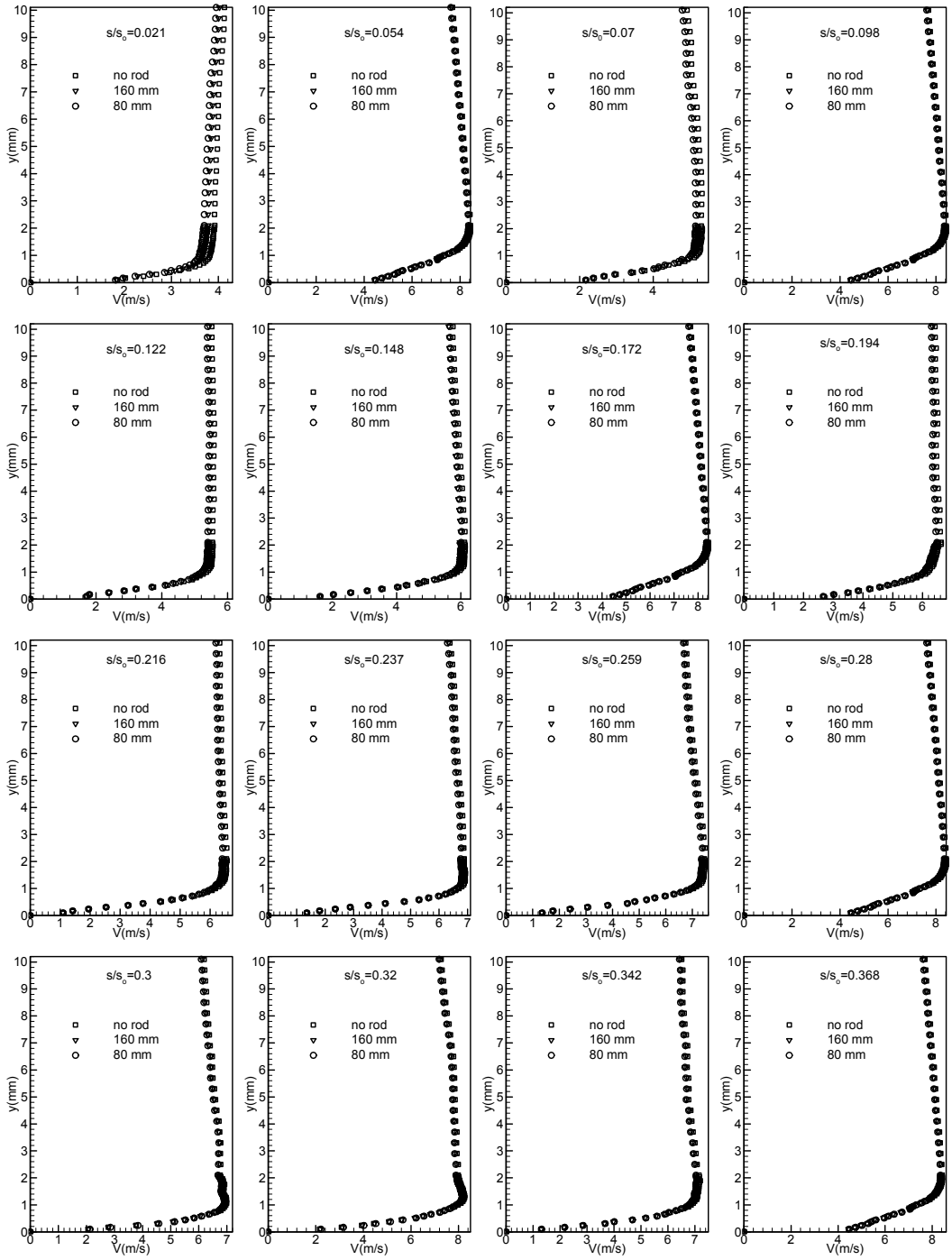

Figure 9.12: Distribution of the time-averaged velocity along the suction surface for three different reduced frequencies of Ω=0 (S_R=∞), Ω=1.59 (S_R=160 mm), Ω=3.18 (S_R=80 mm) at Re=110,000

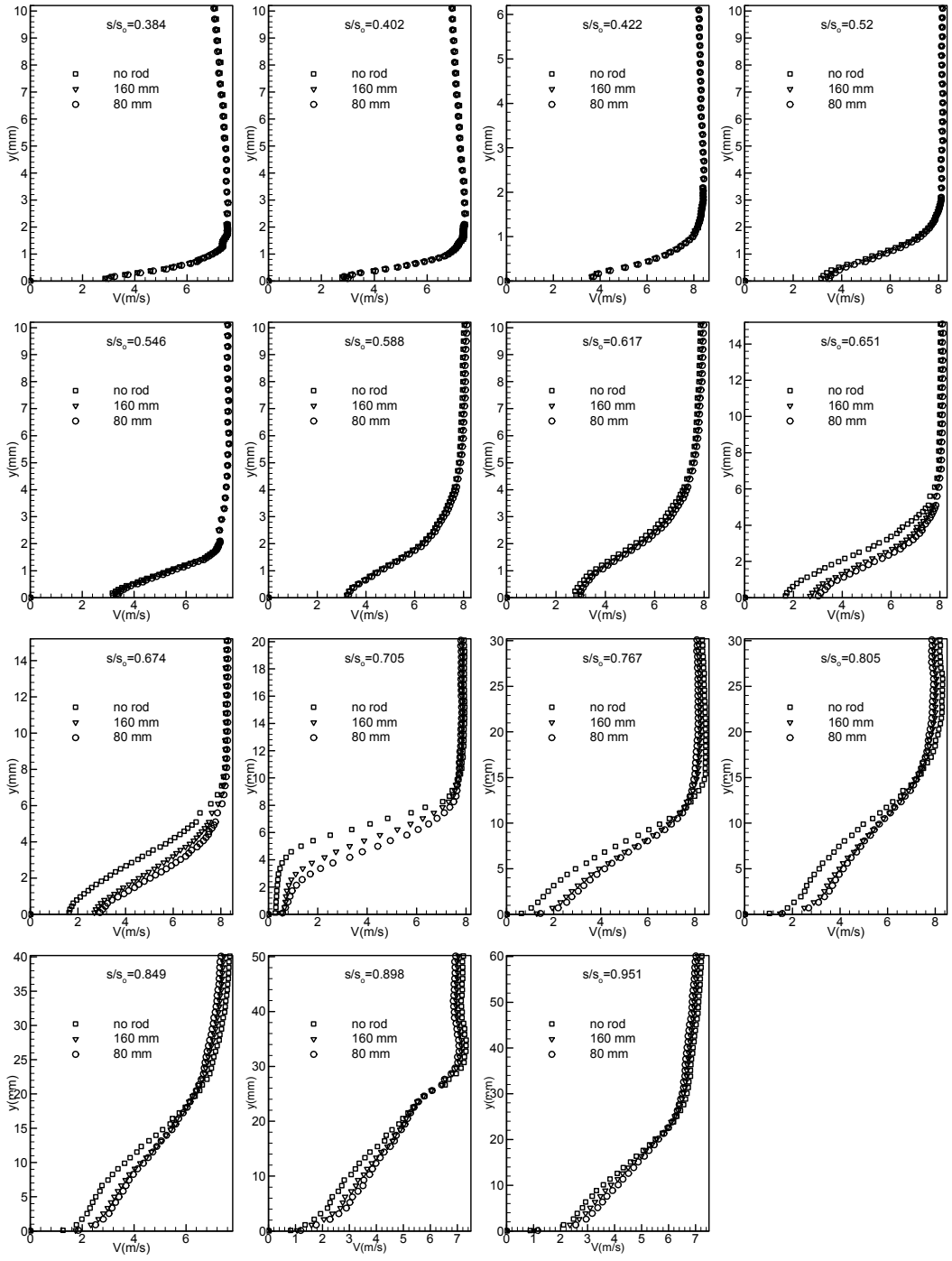

Figure 9.13: Distribution of the time-averaged velocity along the suction surface for three different reduced frequencies of Ω=0 (S_R=∞), Ω=1.59 (S_R=160 mm), Ω=3.18 (S_R=80 mm) at Re=110,000

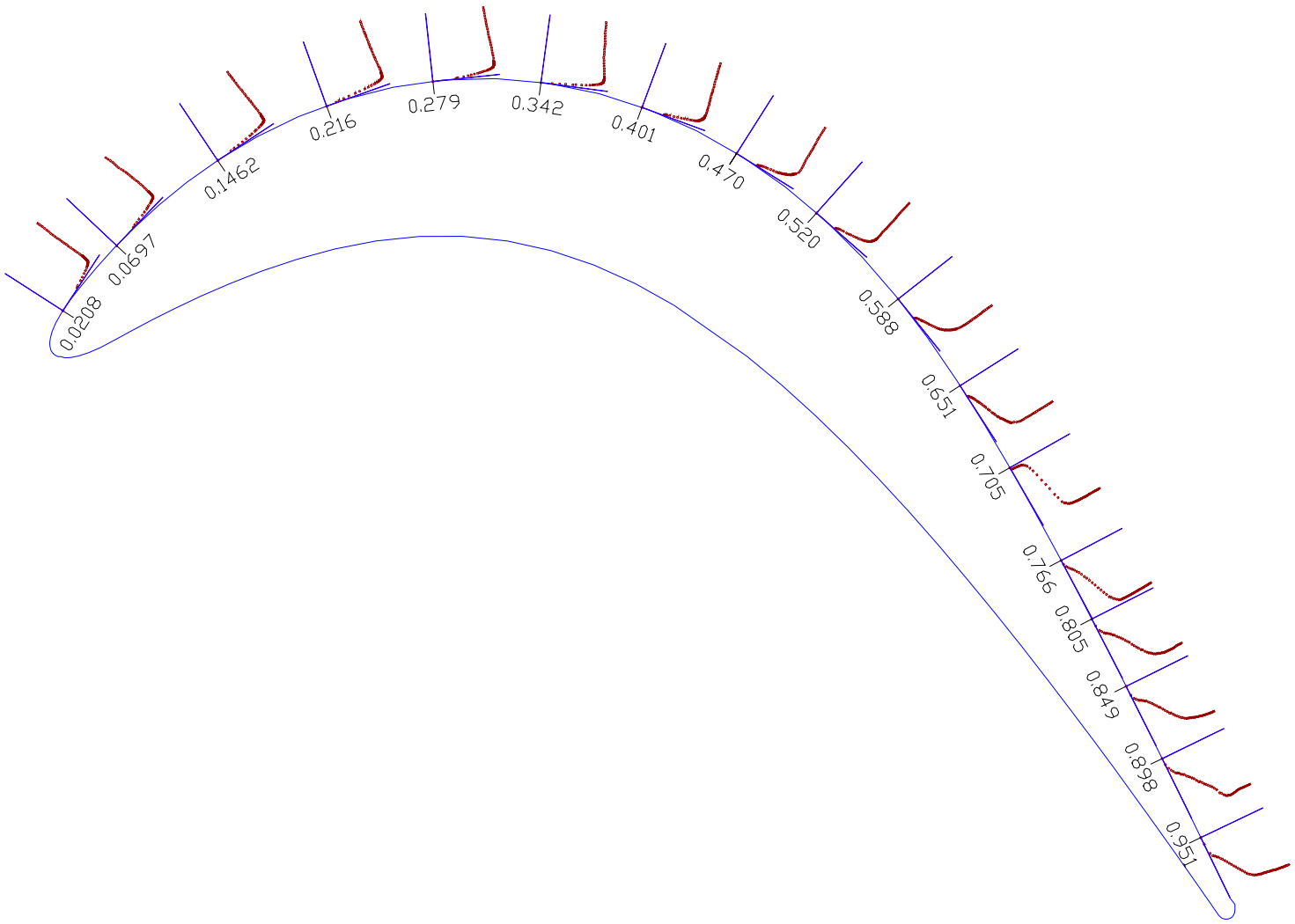

Figure 9.14: Time-averaged velocity profiles along the suction surface of the blade at Ω=0, Re=110,000

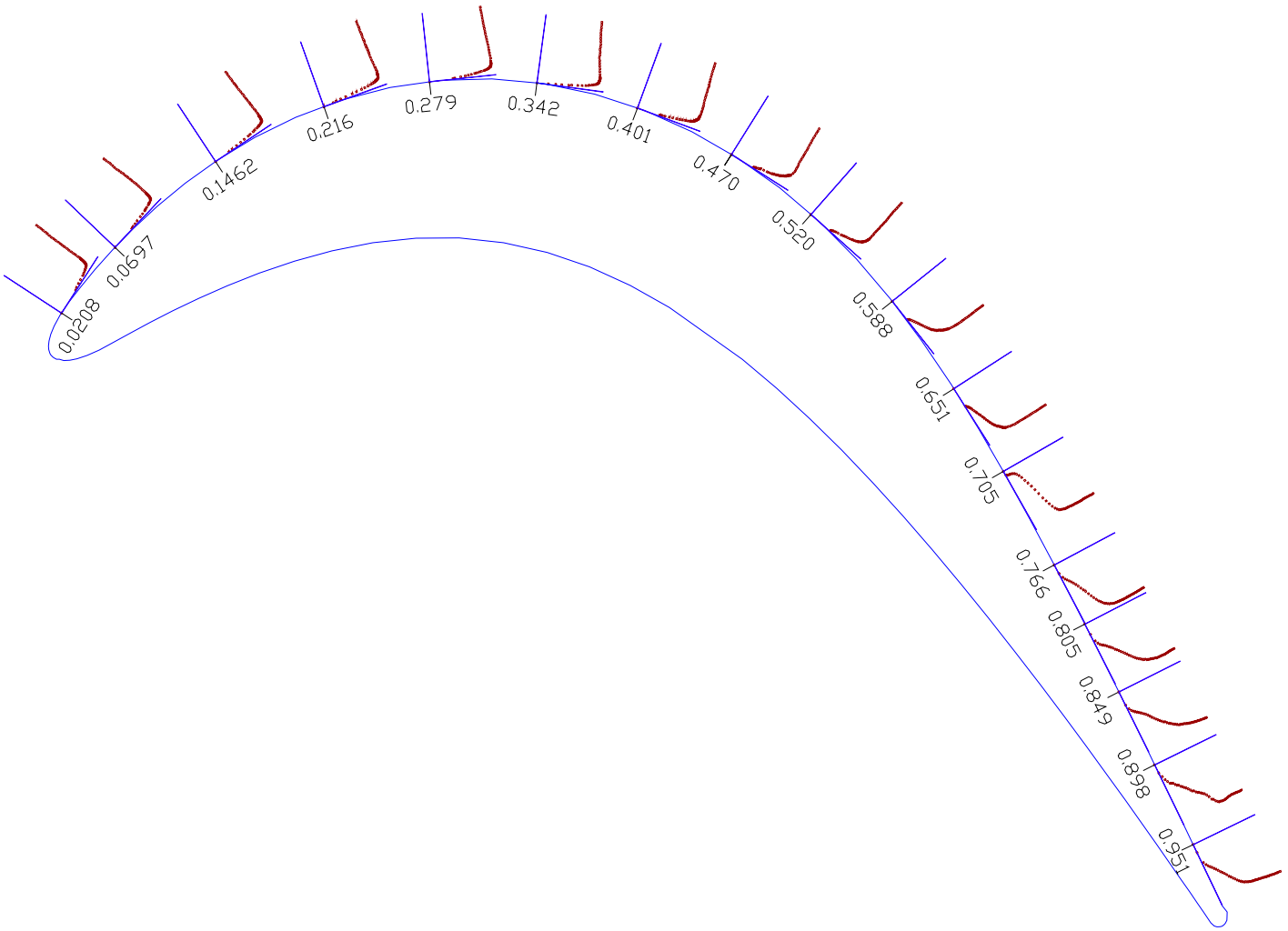

Figure9. 15: Time-averaged velocity profiles along the suction surface of the blade at Ω=1.59, Re=110,000

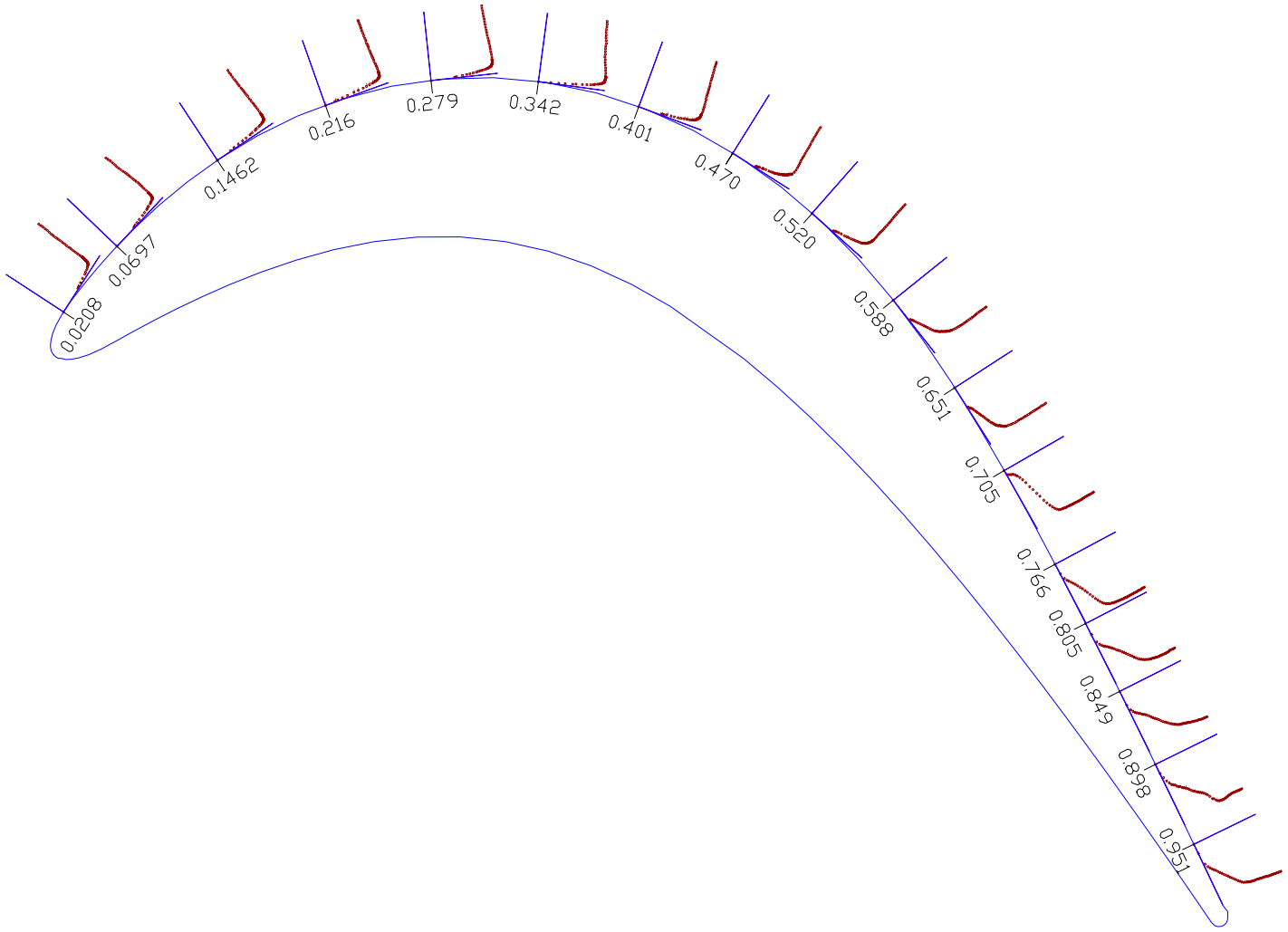

Figure 9.16: Time-averaged velocity profiles along the suction surface of the blade at Ω=3.18, Re=110,000

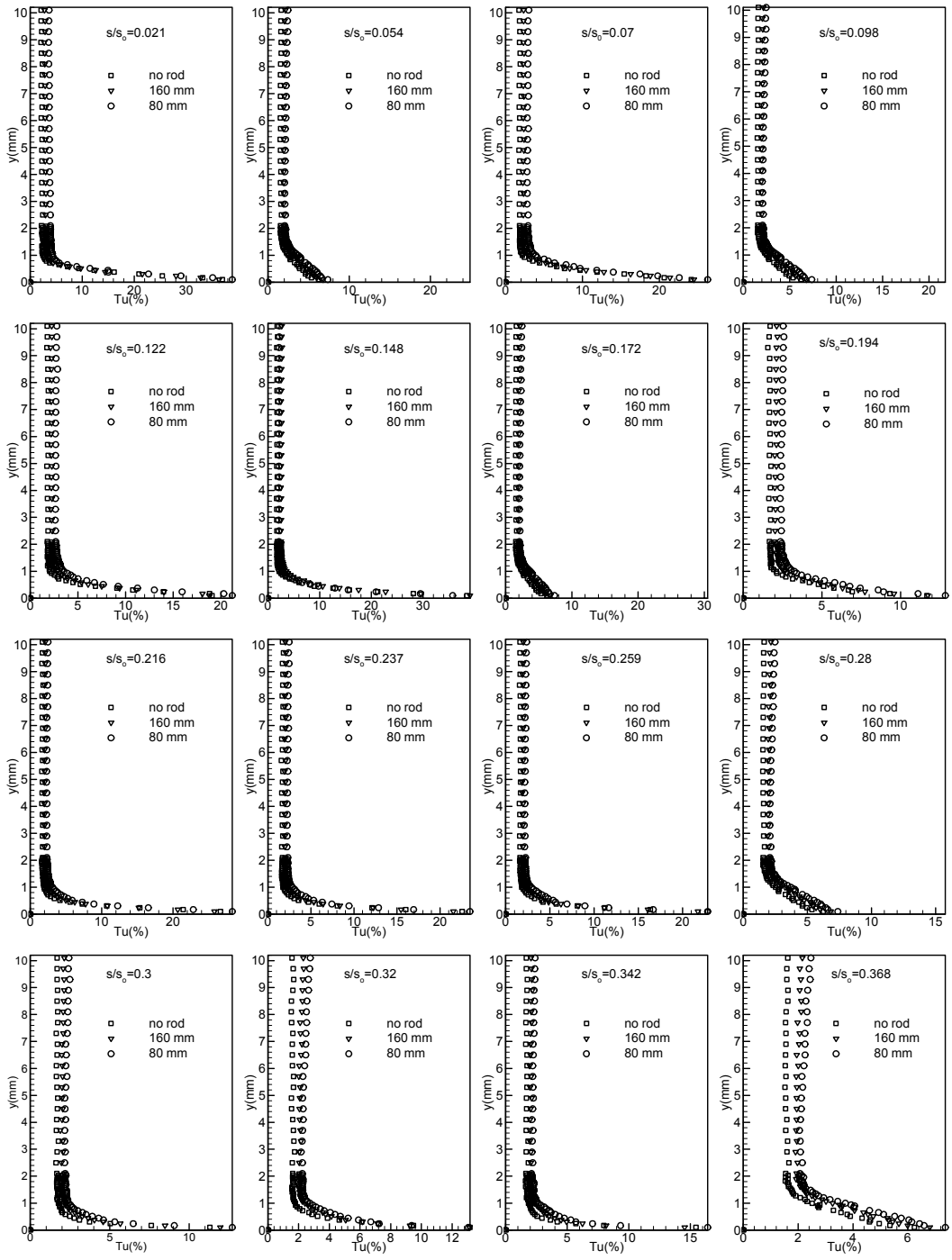

Figure 9.17: Distribution of the time-averaged turbulence intensity along the suction surface for three different reduced frequencies of Ω=0 (S_R=∞), Ω=1.59 (S_R=160 mm), Ω=3.18 (S_R=80 mm) at Re=110,000

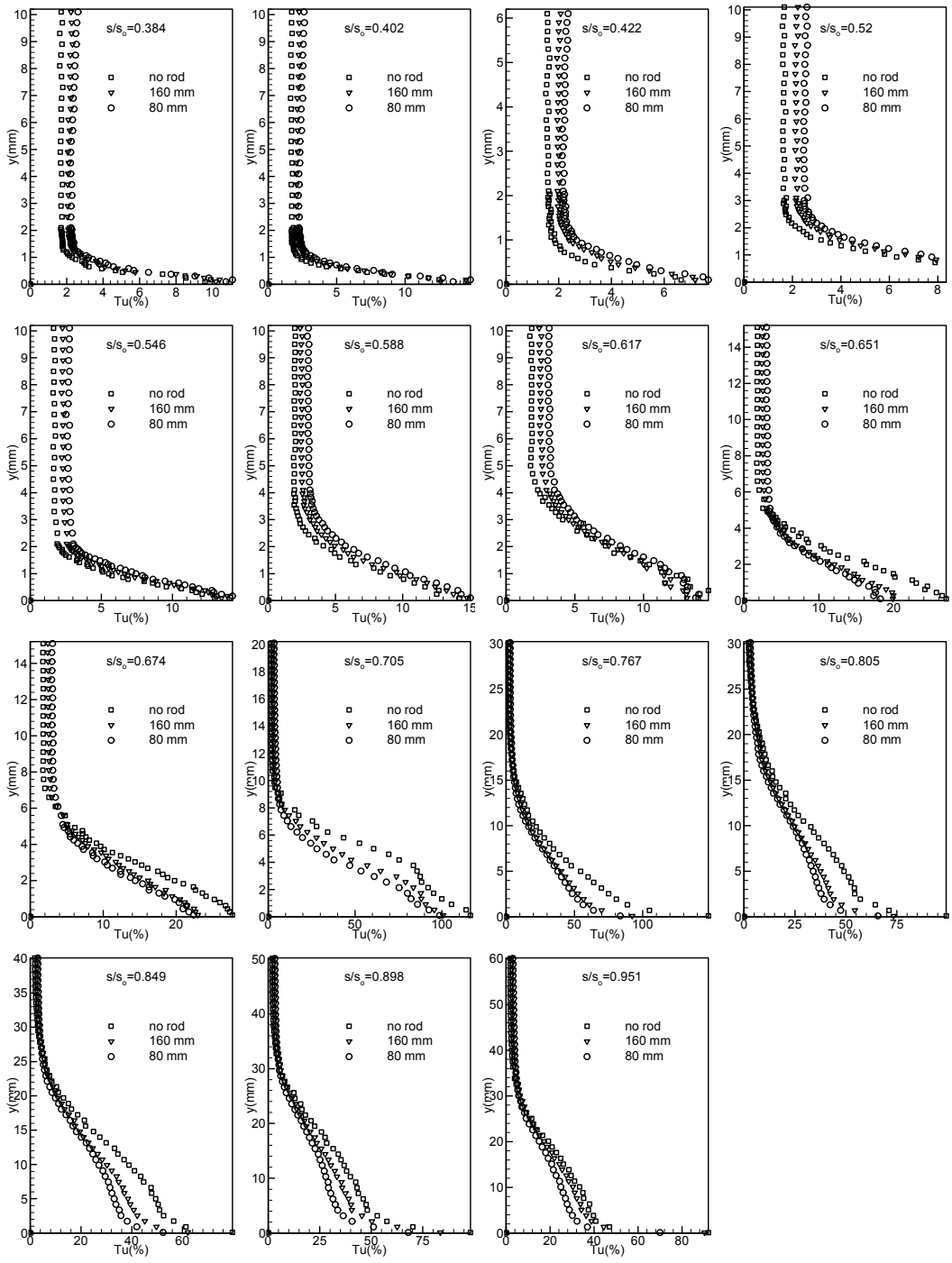

Figure 9.18: Distribution of the time-averaged turbulence intensity along the suction surface for three different reduced frequencies of Ω=0 (S_R=∞), Ω=1.59 (S_R=160 mm), Ω=3.18 (S_R=80 mm) at Re=110,000

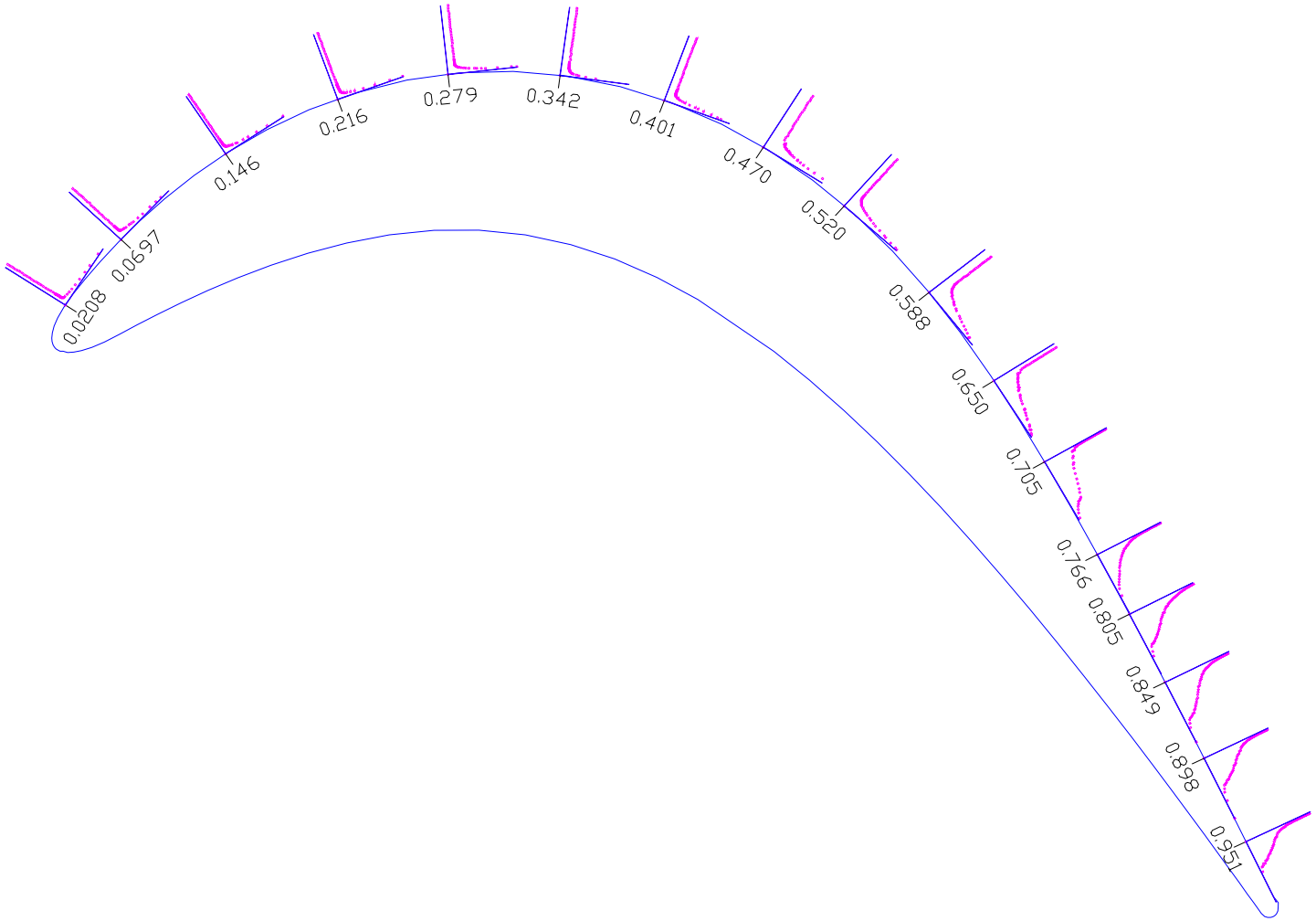

Figure 9.19: Time-averaged turbulence-intensity profiles along the suction surface of the blade at Ω=0, Re=110,000

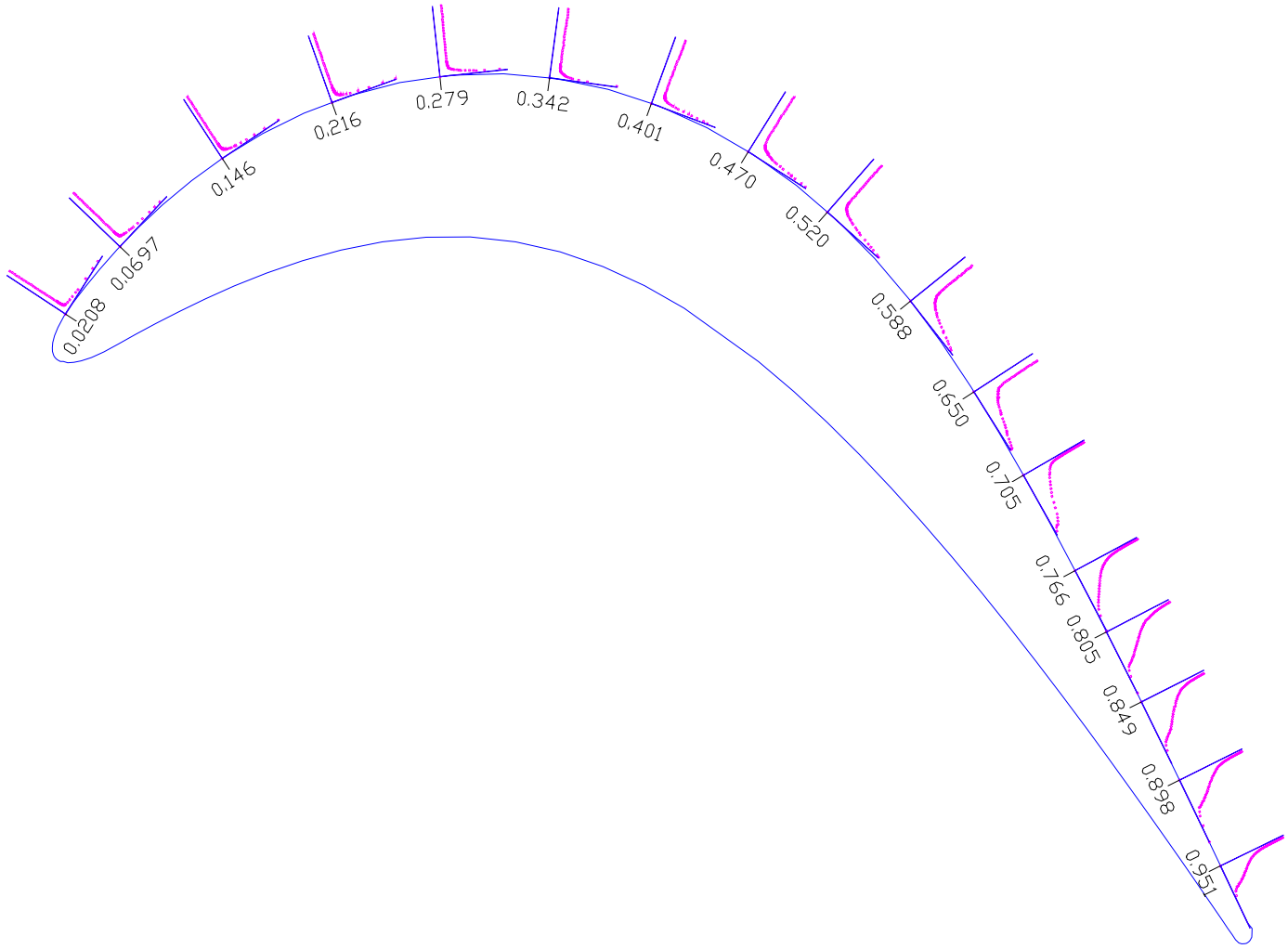

Figure 9.20: Time-averaged turbulence-intensity profiles along the suction surface of the blade at Ω=1.59, Re=110,000

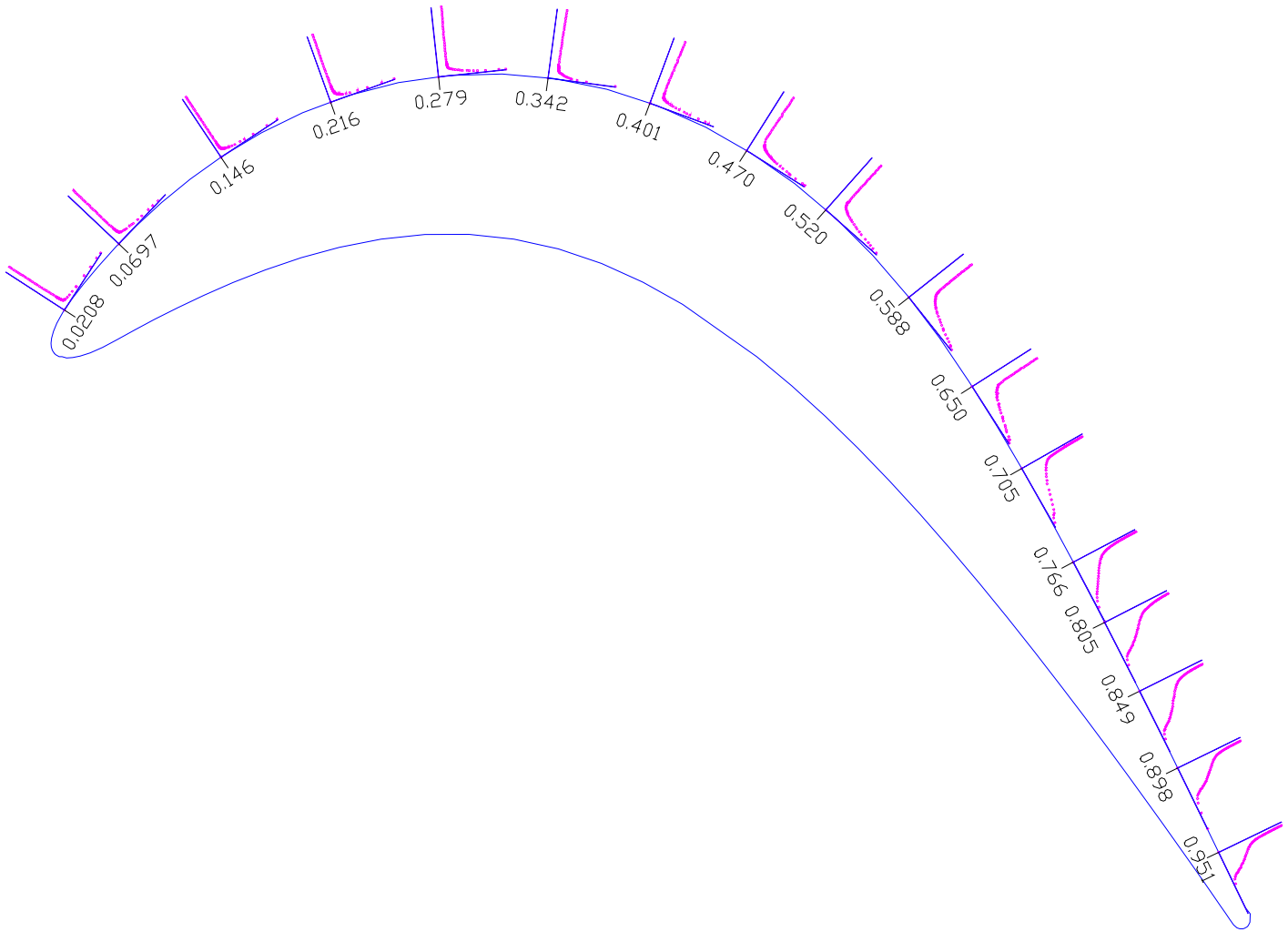

Figure 9.21: Time-averaged turbulence-intensity profiles along the suction surface of the blade at Ω=3.18, Re=110,000

Downstream of the separation zone, where the flow is fully reattached, s/s_o=0.951, the impact of wake on the boundary layer is reduced. This effect is clearly shown in the velocity distribution at s/s_o=0.951 . In accord with the previous investigations by Schobeiri et al. (1997) on a HP-turbine cascade, an increased wake frequency causes turbulence fluctuations to rise inside and outside the boundary layer as shown in Fig 9.17 to 9.21.

9.4 Temporal Behavior of the Separation Zone Under Unsteady Wake Flow

Velocity distributions on the suction surface with time as parameter are plotted in Figure 9.22 and 9.23. The non-dimensional time (t/τ) values are chosen so that they represent the temporal states within one full period of wake passing. As Figures 9.22 (a) to (h) shows, the velocity distributions inside and outside the boundary layer at fixed s/s_0-locations experience moderate to pronounced changes at Ω=1.59. Starting with the initial state of flow being under the influence of free-stream turbulence to the final state where the flow is totally under the influence of wake the boundary layer undergoes a sequence of changes. Figure 9.22 (a) represents the instantaneous velocity distribution upstream of the separation zone followed by Figure 9.22 (b,c,d,e) which represent the velocity distributions inside the separation zone. Figure 9.22 (f) exhibits the instantaneous velocity distribution downstream of the separation zone. Figure 9.22 (g,h) represent the instantaneous velocity distributions, where the flow is fully reattached. In discussing the following results, we simultaneously resort to the wake distribution as well as the turbulence fluctuation results.

Figure 9.22 (a) exhibits the velocity distribution on the suction surface at s/s_0 = 0.402. At this streamwise position, the laminar boundary layer is subjected to a strong negative pressure gradient. The boundary layer distributions at different (t/τ) experience changes in magnitude that reflect the corresponding changes of the impinging periodic wake velocity. It is worth noting, that despite the injection of turbulence kinetic energy by the vortical core of the impinging wakes, no local instantaneous boundary layer transition occurs. This is because of the strong negative pressure gradient that prevents the boundary layer from becoming instantaneously transitional.

Representative for the instantaneous velocity distribution inside the separation zone,

shown in Figure 9.22 (b,c,d,e,f), we discuss the results plotted in Figure 9.22 (e) at s/s_0 = 0.674. During the time interval from t/τ close to 0.5 (1.5, 2.5, etc) to about $t/\tau = 0.75$ (1.75, 2.75 etc) the separation zone is exposed to the wake external flow being under the influence of relatively lower turbulence does not have the capability to suppress the separation zone. Thus, the separation region is clearly shown by the velocity distributions at $t/\tau = 0.5$ and $t/\tau = 0.75$. As the wake passes over the blade at $s/s_0 = 0.674$ introducing high turbulence kinetic energy into the boundary layer, the boundary layer is energized causing the separation zone to partially reduce or disappear. This leads to an instantaneous re-attachment. This time interval corresponds to the case where the flow is completely under the influence of wake and correspondingly the re-attached velocity distribution assumes a turbulent profile characterized by the curves at $t/\tau = 1.0$, $t/\tau = 0.05$, and $t/\tau = 0.25$ shown in Figure 9.22(e). To underline this statement, the steady state velocity distribution at the same streamwise position is also plotted in Figure 9.22 (e) using full circles. It shows clearly the separated nature of the boundary layer which coincides with the instantaneous velocity profile at $t/\tau = 0.5$. Intermediate times reflect the gradual change between the separation and re-attachment as the flow is undergoing the influence of the oncoming wake. Moving to the trailing edge of the separation zone, at $s/s_0 = 0.705$, when the flow is completely under the influence of the wake corresponding to the curves at $t/\tau = 1.0$, $t/\tau = 0.05$, and $t/\tau = 0.25$ shown in Figure 9.22 (f), a partial reduction in boundary layer thickness as a result of wake impingement is visible, however, the separation zone does not seem to disappear. But, the compression of the bubble height is very clear.

Figure 9.22 (g,h) exhibits the velocity distributions on the suction surface respectively at $s/s_0 = 0.849$ and $s/s_0 = 0.898$ where the flow is fully reattached. At this streamwise position, the boundary layer distributions at different (t/τ) experience changes in magnitude that reflect the corresponding changes of the impinging periodic wake velocity. Once, the boundary layer is reattached and the velocity distribution assumes a fully turbulent profile, no major changes are observed.

Figures 9.23 (a) to (h) show, the velocity distributions inside and outside the boundary layer at fixed s/s_0-locations experience moderate to pronounced changes at

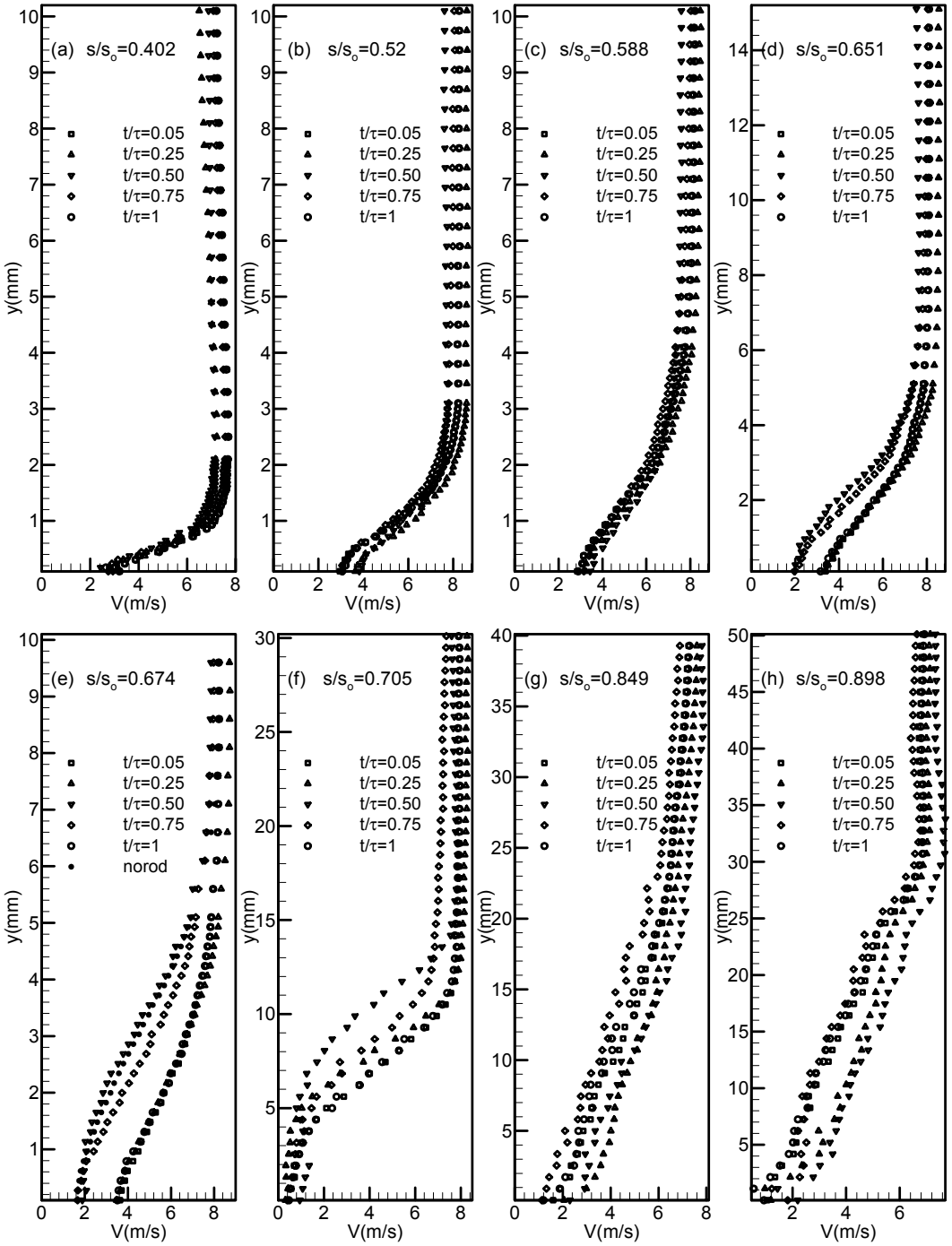

Figure 9.22: Distribution of the ensemble-averaged velocity development along the suction surface for different s/s_o with time t/τ as parameter for Ω=1.59 (S_R=160 mm), Re=110,000

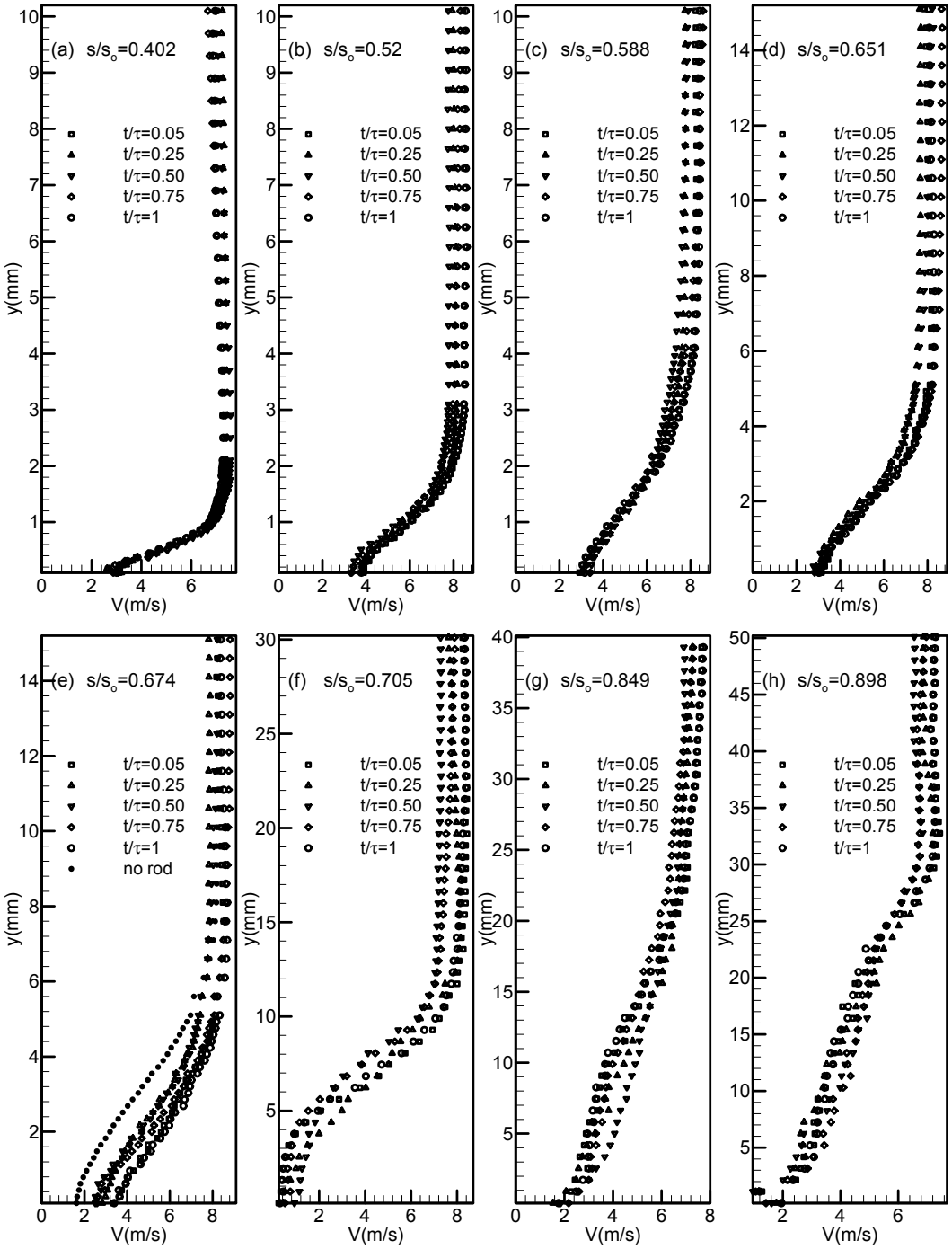

Figure 9.23: Distribution of the ensemble-averaged velocity development along the suction surface for different s/s_o with time t/τ as parameter for Ω=3.18 (S_R= 80 mm), Re=110,000

Ω=3.18. Similar instantaneous velocity distribution is observed when operating at a reduced frequency of Ω=3.18. Compared with Ω=1.59, a stronger suppression of the separation zone is noticed at Ω=3.18. When the wake passing frequency is increased over the blade, it is also increasing high turbulence kinetic energy. Therefore, boundary layer is energized comparatively more than the reduced frequency of Ω=1.59 and it causes the separation zone to partially reduce more.

9.5 Temporal-Spatial Resolution of the Separation Zone

The separation zone can be thought of as a curve that connects the velocity inflection points along the suction surface. Starting with a reduced frequency of Ω = 1.59 (S_R = 160 mm) at s/s_o=0.520 , Figure 9.24 (a) exhibits the start of the separation zone with a lateral extension of about 0.2 mm. The impingement of the periodic wake vortical core with the high turbulence intensity causes a local periodic contraction of the zone in lateral direction. Convecting downstream, the lateral extension increases, thus the contraction appears more pronounced, Figure 9.24 and 9.25 (b,c,d). Substantial contraction occurs toward the trailing edge of the separation zone as shown in Figure 9.26 (e,f). At this streamwise position, the separation zone starts to contract at t/τ=1.25 and 2.25. This points coincides with the streamwise position of the velocity maximum, which exactly correspond to the position of the minimum fluctuation. Similar results are observed when operating at a reduced frequency of Ω=3.18 which is shown in Figure 9.27 to 9.29 (a,b,c,d,e,f) . As we discussed earlier from the other results, increasing the reduced frequency help to reduce more separation boundary layer. As a result, it helps to decrease the losses coming from the large bubble.

Increased passing frequency causes an increase in turbulence kinetic energy. This in turn energizes the boundary layer. This is seen by comparing the velocity distribution for Ω=3.18 and Ω=1.59.

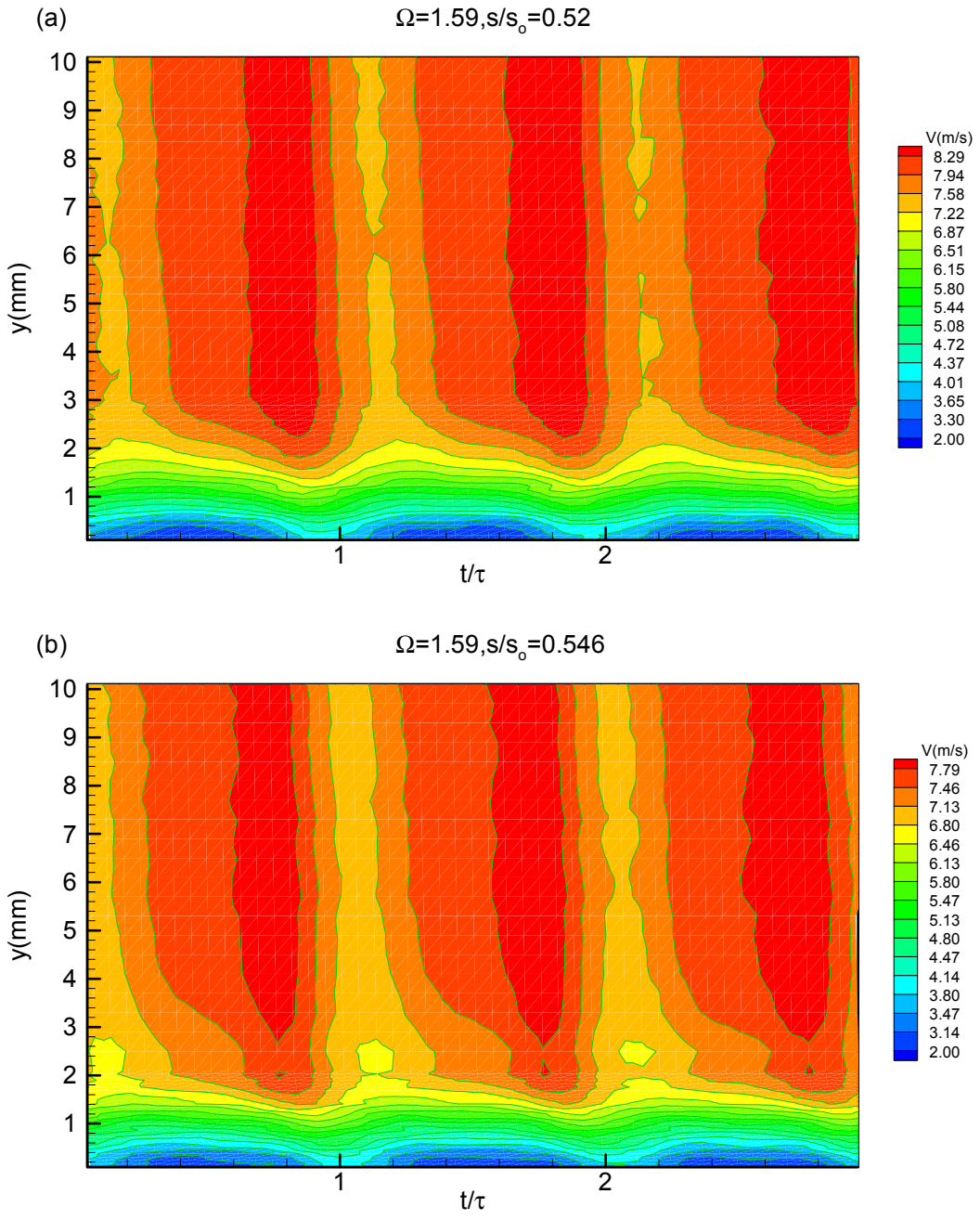

Figure 9.24: Contour plot of ensemble-averaged velocity distribution showing the effect of periodic wakes on the separation zone at Ω=1.59 (S_R=160 mm) at (a) s/s_o=0.52 and (b) s/s_o=0.546, Re=110,000

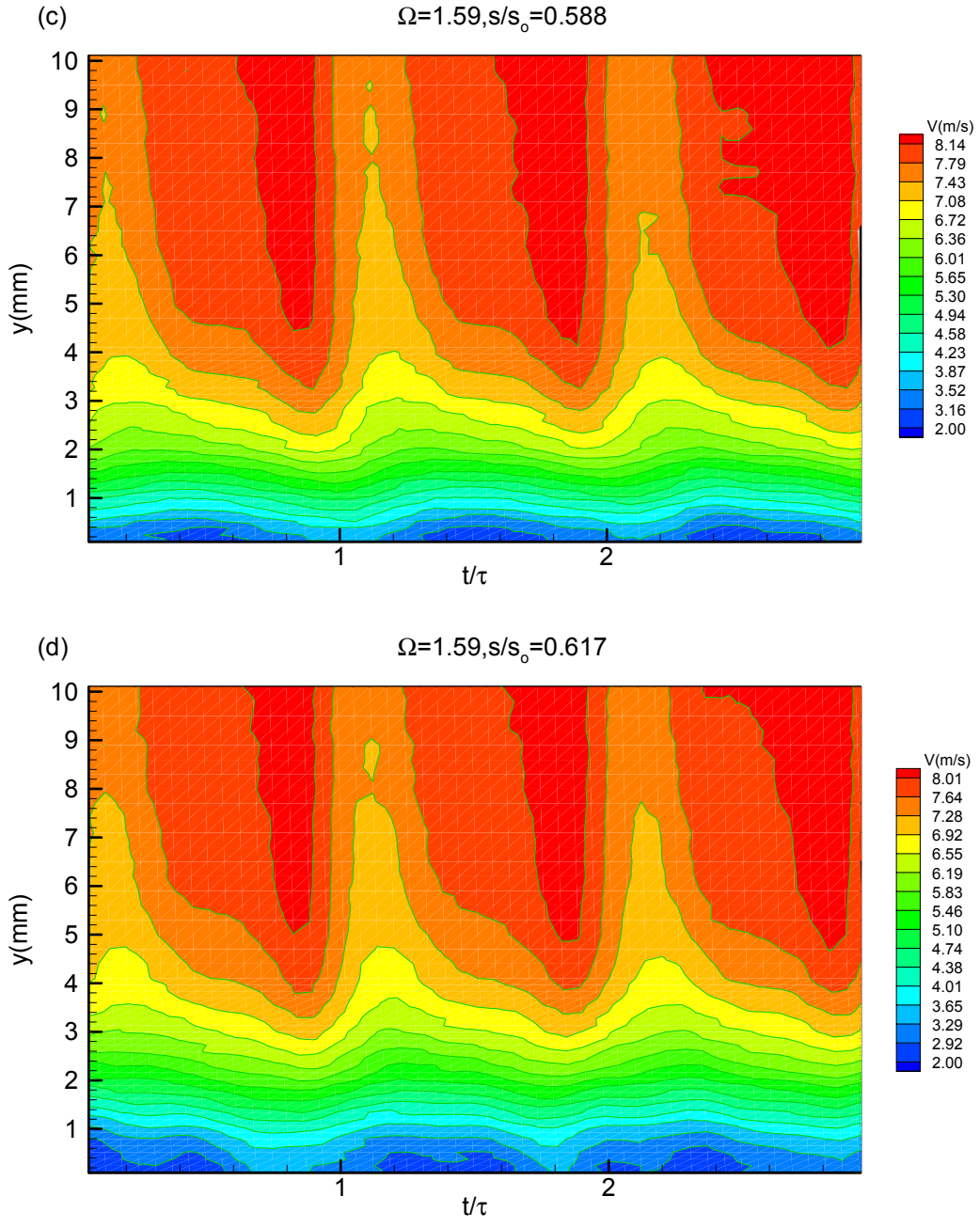

Figure 9.25: Contour plot of ensemble-averaged velocity distribution showing the effect of periodic wakes on the separation zone at Ω=1.59 (S_R=160 mm) at (c) s/s_o=0.588 and (d) s/s_o=0.617, Re=110,000

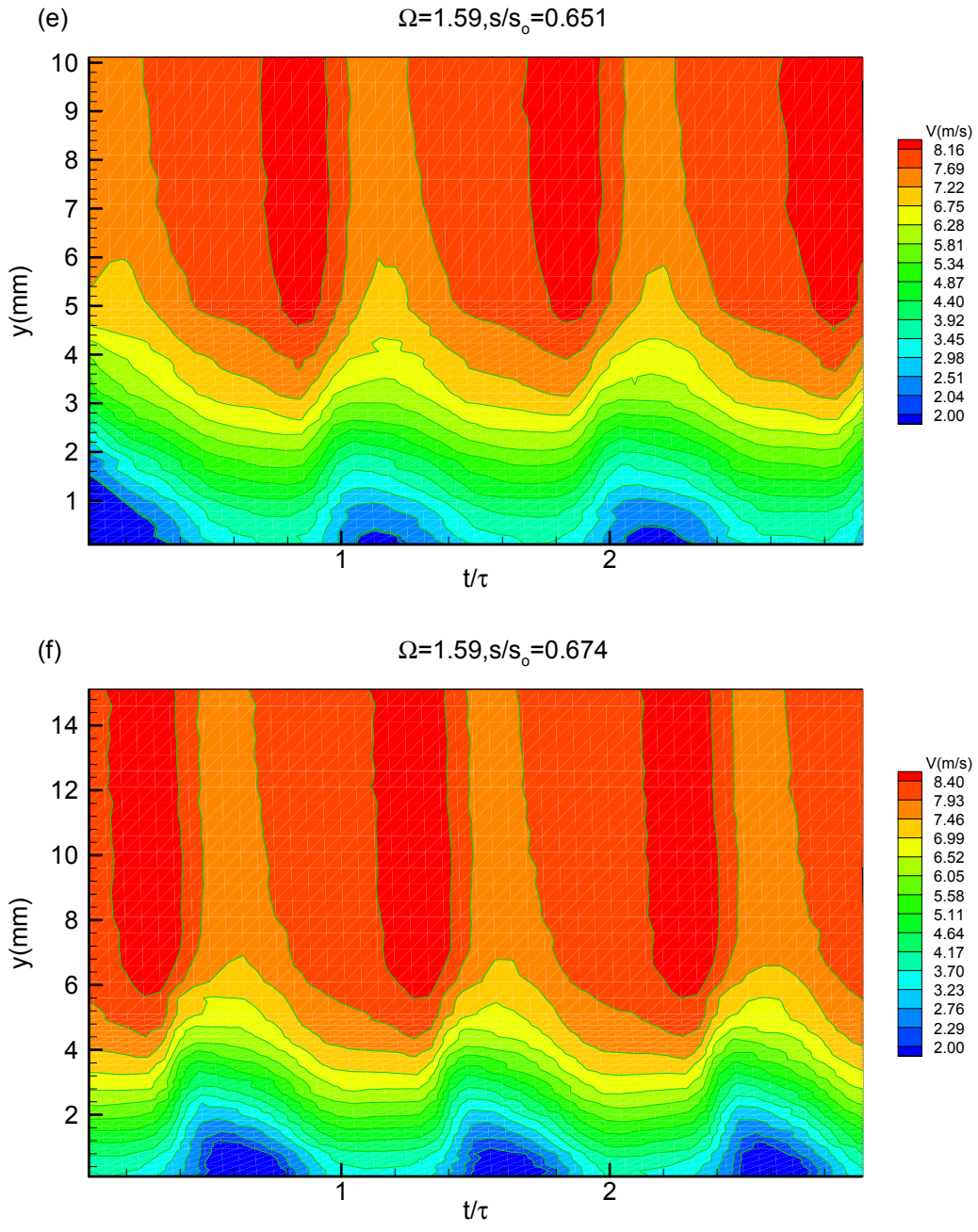

Figure 9.26: Contour plot of ensemble-averaged velocity distribution showing the effect of periodic wakes on the separation zone at Ω=1.59 (S_R=160 mm) at (e) s/s_o=0.651 and (f) s/s_o=0.674, Re=110,000

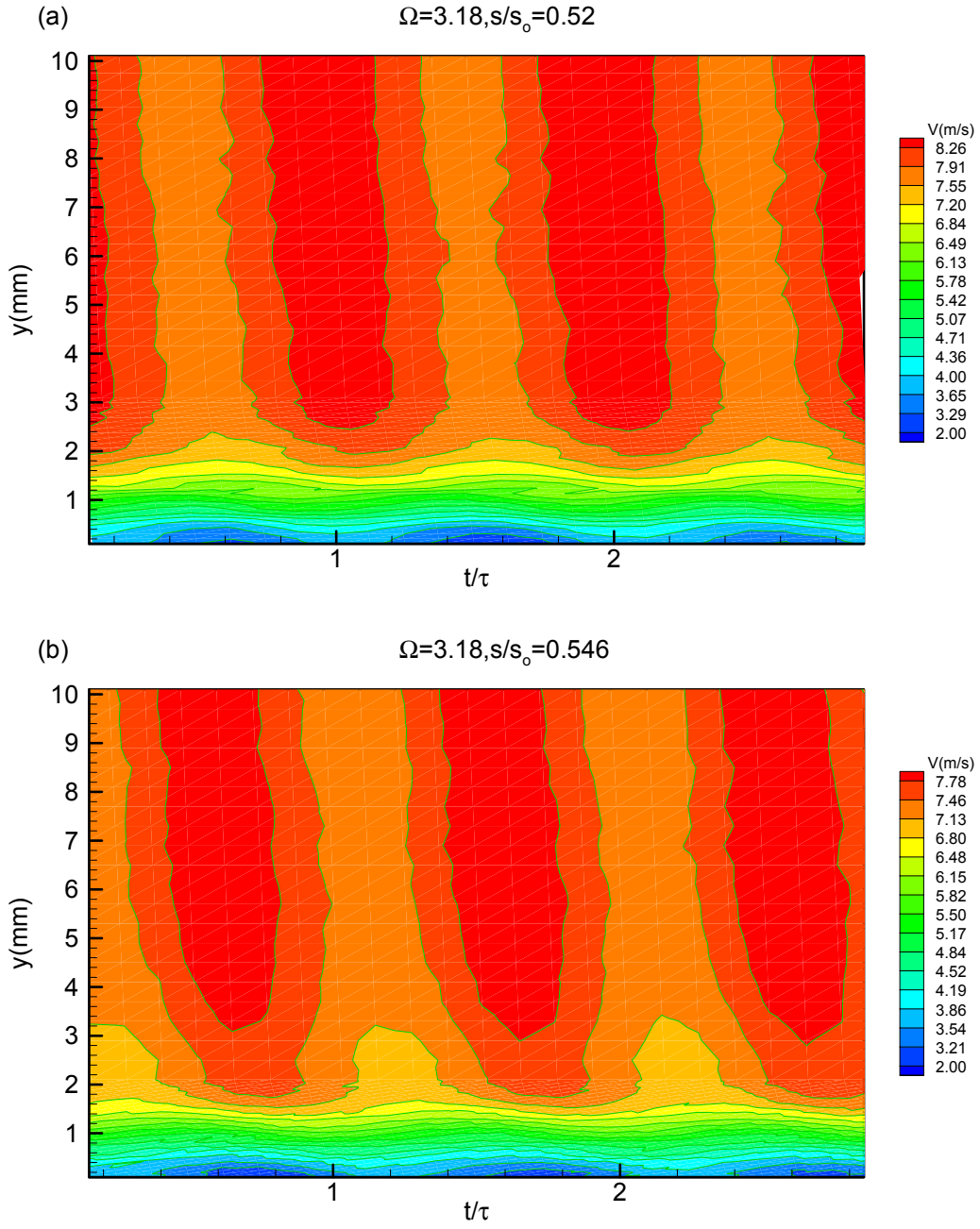

Figure 9.27: Contour plot of ensemble-averaged velocity distribution showing the effect of periodic wakes on the separation zone at Ω=3.18 (S_R=80 mm) at (a) s/s_o=0.52 and (b) s/s_o=0.546, Re=110,000

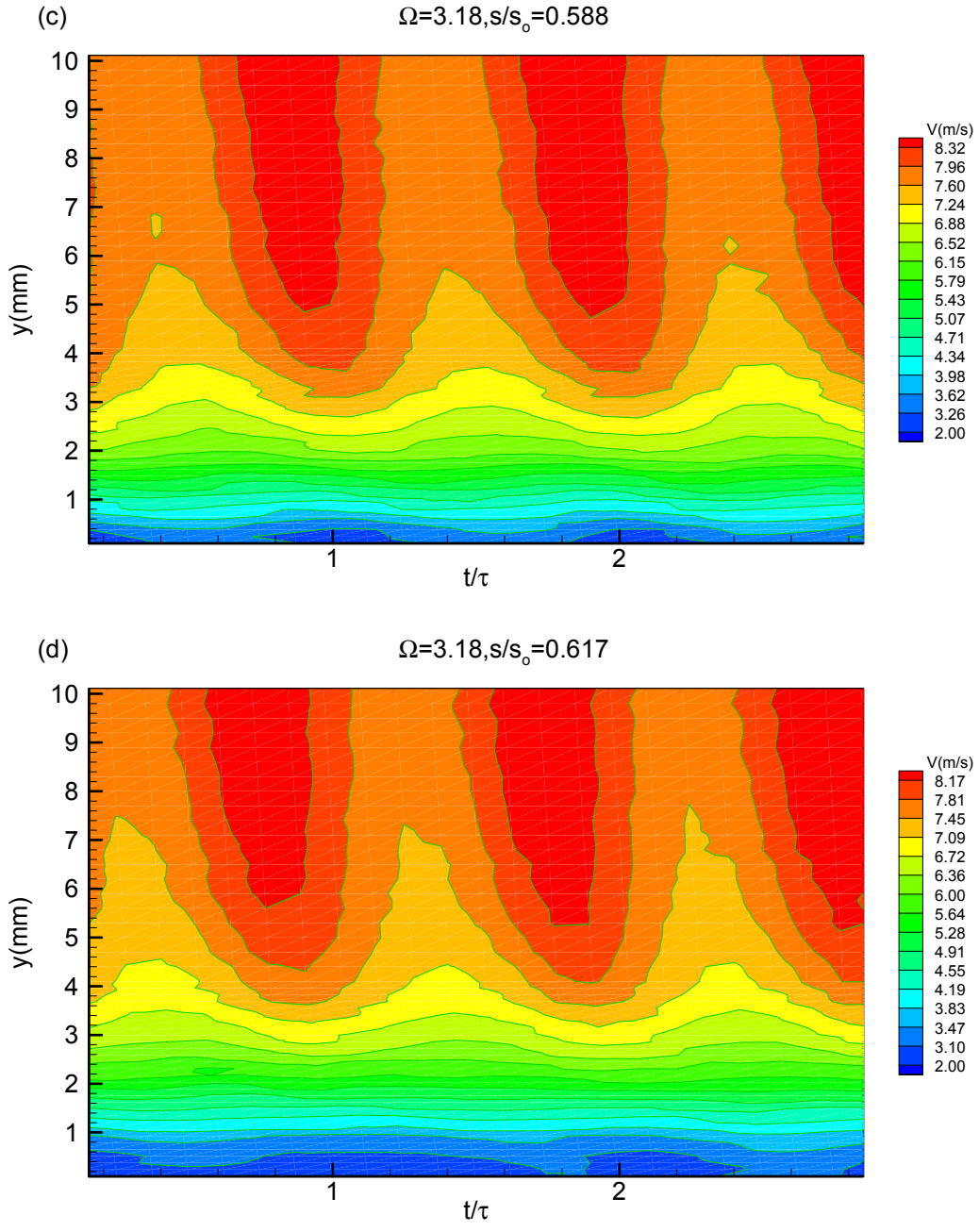

Figure 9.28: Contour plot of ensemble-averaged velocity distribution showing the effect of periodic wakes on the separation zone at Ω=3.18 (S_R=80 mm) at (c) s/s_o=0.588 and (d) s/s_o=0.617, Re=110,000

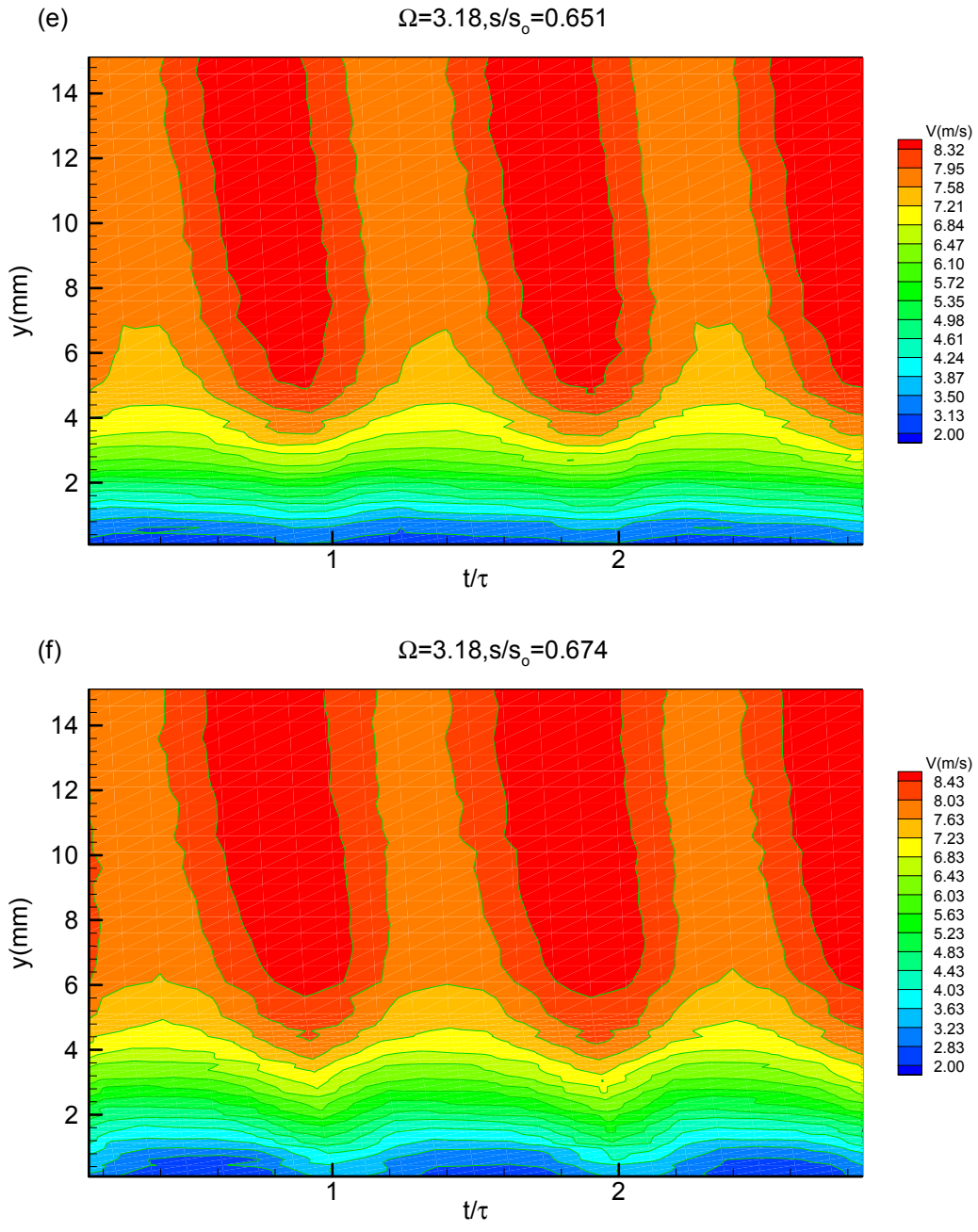

Figure 9.29: Contour plot of ensemble-averaged velocity distribution showing the effect of periodic wakes on the separation zone at Ω=3.18 (S_R=80 mm) at (e) s/s_o=0.651 and (f) s/s_o=0.674, Re=110,000

9.6 Change of Separation Bubble Height Under Unsteady Wake Flow

The shape of the bubble configuration can be identified from the time-averaged velocity distributions. The dividing streamline and the line of inflection points is found by taking second derivative and equating to zero. A similar bubble formation is found for three different frequencies as shown in Figure 9.30. The separation points, where the separation starts and ends, remain the same for the three different frequencies. The separation bubble height decreases with the increase of the reduced frequency. The separation zone is exposed to wake external flow being under the influence of relatively lower turbulence followed by a periodic sequence of wake impingements. When the wake passes over the blade introducing high turbulence kinetic energy into the boundary layer, the boundary layer is energized causing the separation zone to partially reduce. Thus, this flow does not have the capability to completely suppress the separation zone. The main parameters describing the separation bubble for the three test frequencies are presented in Table 9.1.

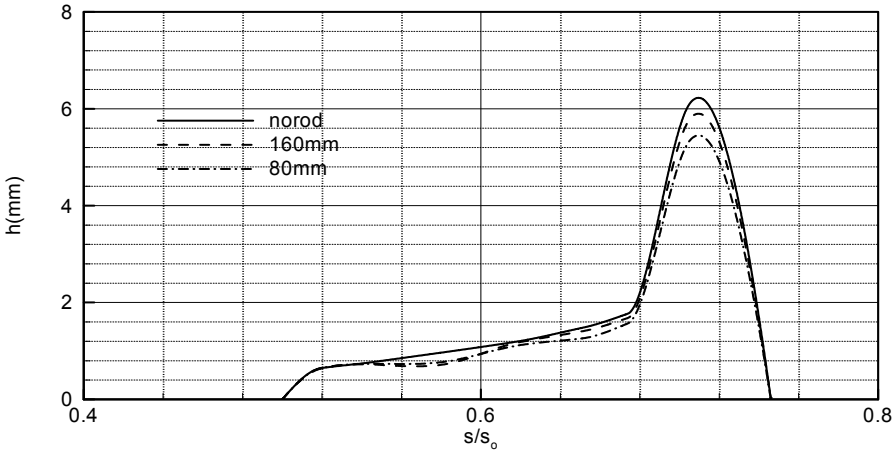

Figure 9.30: Change of separation bubble height under the influence of different reduced frequencies of Ω=0, 1.59, 3.18 (S_R=∞, 160 mm, 80 mm), Re=110,000

Table 9.1: Parameters describing separation bubble for three different frequencies

Parameters	Ω=0.0	Ω=1.59	Ω=3.18
s_s/s_o	0.5	0.5	0.5
s_m/s_o	0.705	0.705	0.705
s_r/s_o	0.746	0.746	0.746
h_m(mm)	6.123	5.818	5.358

9.7 Separation Bubble Behavior Under Wake Propagation

The effect of periodic unsteady wakes on the onset and extent of the separation zone is shown in Figure 9.31 to 9.36 for two different frequencies, namely Ω=1.59 and Ω=3.18. The wake propagation for Ω=1.59 and Ω=3.18 is analyzed and the value of t/τ corresponds to the point in the cycle at which data acquisition system is triggered. During a rod passing period, the wake flow and the separation zone undergo a sequence of flow states which are not noticeably different when the unsteady data are time-averaged. Starting with a reduced frequency of Ω=1.59 at t/τ=0.05, the wake hits the blade leading edge and there is no effect on the separation zone. As the wake convects downstream, at t/τ=0.50, the wake passing over the blade introducing high turbulence kinetic energy into the boundary layer, the energized boundary layer is partially reduced or disappeared. Becalmed regions generated by the turbulent spot produced in the wake paths, were effective in suppressing or reducing the flow separation. At s/s_o=0.705 the core region has slightly moved towards to the leading edge. At t/τ=1, the full effect of the wake on the boundary layer can be seen before another wake appears and the bubble moves back to the original position. Once the wake starts to penetrate the separation zone, the turbulent spot produced in the wake paths caused total suppression at some streamwise positions. Similar results are observed when operating at a reduced frequency of Ω=3.18. The wake frequency exerts no influence on the position of the separation zone.

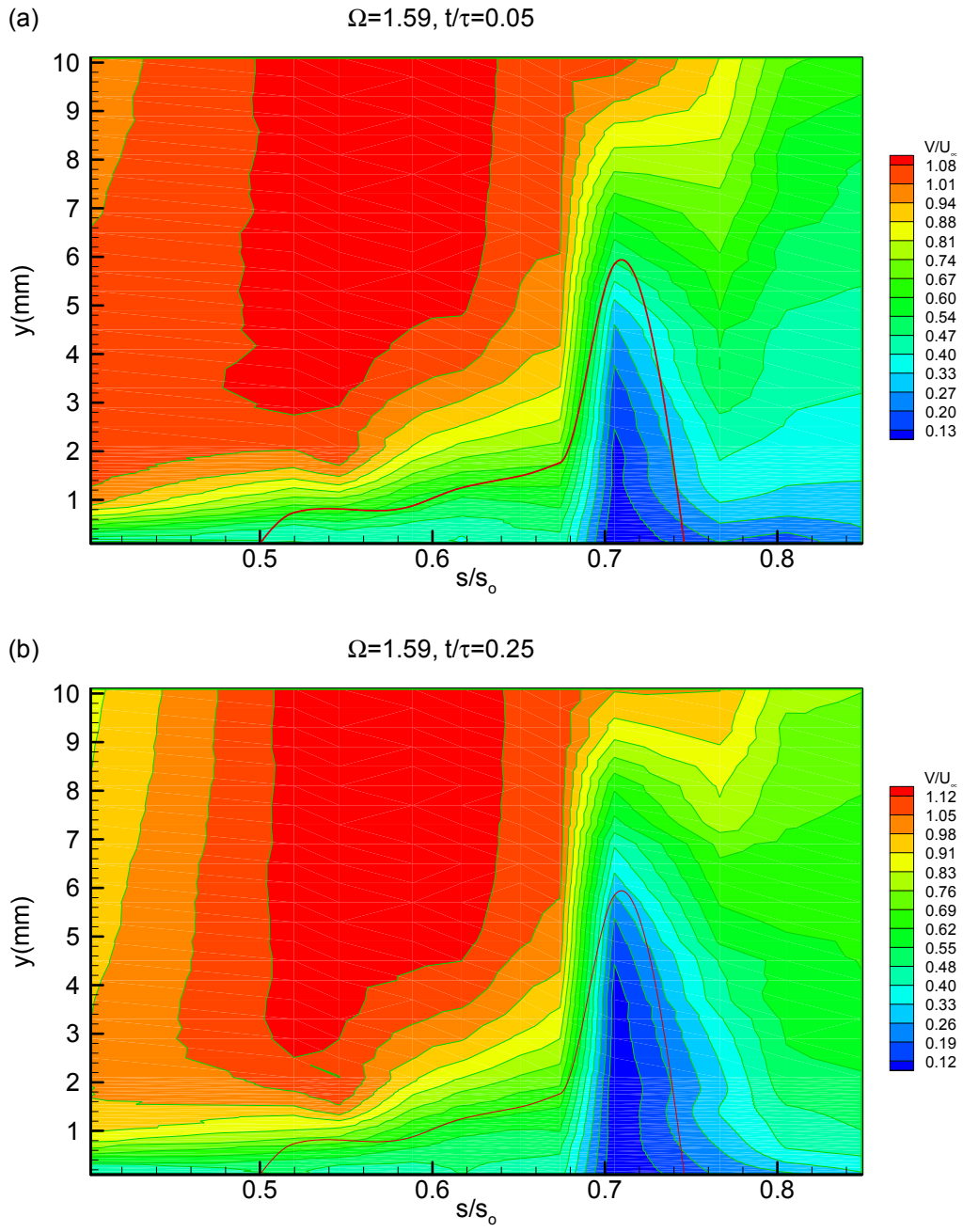

Figure 9.31: Ensemble-averaged velocity contours along the suction surface for different s/s_o with time (a) t/τ=0.05 and (b) t/τ=0.25 as parameter for Ω=1.59 (S_R=160 mm), Re=110,000

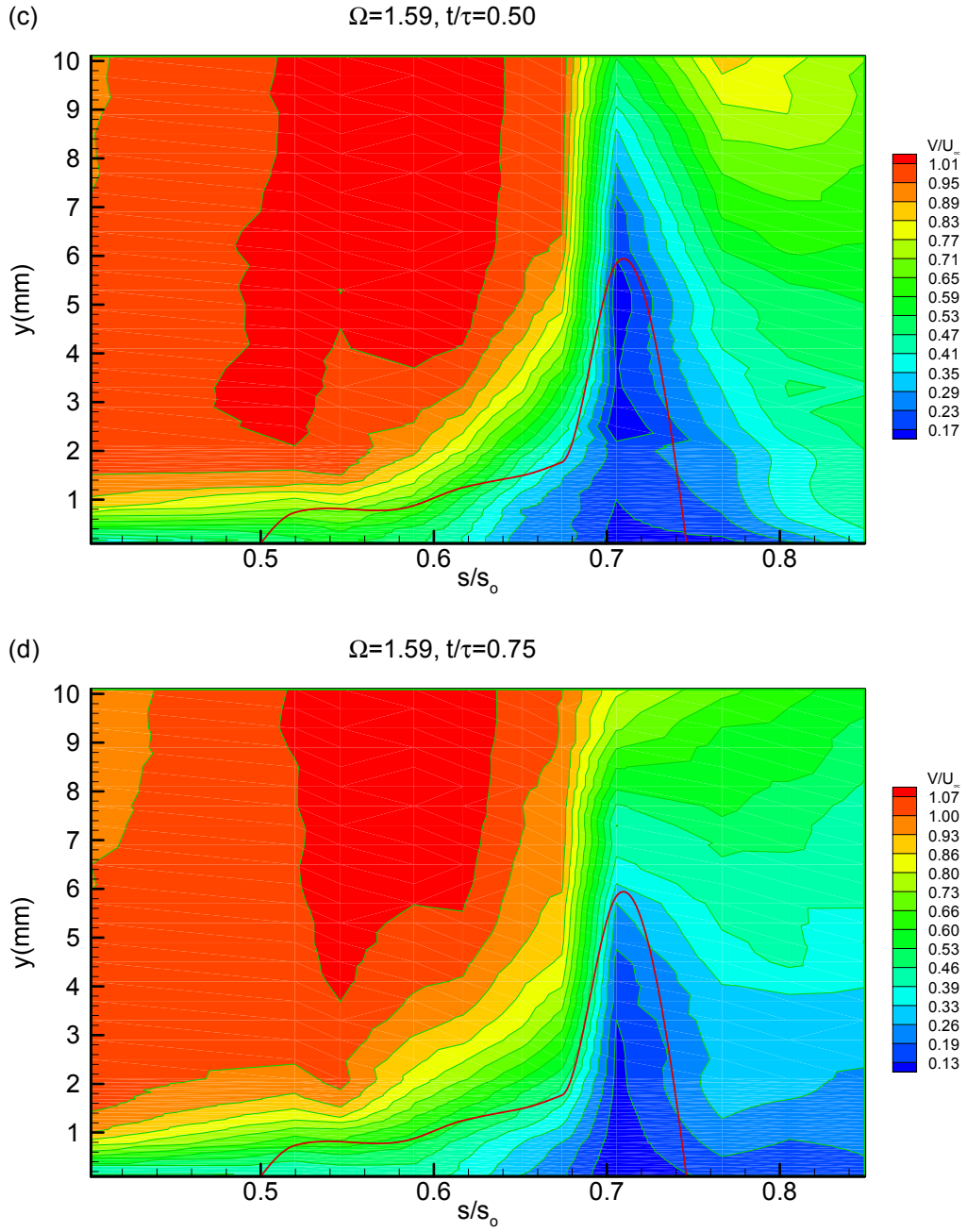

Figure 9.32: Ensemble-averaged velocity contours along the suction surface for different s/s_o with time (c) t/τ=0.50 and (d) t/τ=0.75 as parameter for Ω=1.59 (S_R=160 mm), Re=110,000

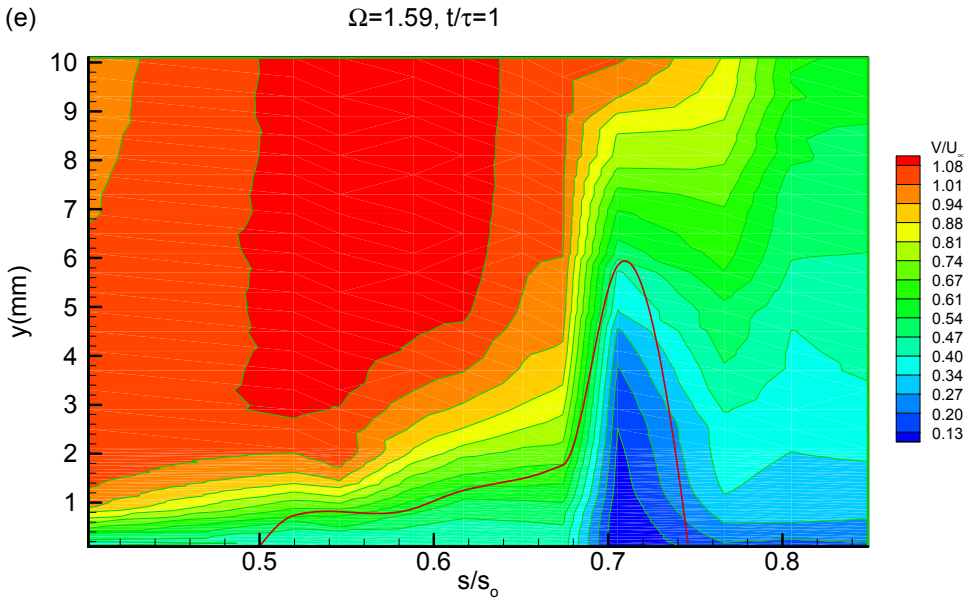

Figure 9.33: Ensemble-averaged velocity contours along the suction surface for different s/s_o with time (e) t/τ=1 as parameter for Ω=1.59 (S_R=160 mm), Re=110,000

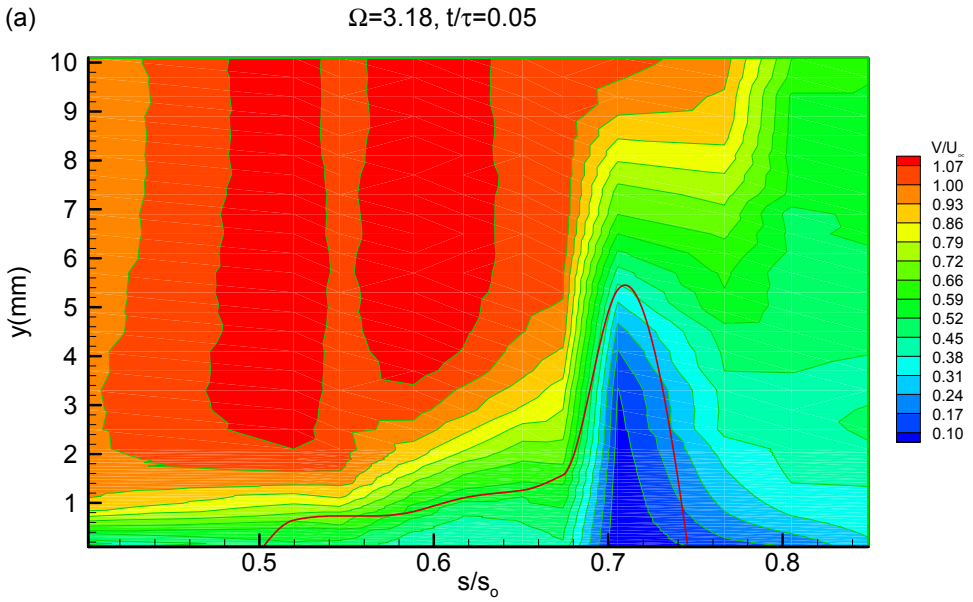

Figure 9.34: Ensemble-averaged velocity contours along the suction surface for different s/s_o with time (a) t/τ=0.05 as parameter for Ω=3.18 (S_R=80 mm), Re=110,000

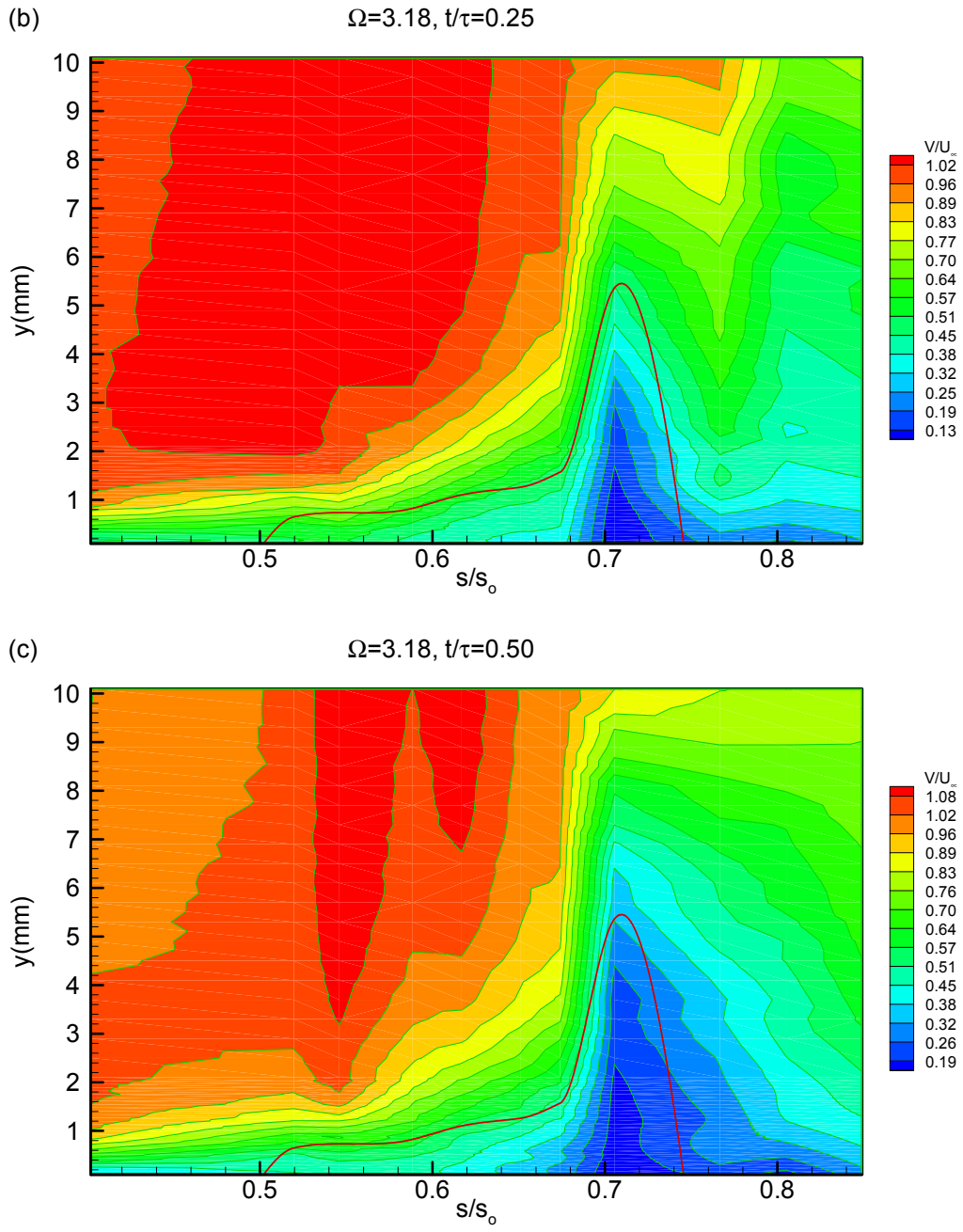

Figure 9.35: Ensemble-averaged velocity contours along the suction surface for different s/s_o with time (b) t/τ=0.25 and (c) t/τ=0.50 as parameter for Ω=3.18 (S_R=80 mm), Re=110,000

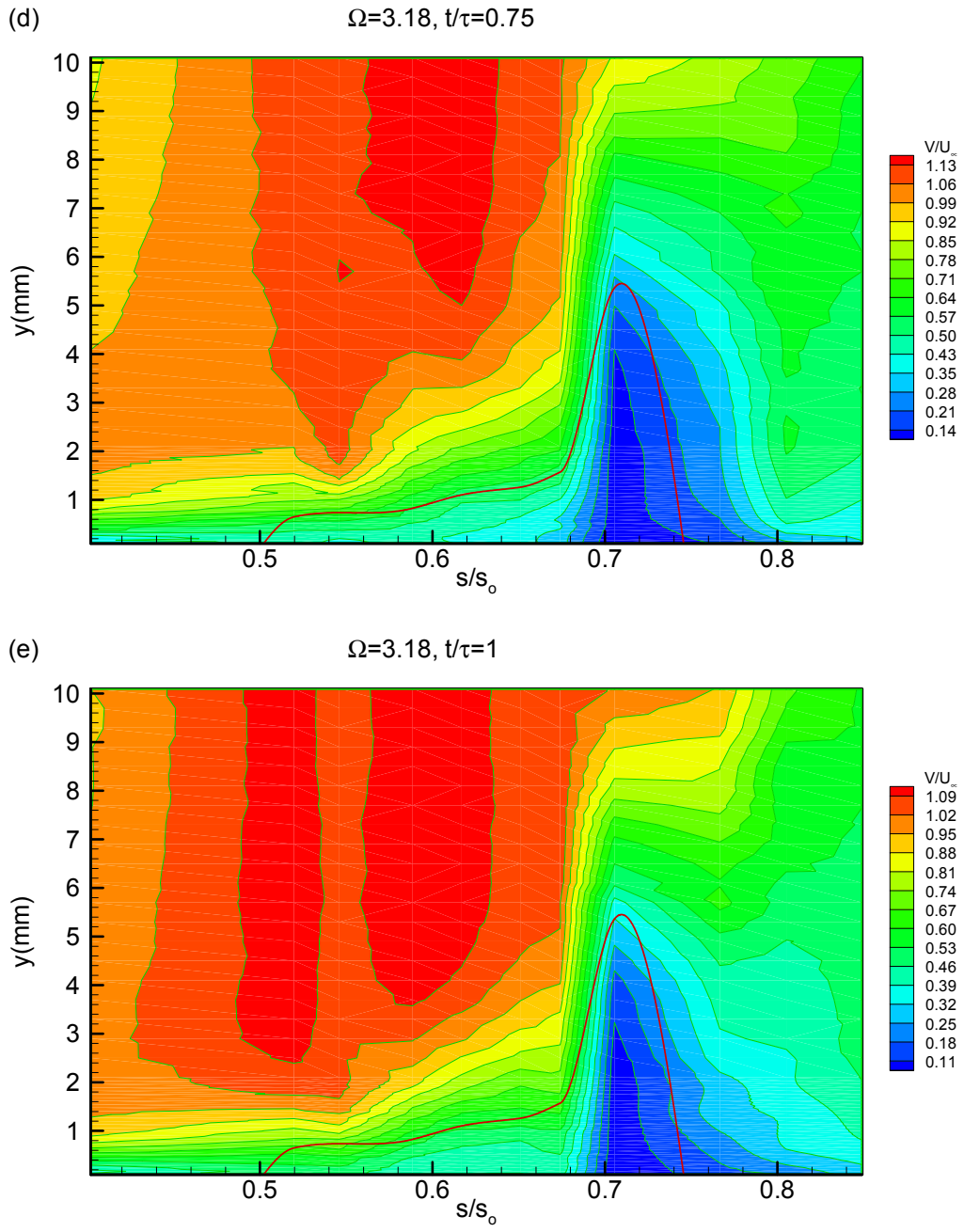

Figure 9.36: Ensemble-averaged velocity contours along the suction surface for different s/s_o with time (d) t/τ=0.75 and (e) t/τ=1 as parameter for Ω=3.18 (S_R=80 mm), Re=110,000

9.8 Contraction, Separation and Regeneration of the Separation Zone

Studying the temporal distribution of the turbulence fluctuations along the longitudinal extension of the separation zone, it becomes clear that, in conjunction with the pressure gradient and periodic wakes, there is another crucial mechanism responsible for the lateral and longitudinal decrease of the separation zone. This mechanism constitutes a combination of the high turbulence fluctuation level and its gradient. It is the temporal gradient of the turbulence fluctuation, or more precisely the fluctuation acceleration $\partial v_{rms}/\partial t$ that provides higher momentum and energy transfer into the boundary layer energizing the separation zone and causing it to partially or entirely disappear.

For better understanding this phenomenon, the wake and the fluctuation velocity is presented in Figure 9.37 for the streamwise position s/s_o=0.651. The fluctuation rms velocity is scaled up with the factor of 4 to make it clear and an arbitrary normal position of y=2.85mm is chosen which is sufficiently above the separation zone for a given normal distance.

Figure 9.37 (a) shows two separate regions: (1) a wake vortical core, occupied by vortices that originate from the moving cylindrical rods and generate high turbulence fluctuations, and (2) a wake external region between the adjacent vortical cores with relatively low turbulence activities. The wake configuration is asymmetric as shown in Figure 9.38. As Figure 9.38 shows, the separation zone starts to contract at t/τ=1.25. This point coincides with the streamwise position of the velocity maximum, which exactly corresponds to the position of the fluctuation minimum, as shown in Figure 9.37 (b). At this point, the fluctuation within the vortical core starts to increase while the velocity continuously decreases. This process continues until the end contraction at t/τ=1.41 has been reached. Thereafter, the separation zone is subjected to a process of intensive exchange of momentum and energy that causes the separation to diminish, as shown in Figure 9.38. The process of separation contraction, suppression, and regeneration is summarized in Figure 9.37 (b). It shows more details of separation contraction and suppression. In this context, it is necessary to subdivide the vortical core shown in Figure 9.37 (b) into four distinct regions, separated by thick dashed lines, as presented in Figure 9.37 (b). Region (a)

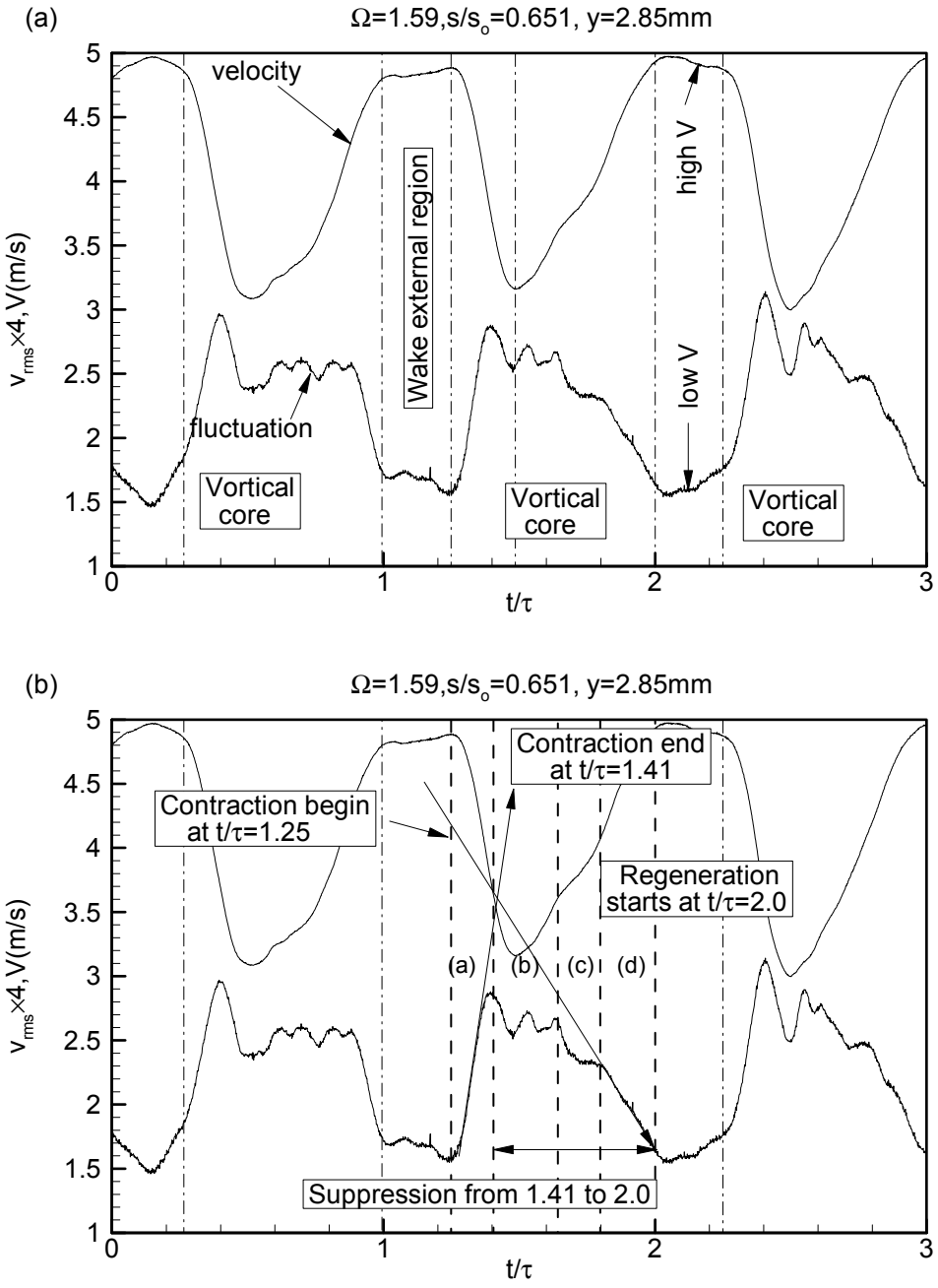

Figure 9.37: Separation, contraction, suppression and regeneration at Re=110,000

is characterized by the initial positive gradient of the fluctuation $\partial v_{rms}/\partial t>0$ marked with an upward arrow. Region (b) represents the substantial part of the vortical core with an intense turbulence activity. Region (c) serves as a transition between region (b) and the relatively calm region (d) characterized by $\partial v_{rms}/\partial t<0$.

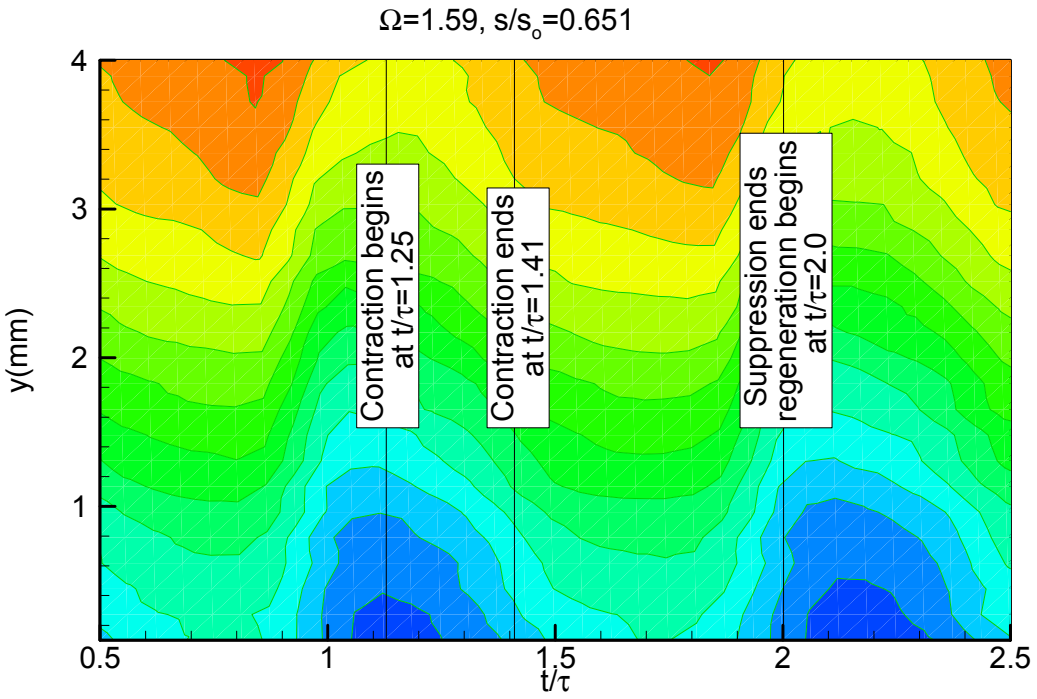

Figure 9.38: Separation zone, definition of contraction begin, contraction end, suppression, and regeneration

For an initial fluctuation gradient $\partial v_{rms}/\partial t>0$, the separation zone begins to contract at t/τ=1.25. This initial gradient is crucial for initiating the contraction process. Once the maximum fluctuation velocity with the temporal gradient $\partial v_{rms}/\partial t=0$ at t/τ=1.41 is reached (region a), the process of energizing the separation zone, thereby preventing its regeneration (region b). Passing the transition region (c), the process of suppression continues until the end of the vortical region at t/τ=2.0 is reached. At this point the external wake region with its low turbulence content arrives causing a regeneration of the separation zone, thus reversing the entire suppression process.

While the existence of higher turbulence fluctuations expressed in terms of higher turbulence intensity is well known for influencing the flow separation, its gradient is crucial in suppressing or preventing the onset and the extension of the separation zone. The fluctuation gradient is an inherent feature of the incoming periodic wake flow and does not exist in a statistically steady flow, that might have high turbulence intensity.

The results clearly indicate that for the particular blade under investigation, one has to do with a massive separation on the suction surface. These observations in comparison with the steady state reference case suggest that, once a massive separation zone is manifested, its size can be significantly reduced by periodic wake impingement, but it cannot be completely removed. The results presented here are valid for blades with a similar pressure distribution discussed earlier. Since the onset and extent of the separation zone is uniquely associated with the pressure gradient, blades can be designed with less local adverse pressure gradient, whose onset can completely be suppressed by impinging wakes.

9.9 Ensemble-Averaged Fluctuation RMS Velocity Distribution

The temporal-spatial contours of the ensemble-averaged fluctuation rms velocity at three different lateral positions for two reduced frequencies are presented in Figures 9.39, 9.40 and 9.41. As shown in Figure 9.39, the wakes periodically disturb the boundary layer with high turbulence intensity cores. As Figure 9.39 (a) shows, three wake passings are visible for Ω=1.59 at a normal distance from the wall of y=1.065m. At s/s_o=0.52, the visibility of the wake is vanished due to separation. As explained earlier the separation zone starts at s/s_o=0.52 and extends up to s/s_o=0.746, thus occupying more than 24% of the suction surface and forming a massive separation. It is perfectly matching the result obtained from the Figure 9.1 and Figure 9.2. At s/s_o=0.746, the fluctuation rms velocity field in Figure 9.39 (a) shows the stagnant fluid region and the area of the rms maximum, which indicates the development of transition and reattachment. Increasing Ω to 3.18 causes an earlier mixing of the impinging wakes that leads to a complete degeneration of the deterministic periodic flow into a stochastic turbulent flow. For the highest reduced frequency of Ω=3.18, the flow is highly turbulent all along the blade surfaces. As it can be

seen from the Figure 9.40 (b), increasing the reduced frequency has not brought major changes, regarding the structure of the separation zone. The laminar boundary layer and the onset of the separation zone remain the same.

As shown in Figure 9.40 at y=10.1 mm and Ω=1.59, the wakes are visible up to s/s_o=0.676. Up to this particular location, the wake convects above the separation zone, however by moving downstream the same lateral position is within the separation zone. This explains the sharp separation line where the wakes are not visible anymore. This implies that the wakes here, is in the previous figure have not penetrated into the separation zone. As shown in Figure 9.41, farther from the wall at y=60.1 and Ω=1.59, the wake passings are visible, because the wake convects outside the boundary layer and the separation zone.

9.10 Boundary Layer Ensemble-Averaged Integral Quantities

The integral parameters, such as momentum thickness and shape factor, are of particular interest to turbine designer, since they provide an accurate first estimation of the quality of the designed blade. The ensemble-averaged distributions of the momentum deficiency thickness and shape factor for the suction surface at different streamwise positions are shown in Figure 9.42 and 9.43 for $\Omega = 1.59$. The momentum thickness values are non-dimensionalized with respect to the value corresponding to the steady case with $\Omega = 0$. The period τ represents the wake-passing period that is specific to the individual wake generating cluster, which is characterized by the Ω - value under investigation. The results are shown for three wake passing periods. The periodic behavior of the ensemble-averaged momentum thickness over the entire suction surface as a result of the embedded periodic wake flow, is clearly visible from Figure 9.42. It represents the momentum thickness behavior at different s/s_0 -locations upstream, within and outside the separation zone. The relative momentum thickness distribution upstream of the separation zone in Figure 9.42 (b) integrally exhibits a slight increase, whereas inside the zone shown in Figure 9.43 (c), a substantial decrease is apparent. At the immediate vicinity of the trailing edge, $s/s_0 = 0.705$ close to re-attachment, Figure 9.43 (d), the momentum thickness experiences a noticeable increase, which by convecting downstream decreases again and approaches the integral

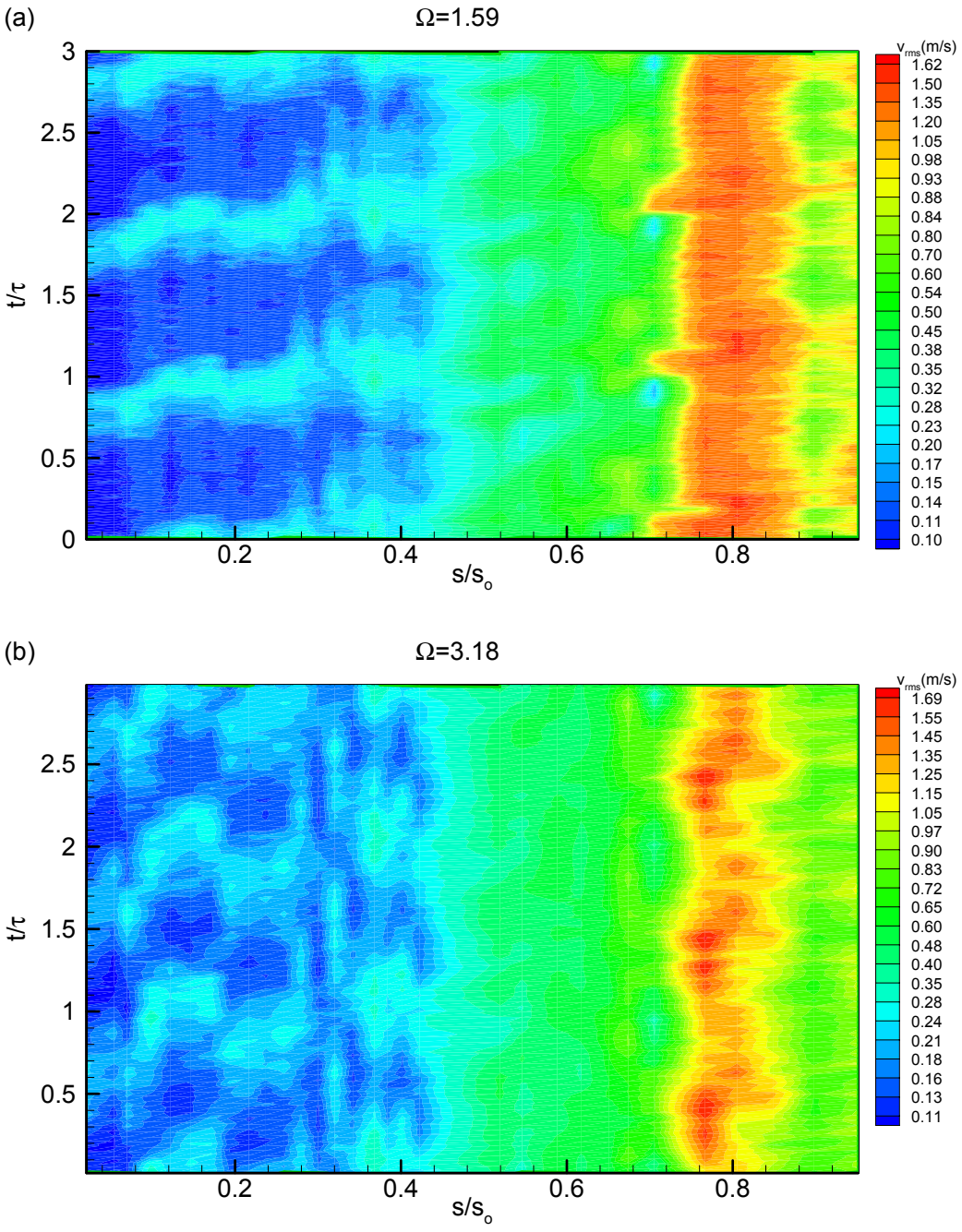

Figure 9.39: Ensemble-averaged rms fluctuation velocity in the temporal-spatial domain at y=1.065 mm for (a) Ω=1.59 (S_R=160 mm), and (b) 3.18 (S_R=80 mm), Re=110,000

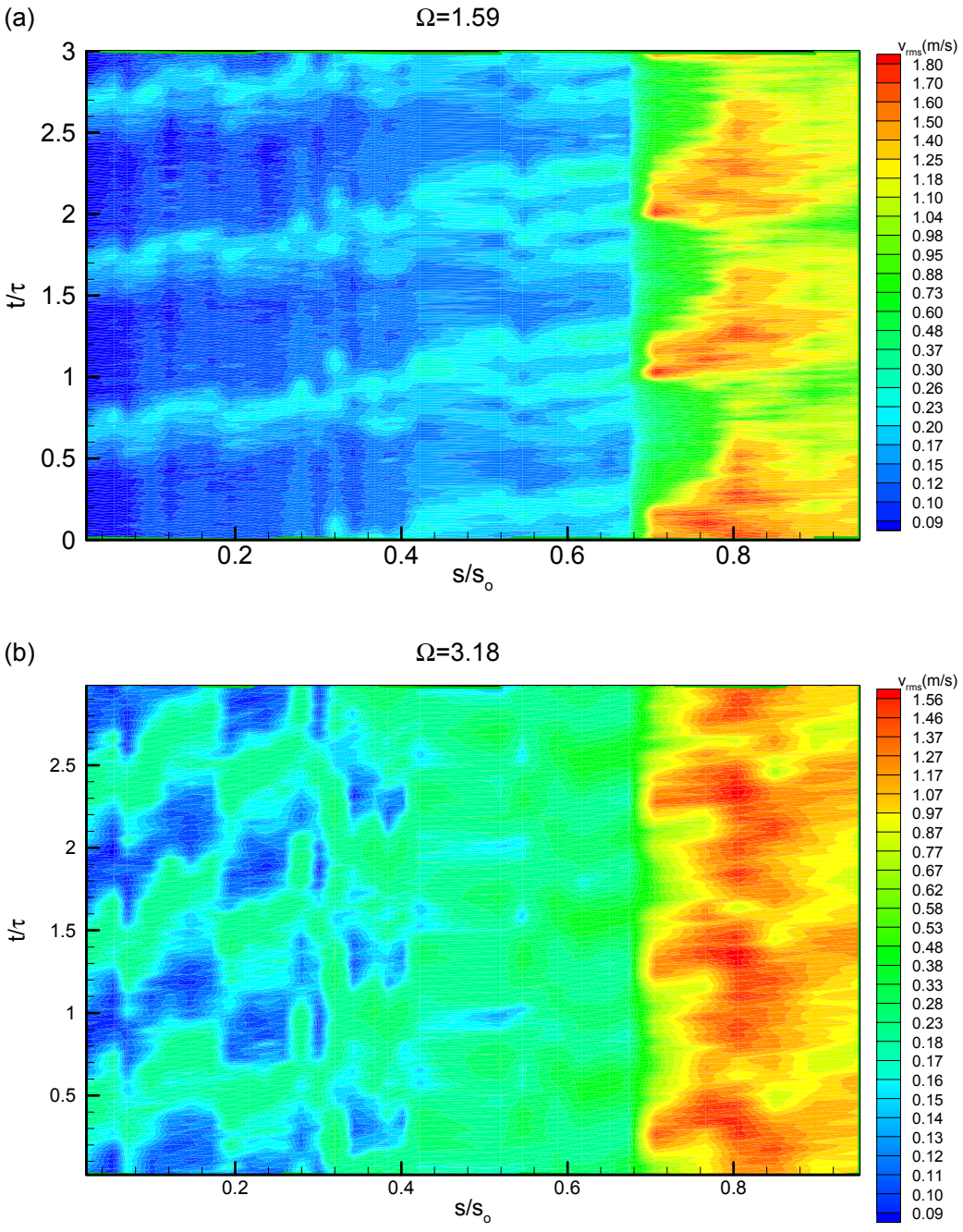

Figure 9.40: Ensemble-averaged rms fluctuation velocity in the temporal-spatial domain at y=10.1 mm for (a) Ω=1.59 (S_R=160 mm), and (b) 3.18 (S_R=80 mm), Re=110,000

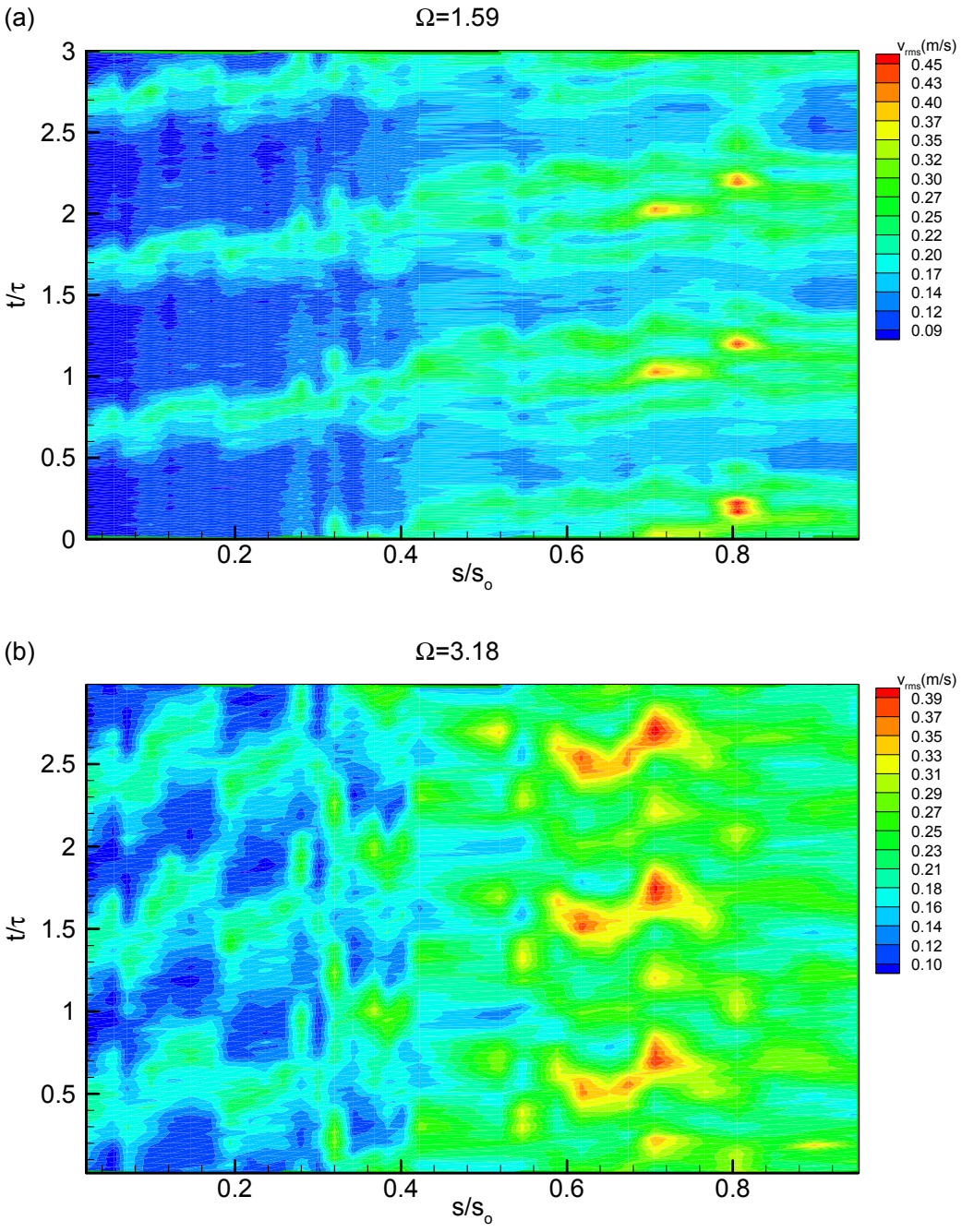

Figure 9.41: Ensemble-averaged rms fluctuation velocity in the temporal-spatial domain at y=60.1 mm for (a) Ω=1.59 (S_R=160 mm), and (b) 3.18 (S_R=80 mm), Re=110,000

values that are close to the steady state case.

The ensemble averaged relative shape factor H_{12} -distributions on the suction surface at the same streamwise locations are plotted in Figure 9.44 and 9.45 (a,b,c,d). Upstream of the separation zone, Figure 9.44 (b) they experience a similar periodic change with an average slightly close the steady case. Moving into the separation zone, Figure 9.44 and 9.45 (b,c), each streamwise location presents its own form parameter that is specific to the velocity distribution. Similar results is observed when operating at a reduced frequency of Ω=3.18 which is shown in Figure 9.46 to 9.49.

9.11 Boundary Layer Time-Averaged Integral Quantities

The time-averaged distribution of the boundary layer thickness, displacement thickness, the momentum deficiency thickness and the shape factor for the suction surface are shown in Figure 9.50 and 9.51. The momentum thickness values for three different reduced frequencies remain the same along the blade and do not reveal any unusual behavior within the separation bubble between the start s_s and reattachment s_r. The initial growth of the boundary layer displacement thickness and the shape factor, is comparatively small up to the maximum displacement location. As shown in Figures 9.50 and 9.51, both the boundary layer displacement thickness and shape factor are decreasing in the separation zone and after the reattachment as the reduced wake frequency is increased. This results clearly show the impact of the unsteady wake flow on the boundary layer parameters and hence on the profile loss coefficient and efficiency. Unsteady wake flow cause a reduction of the losses due to suppressed or reduced separated boundary layer. All of this results show that the steady state data cannot be transformed to the unsteady turbine design technology without modification.

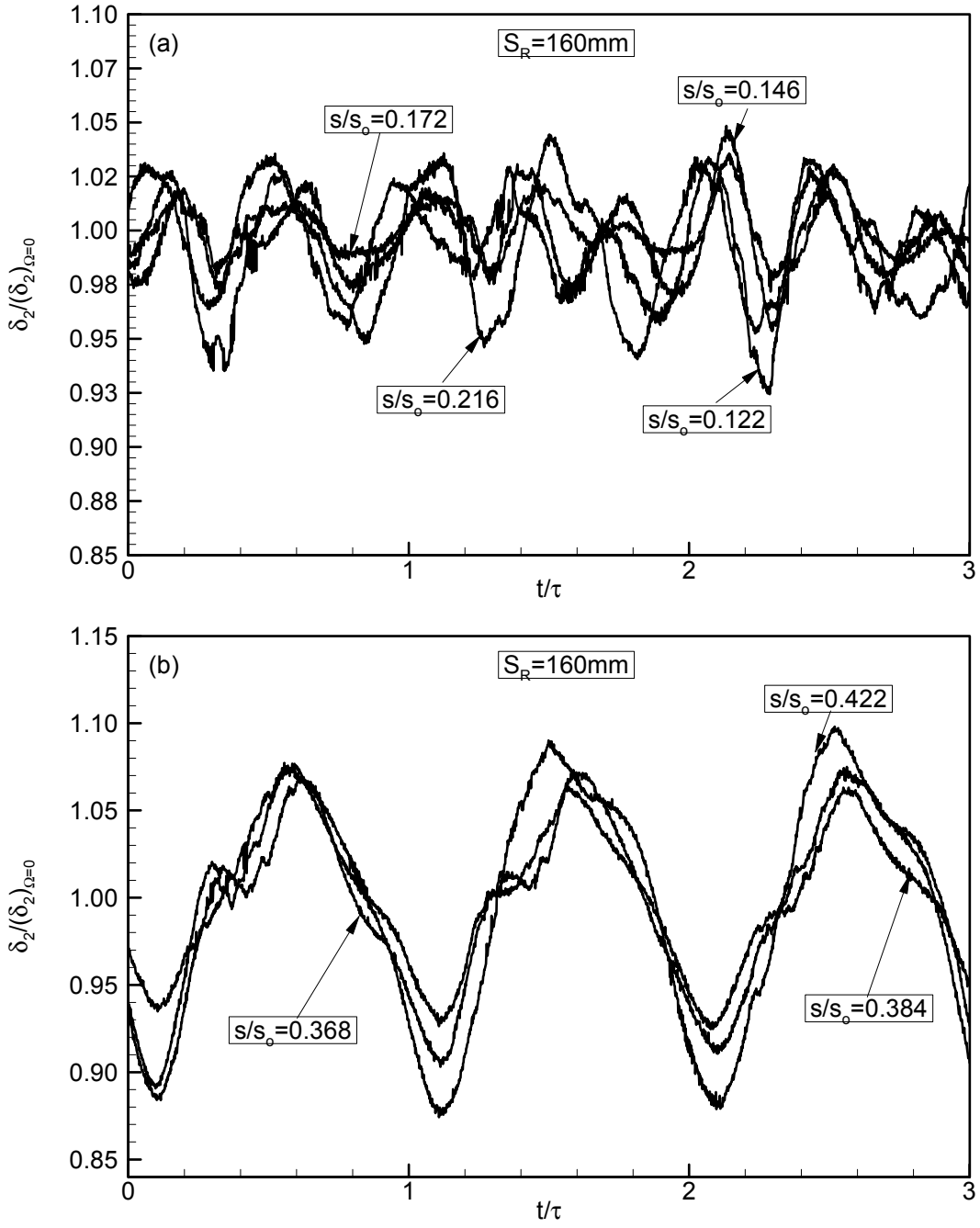

Figure 9.42: (a) and (b):Ensemble-averaged relative momentum thickness distribution along the suction surface for different streamwise positions at Ω=1.59 (S_R=160 mm), Re=110,000

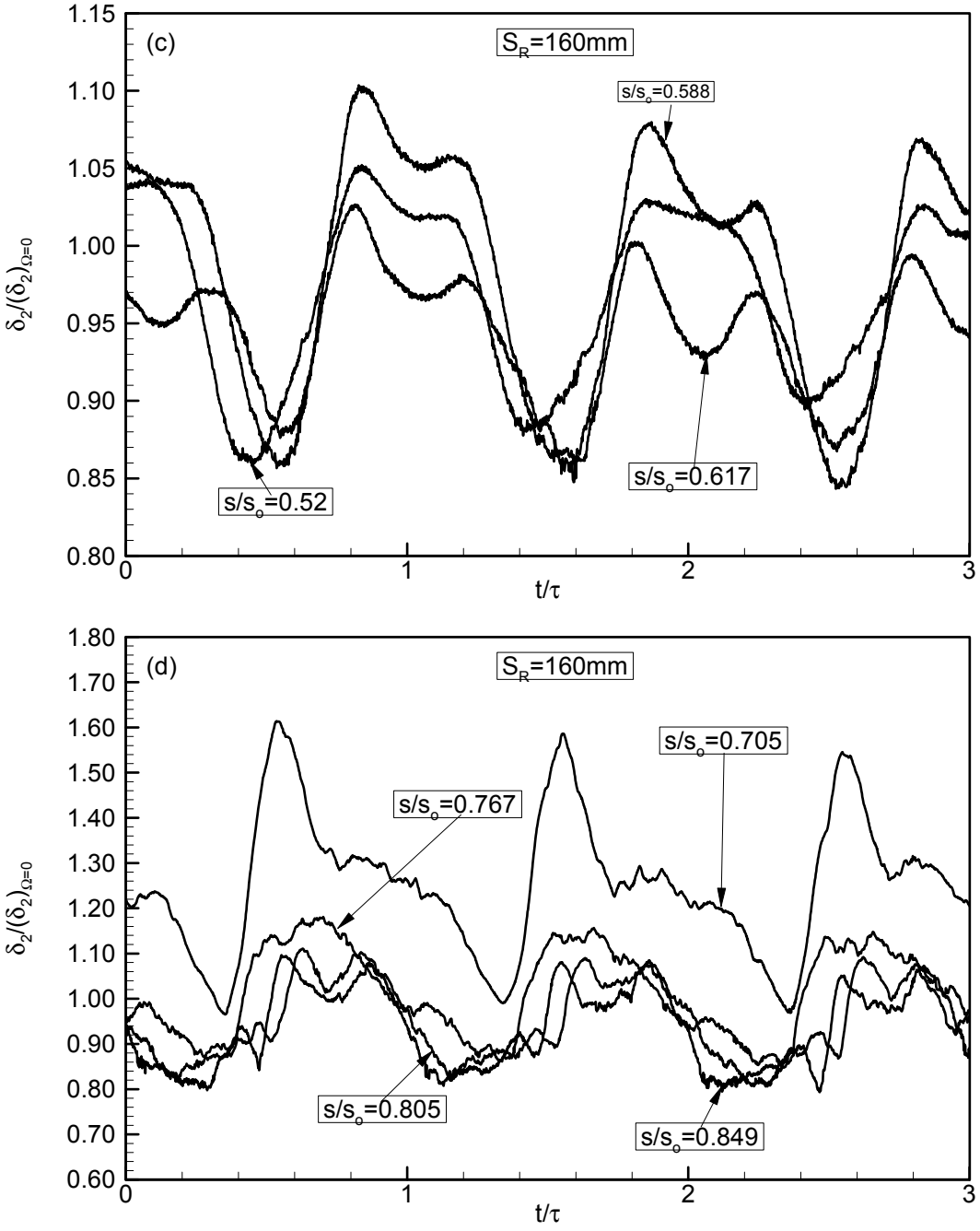

Figure 9.43: (c) and (d):Ensemble-averaged relative momentum thickness distribution along the suction surface for different streamwise positions at Ω=1.59 (S_R=160 mm),Re=110,000

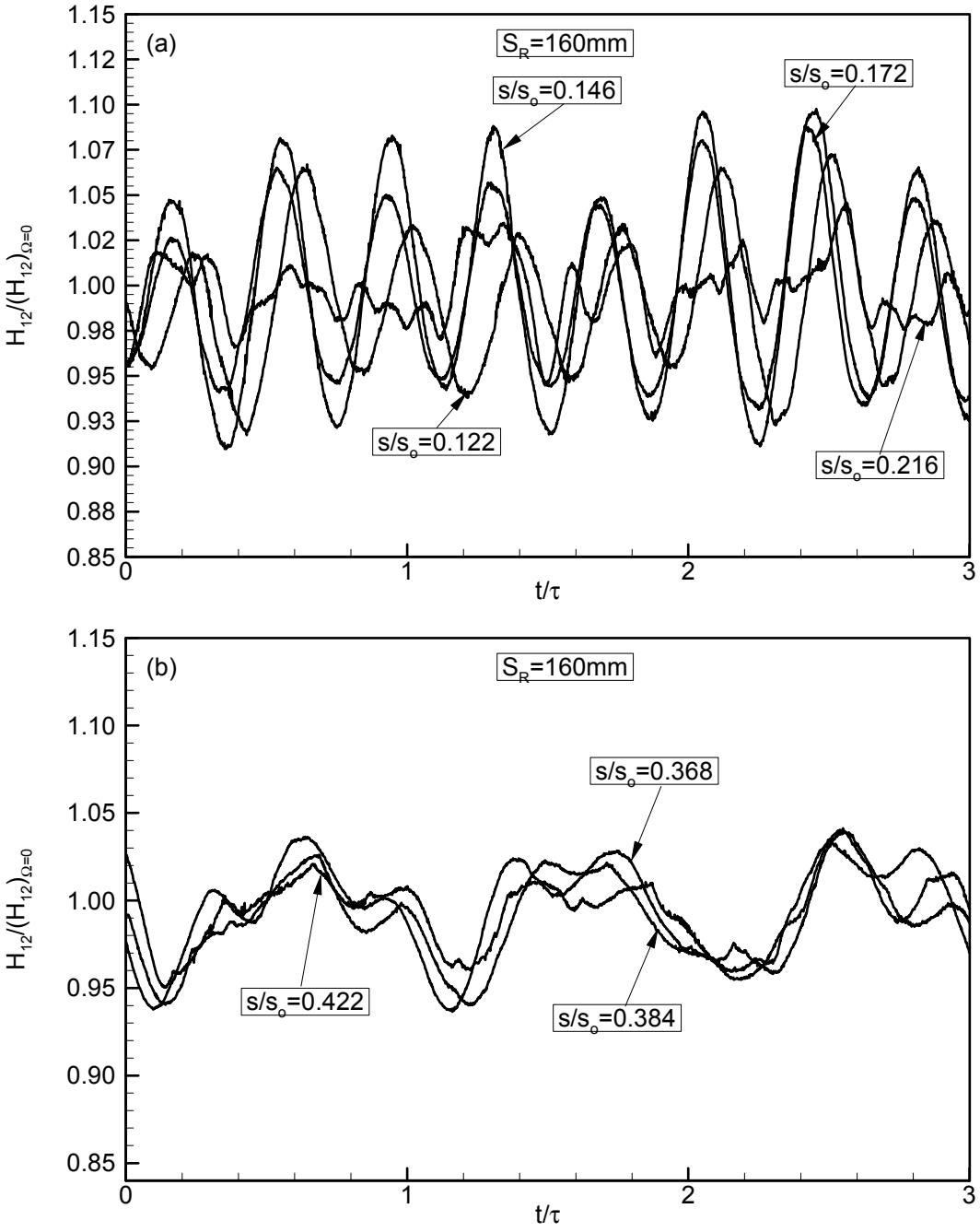

Figure 9.44: (a) and (b):Ensemble-averaged relative form parameter distribution along the suction surface for different streamwise positions at Ω=1.59 (S_R=160 mm) ,Re=110,000

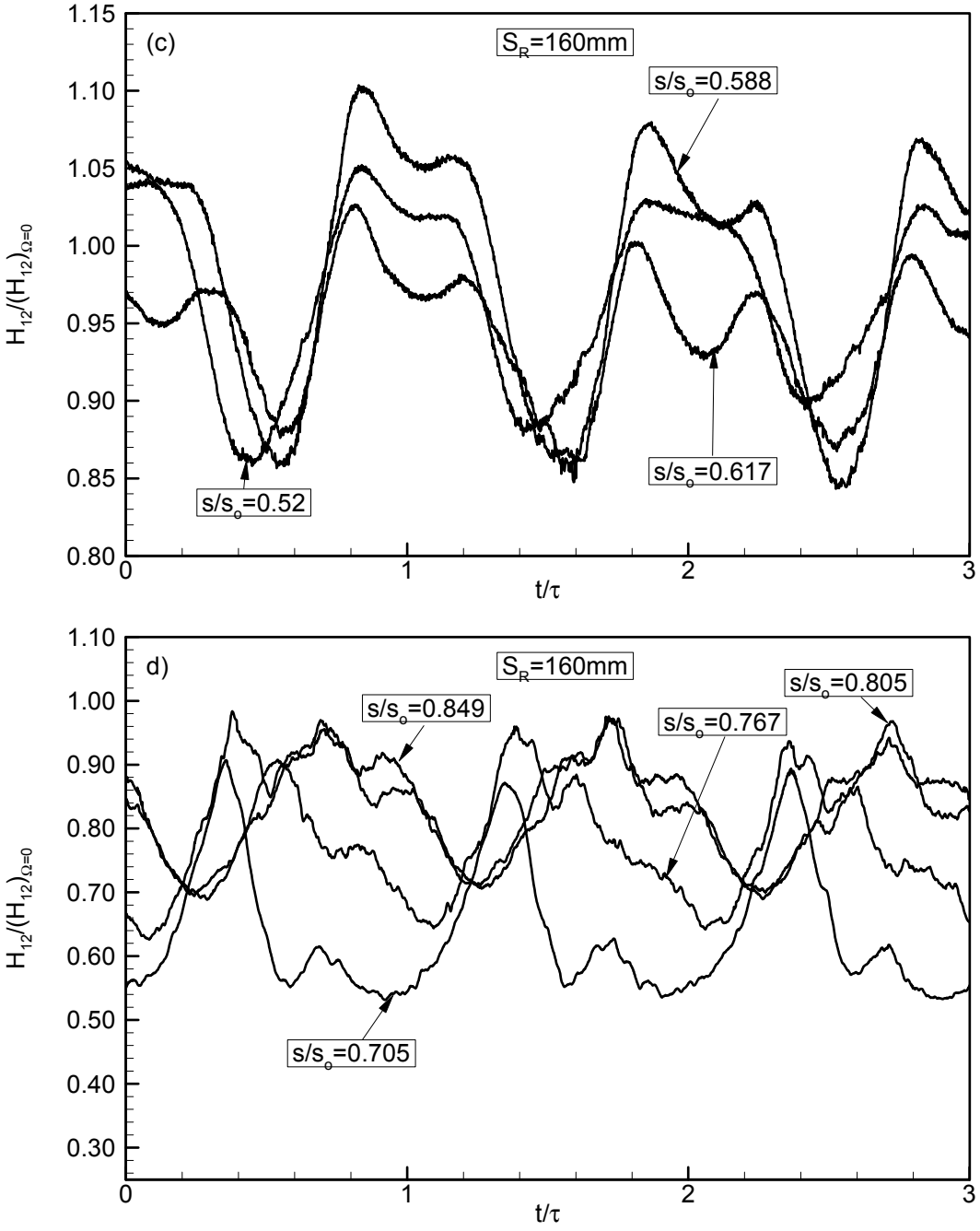

Figure 9.45: (c) and (d):Ensemble-averaged relative form parameter distribution along the suction surface for different streamwise positions at Ω=1.59 (S_R=160 mm) ,Re=110,000

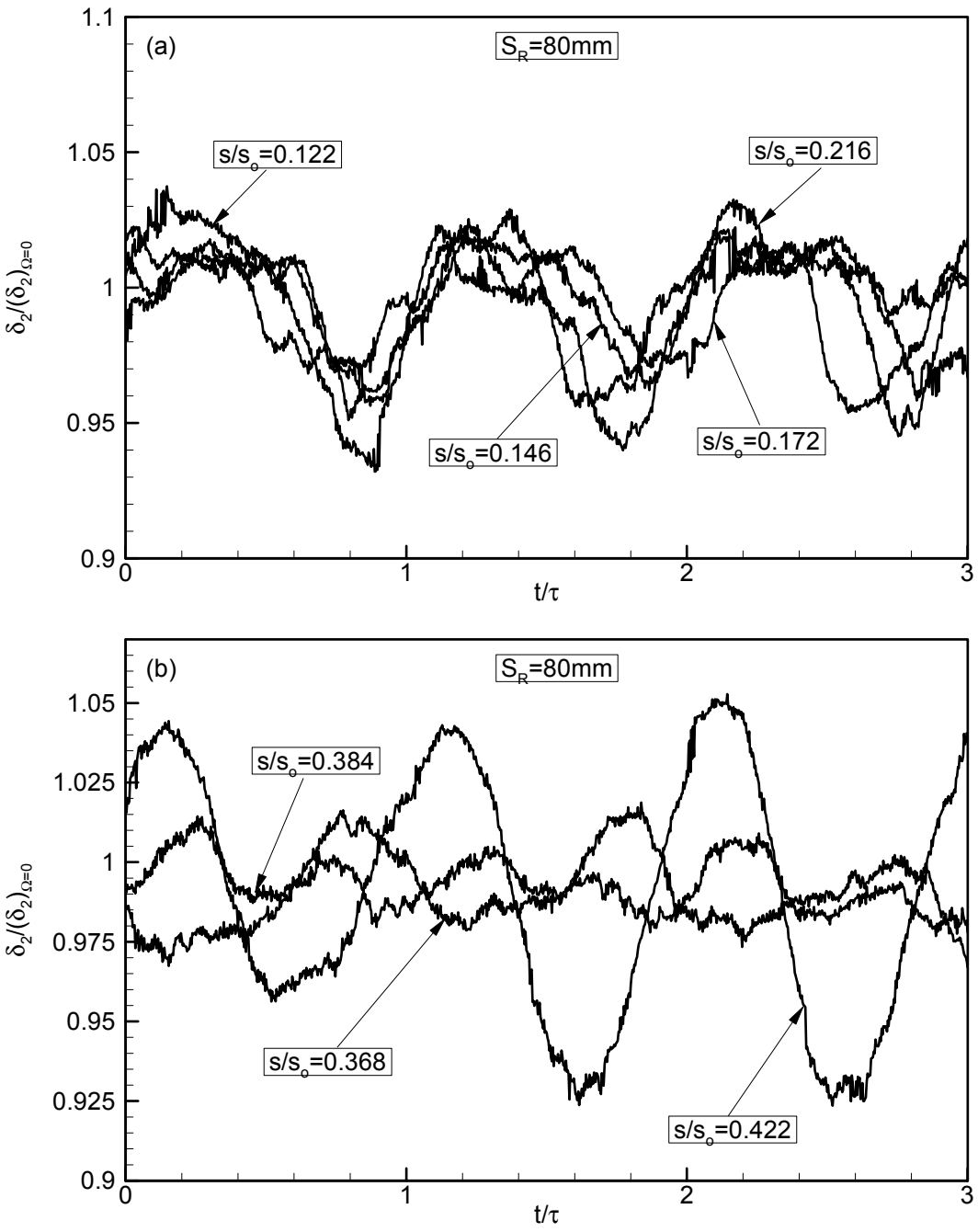

Figure 9.46: (a) and (b):Ensemble-averaged relative momentum thickness distribution along the suction surface for different streamwise positions at Ω=3.18 (S_R=80 mm) ,Re=110,000

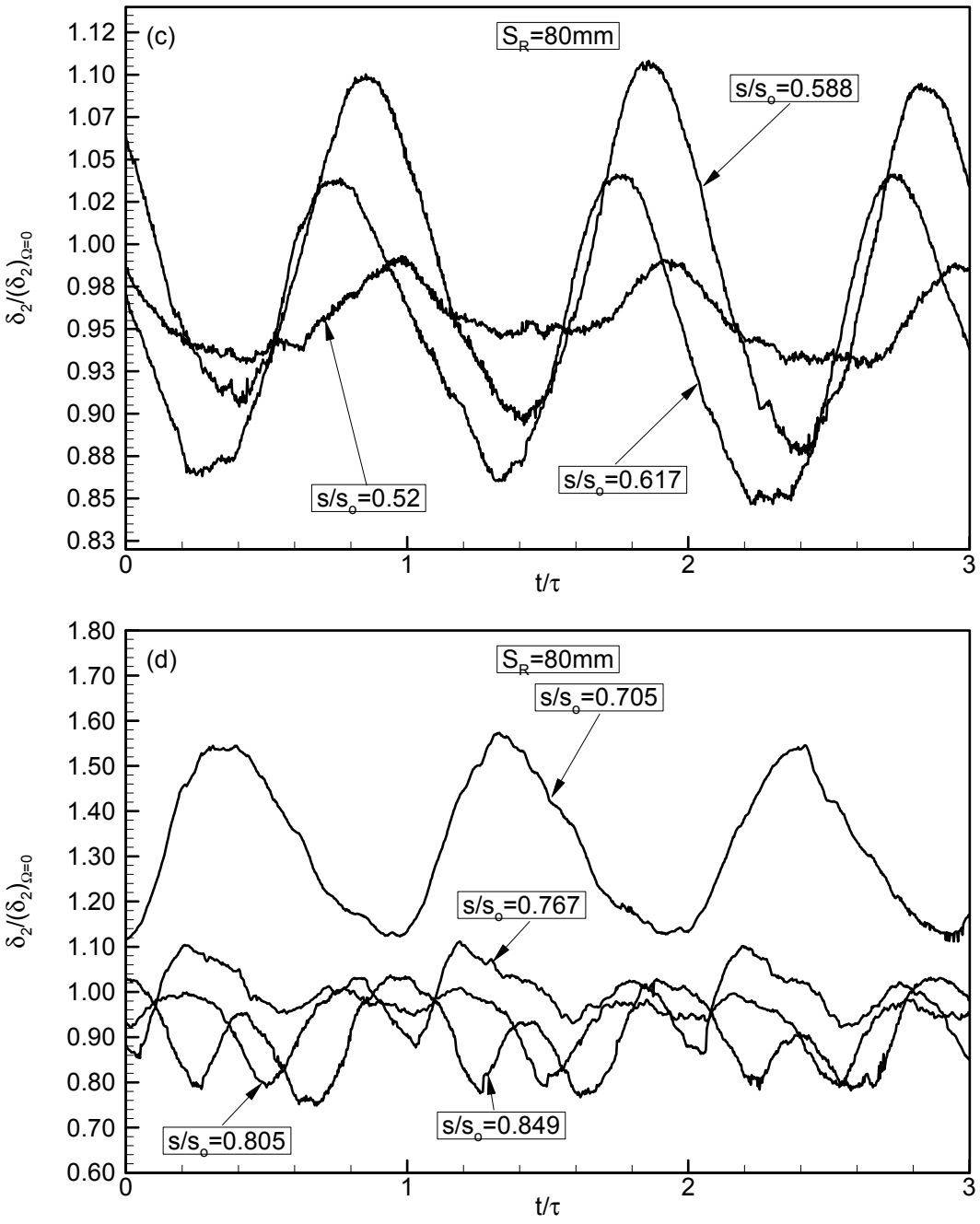

Figure 9.47: (c) and (d):Ensemble-averaged relative momentum thickness distribution along the suction surface for different streamwise positions at Ω=3.18 (S_R=80 mm) ,Re=110,000

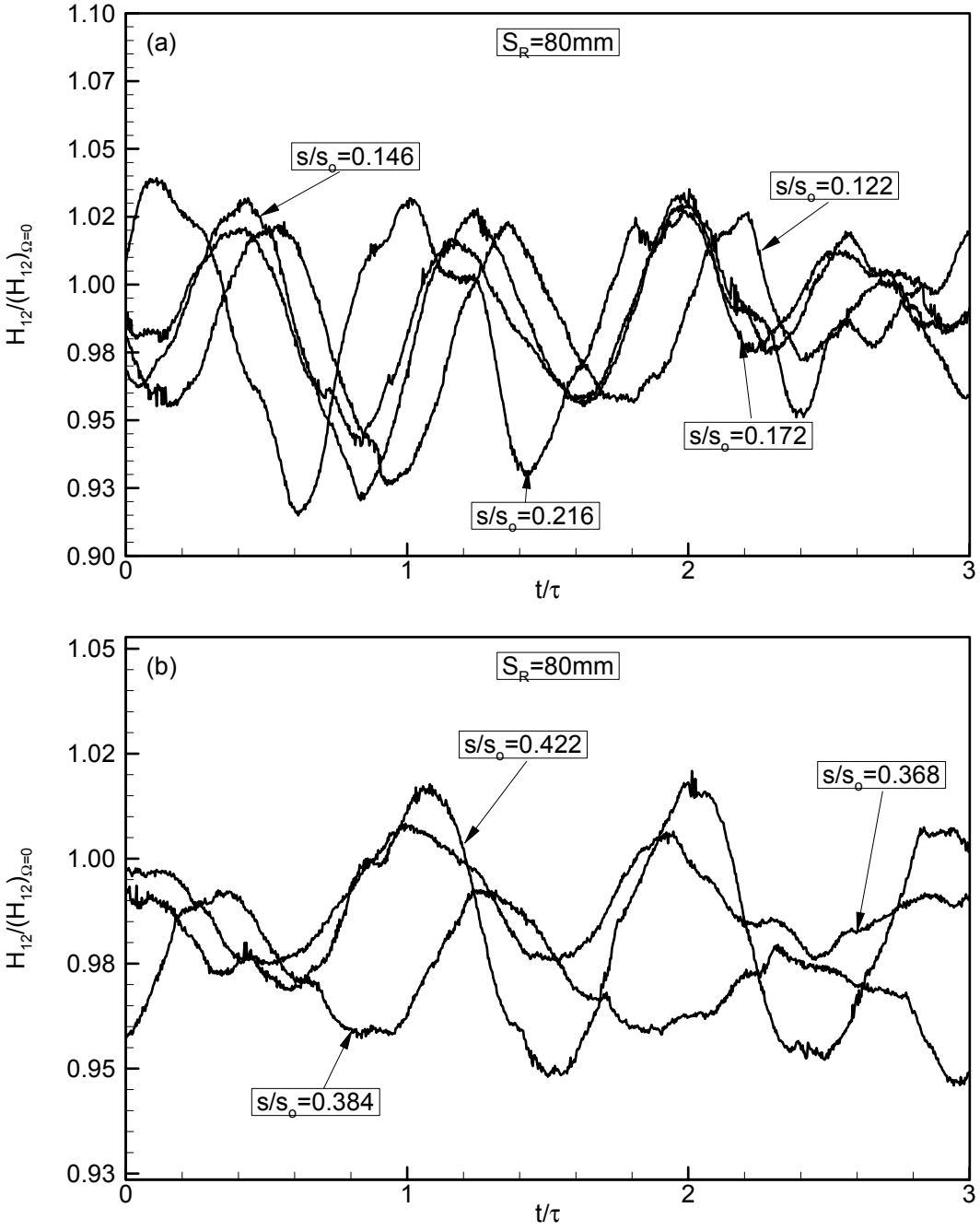

Figure 9.48:: (a) and (b):Ensemble-averaged relative form parameter distribution along the suction surface for different streamwise positions at Ω=3.18 (S_R=80 mm) ,Re=110,000

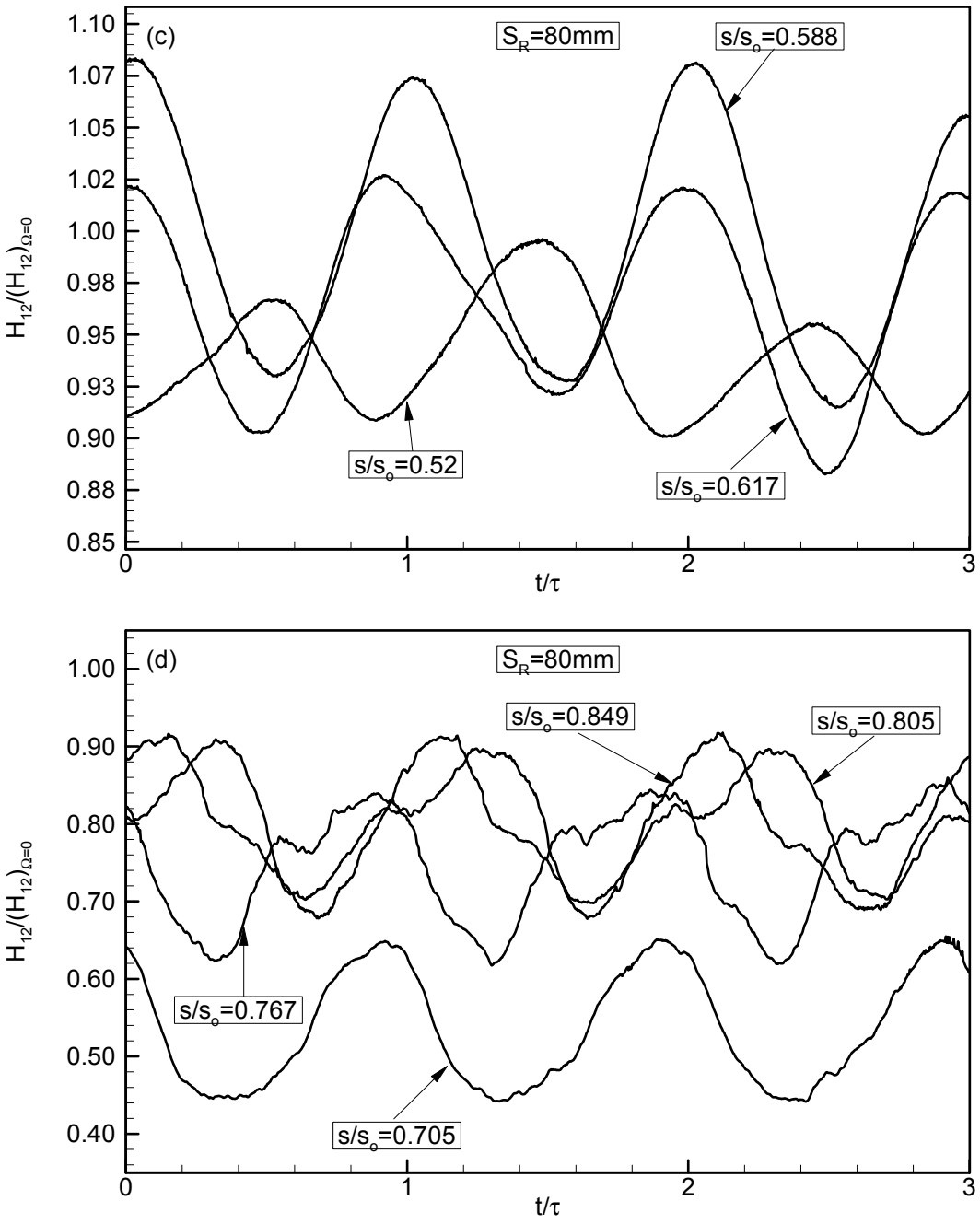

Figure 9.49: (c) and (d):Ensemble-averaged relative form parameter distribution along the suction surface for different streamwise positions at Ω=3.18 (S_R=80 mm) ,Re=110,000

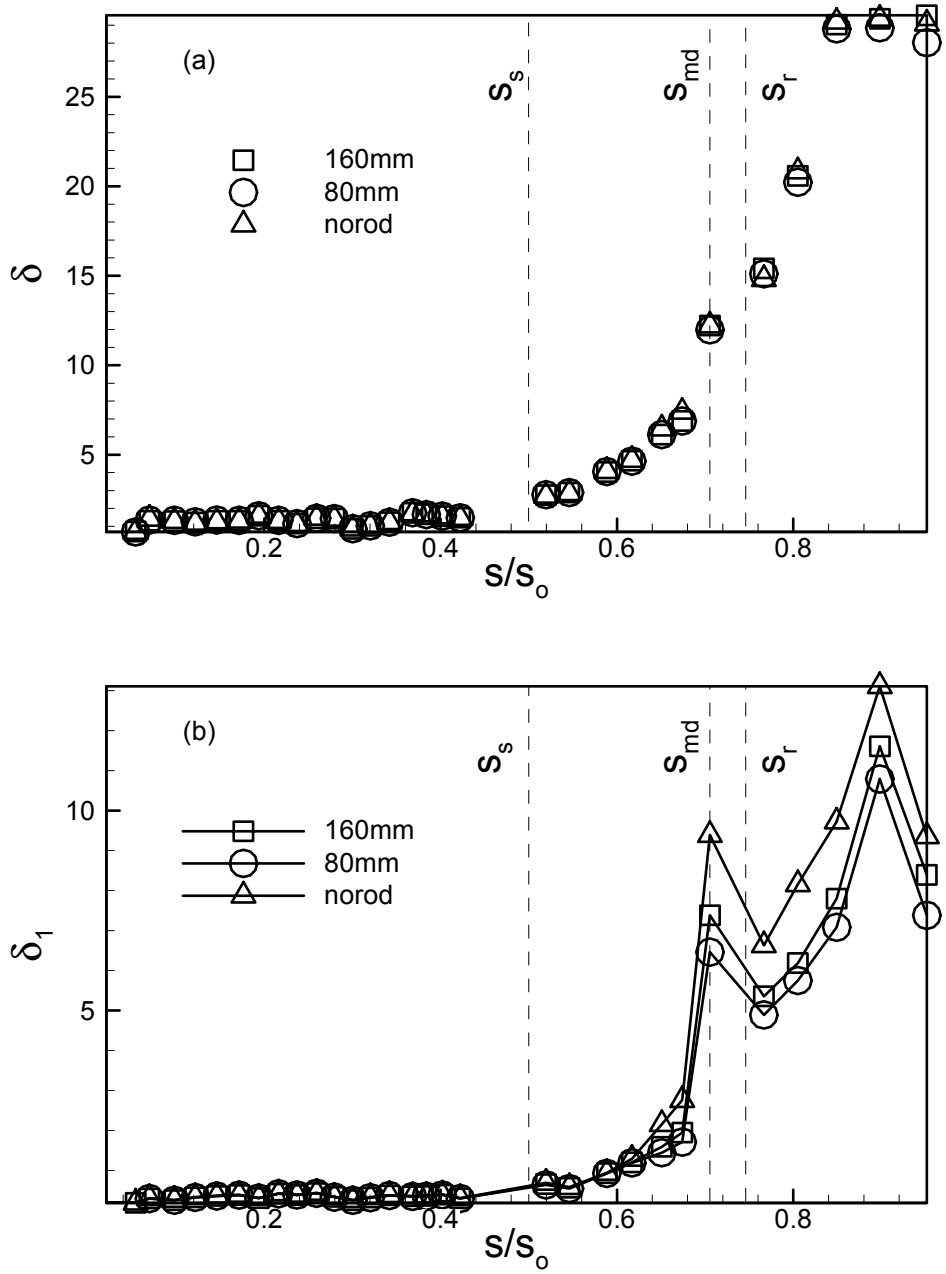

Figure 9.50: Time-averaged boundary layer thickness and displacement thickness for three different reduced frequency of Ω=0, 1.59, 3.18 (S_R=∞, 160 mm, 80 mm), Re=110,000

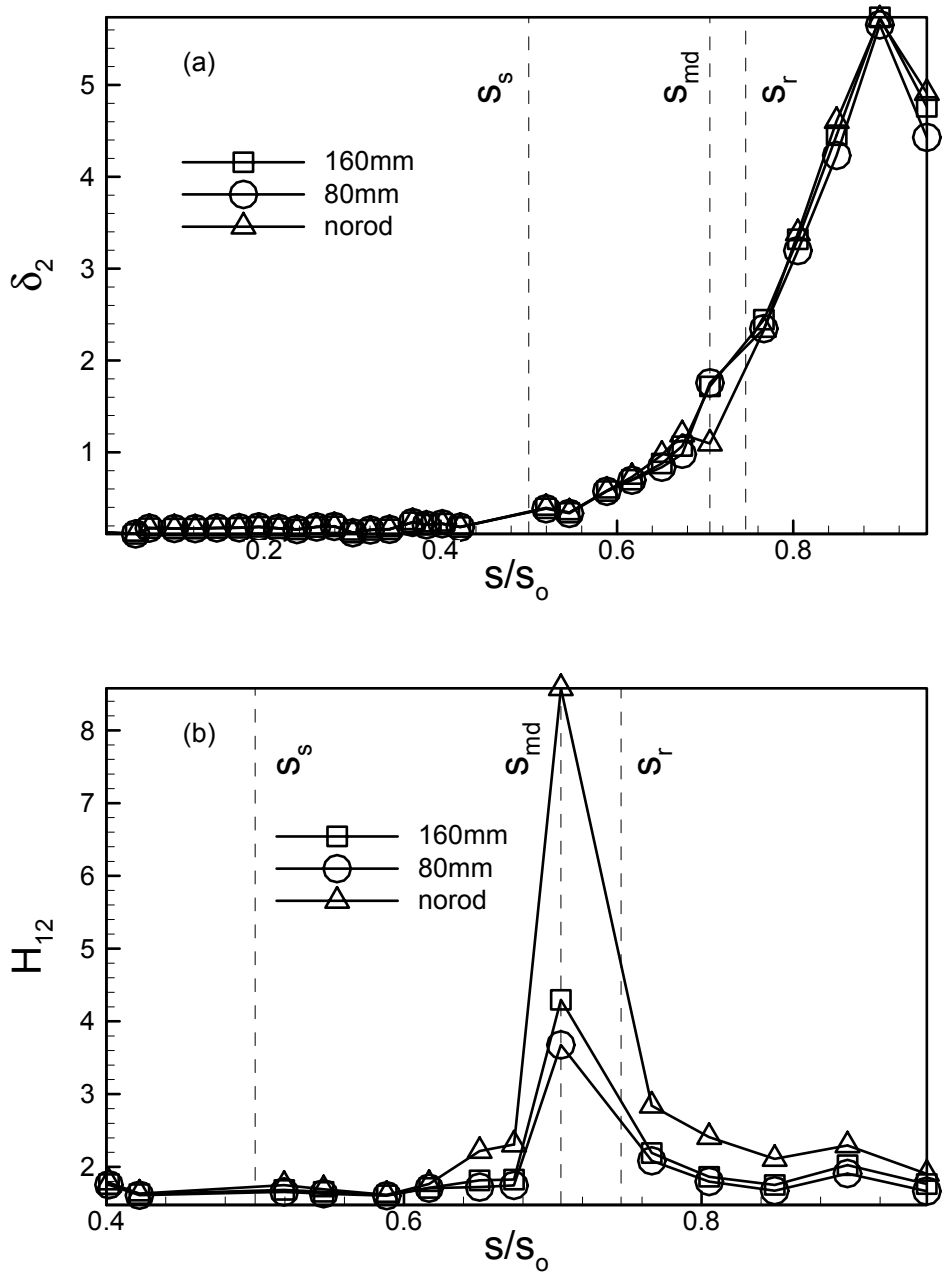

Figure 9.51: Time-averaged boundary layer momentum thickness and form parameter for three different reduced frequency of Ω=0, 1.59, 3.18 (S_R=∞, 160 mm, 80 mm), Re=110,000

9.12 Application of Boundary Layer Transition Models

In order to predict the location of the boundary layer transition, some emprical transition models are used in CFD. One of them, is proposed by Mayle (1991) and Malkiel&Mayle (1996) was included in this investigation. This model predicts the transition location based on the conditions at the separation point. A plot of the Reynolds number $Re_{smd}=U_{\infty}(s_{md}-s_s)/\nu$, based on the conditions at separation and the distance $(s_{md}-s_s)$ versus the momentum thickness Reynolds number $Re_{2s}= U_{\infty}\delta_2/\nu$ is shown in Figure 9.52.

$Re_{smd}=700\ Re_{2s}^{0.7}$ for short bubbles

$Re_{smd}=1400\ Re_{2s}^{0.7}$ for long bubbles

Short bubbles have only a local displacement. Therefore, the pressure distribution is close to that predicted value over the surface without separation. On the other hand, long bubbles interact with the exterior flow so, the pressure distribution over the blade surface is mostly different from the predicted one. Since long bubbles produce large losses and large deviations in exit flow angles, they should be avoided. On the other hand short bubbles are an effective way to force the flow to turbulent and may be considered as a means to control performance. The data are in good agreement with the empirical formula.

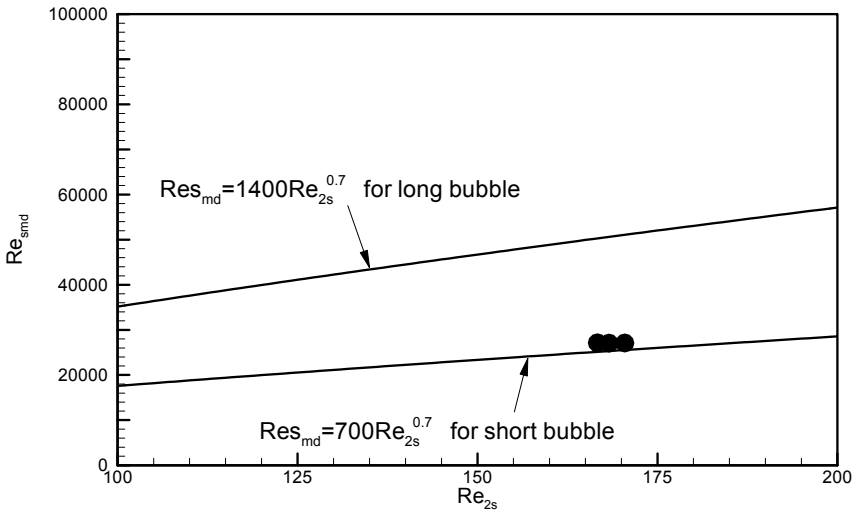

Figure 9.52: Reynolds number based on the length of separation as a function of the momentum thickness Reynolds number at separation point

10. CONCLUSIONS

A detailed experimental study on the behavior of the separation zone on the suction surface of a highly loaded LPT-blade under periodic unsteady wake flow was presented. One steady and two different unsteady inlet wake flow conditions with the corresponding passing frequencies, wake velocity and turbulence intensities were investigated utilizing a new large-scale, high-subsonic research facility The results of the unsteady boundary layer measurements were presented in ensemble-averaged, and contour plot forms. Surface pressure measurements were performed at Re= 50,000, 75,000, 10,0000, and 125,000. At each Reynolds number, one steady and two periodic unsteady inlet flow measurements were performed. The surface pressure distribution showed no major changes with respect to the above Re-number changes. Noticeable changes occurred, while operating at unsteady flow conditions. Detailed unsteady boundary layer measurement identified the onset and extension of the separation zone as well as its behavior under unsteady wake flow. Passing the wake flow with its highly turbulent vortical core over the separation region, caused a periodic contraction and expansion of the separation zone. It was found that, in conjunction with the pressure gradient and periodic wakes, the temporal gradient of the turbulence fluctuation, or more precisely the fluctuation acceleration $\partial v_{rms}/\partial t$ provides higher momentum and energy transfer into the boundary layer energizing the separation zone and causing it to partially or entirely disappear. We found that for $\partial v_{rms}/\partial t > 0$, the separation zone starts to contract whereas for $\partial v_{rms}/\partial t < 0$ it gradually assumes the shape before the contraction. The existence of higher turbulence fluctuations expressed in terms of higher turbulence intensity is well known for influencing the flow separation, its gradient is of crucial importance in suppressing or preventing the onset and the extension of the separation zone. The fluctuation gradient is an inherent feature of the incoming periodic wake flow and does not exist in a statistically steady flow, that might have high turbulence intensity.

REFERENCES

Arndt, N., 1993, "Blade Row Interaction in a Multistage Low Pressure Turbine," ASME J. of Turbomachinery, Vol. 115, pp. 137-146.

Bons, J. P., Sondergaard, R., and Rivir, R.B, 1999, " Control of Low pressure Turbine Separation Using Vortex Generator Jets," AIAA Paper No. 99-0367.

Cardamone, P, Stadtmüller, Fottner, L, Schiffer, 2000, "Numerical investigation of the wake-boundary layer interaction on a highly loaded LP turbine cascade blade," ASME 2002-GT-30367, presented at the International Gas Turbine and Aero-Engine Congress and Exposition, Amsterdam, Holland, June 3-6, 2002.

Chakka, P., Schobeiri, M.T. , 1999, "Modeling of Unsteady Boundary Layer Transition on a Curved Plate under Periodic Unsteady Flow Condition: Aerodynamic and Heat Transfer Investigations," ASME Transactions, Journal of Turbo machinery, January 1999, Vol. 121, pp. 88-97.

Dullenkopf, K., Schulz, A., and Wittig, S., 1991, "The Effect of Incident Wake Conditions on the Mean Heat Transfer of An Airfoil," ASME, J. of Turbomachinery. Vol. 113, pp. 412-418.

Fottner, L, Brunner, S Schiffer, 2000, "Comparison of two highly loaded turbine cascade under the influence of wake-induced transition," ASME 2000-GT-268, presented at the International Gas Turbine and Aero-Engine Congress and Exposition, Munich, Germany, May 8-11, 2000.

Halstead, D. E., Wisler, D. C., Okiishi, T. H., Walker, G. J., Hodson, H. P., and Shin, H. W., 1997, " Boundary Layer Development in Axial Compressors and Turbines: Part 3 of 4 LP Turbines, " ASME J. Turbomachinery, 119, pp. 225-237.

Howell, R. J., Ramesh, O.N., Hodson, H.P., Harwey, N. W., Schulte, V., 2001, "High Lift and Aft-Loaded Profiles for Low-Pressure Turbines," ASME, J. of Turbomachinery, Vol. 123, pp. 181-188.

Kaszeta, R., W., Simon T. W, Ashpis, D.E., 2001,"Experimental Investigation of Transition to Turbulence as Affected by Passing Wakes ," ASME Paper 2001-GT-0195.

Kline, S. J., and McKlintock, F. A., "Describing Uncertainties in Single-Sample Experiments," *Mechanical Engineering*, Vol. 75, Jan. 1953, pp. 3-8.

Lake, J. P., King, P. I., and Rivir, R.B., 2000, "Low Reynolds Number Loss Reduction on Turbine Blades With Dimples and V-Grooves," AIAA Paper No. 00-0738.

Lin, J. C., 1999, " Control of Turbulent Boundary Layer Separation Using Micro-Vortex Generators," AIAA Paper No. 99-3404

Liu, X., Rodi, W., 1989, "Measurement of Unsteady Flow Over and Heat Transfer From a Flat Plate," ASME Paper No. 89-GT-2.

Liu, X., Rodi, W., 1991, "Experiments on Transitional Boundary Layers with Wake-Induced Unsteadiness," Journal of Fluid Mechanics, Vol. 231 pp. 229-256.

Lou, W., Hourmouziadis, J., 2000,"Separation bubbles under Steady and Periodic Unsteady Main Flow Conditions,"ASME Paper 2000, Vol. 122, pp, 634-643.

Malkiel, E., and Mayle, R. E. , 1996, "Transition in a Separation Bubble," ASME J. Turbomachinery, Vol. 118, pp. 752-759.

Mayle, R. E., 1991, "The Role of Laminar-Turbulent Transition in Gas Turbine Engines," ASME J. Turbomachinery, Vol. 113, pp.509-537.

Orth, U., 1993, "Unsteady Boundary Layer Transition in Flow Periodically Disturbed by Wakes," ASME Journal of Turbomachinery, Vol. 115, pp. 707-713.

Pfeil, H., and Pache, W., 1977, "Messungen von Strömungsgrenzschichten unter Turbo-maschinenbedingungen," Zeitschrift fur Flugwissenschaften und Weltraumforschung 1, Heft 4, pp. 267-278.

Pfeil, H., Herbst R., 1979 "Transition Procedure of Instationary Boundary Layers," ASME Paper No. 79-GT-128.

Pfeil, H., Herbst, R., Schröder, T., 1983, "Investigation of the Laminar Turbulent Transition of Boundary Layers Disturbed by Wakes," ASME Journal of Engineering for Power, Vol. 105, pp. 130-137.

Schobeiri, M. T., Radke, R. E., 1994, "Effects of Periodic Unsteady Wake Flow and Pressure Gradient on Boundary Layer Transition along the Concave Surface of a Curved Plate," Presented at the International Gas Turbine and Aeroengine Congress and Exposition, The Hague, Netherlands, 94-GT-327.

Schobeiri, M. T., Pappu, K., Wright, L., 1995, "Experimental Sturdy of the Unsteady Boundary Layer Behavior on a Turbine Cascade," ASME 95-GT-435, presented at the International Gas Turbine and Aero-Engine Congress and Exposition, Houston, Texas, June 5-8, 1995.

Schobeiri, M. T., John, J., Pappu, K., 1996, “Development of Two-Dimensional Wakes Within Curved Channels, Theoretical Framework and Experimental Investigation,” an honor paper, ASME Transactions, Journal of Turbomachinery, July, 1996, Vol. 118, pp. 506-518.

Schobeiri, M. T., John, J., Pappu, K., 1997, “Experimental Study on the effect of Unsteadiness on Boundary layer Development on a Linear Turbine Cascade,” Journal of Experiments in Fluids, 23 91997), pp. 303-316.

Schobeiri, M.T., Wright., L., Chakka, P., 1998, "Periodic Unsteady Flow Aerodynamics and Heat Transfer Studies on a Curved Surface, Combined Part I and II," in press, International Journal of Rotating Machinery.

Schobeiri, M. T., Chakka, P., 2002, “Prediction of Turbine Blade Heat Transfer and Aerodynamics Using Unsteady Boundary Layer Transition Model,” International Journal of Heat and Mass Transfer, 45 (2002) pp. 815-829.

Schobeiri, M.T., Read, K., Lewalle, J.2002, “Effect of Unsteady Wake Passing Frequency on Boundary Layer Transition, Experimental Investigation and Wavelet Analysis,” Journal of Fluids Engineering, in press.

Schobeiri, M.T., “Turbomachinery Flow Physics and Dynamic Performance”, to be published October 2003 by Springer-Verlag.

Schröder, Th. 1989, “Measurements with hot-film probes and surface mounted hot film gages in a multi-stage low-pressure turbine,” European Propulsion Forum, Bath, UK.

Schulte, V., Hodson, H. P., 1996, “Unsteady Wake-Induced Boundary Layer Transition in High Lift LP Turbines,” ASME Paper No. 96-GT-486.

Schultz, M. P., and Volino, R. J., 2001, “Effects of Concave Curvature on Boundary Layer Transition under High Free-Stream Turbulence Conditions,” ASME Paper 2001-GT-0191.

Shyne, R. J., Sohn K. H., De Witt, K. J., 2000, “ Experimental Investigation of Boundary Layer Behavior in a Simulated Low Pressure Turbine,” ASME, Journal of Fluids Engineering, Vol. 122, pp. 84-89.

Treuren, K. W. V., Simon T., Koller M. V., Byerley A. R., Baughn J. W., Rivir, R., 2002, “ Measurements in a Turbine Cascade Flow under Ultra Low Reynolds Number Conditions,” ASME, J. of Turbomachinery, Vol. 124, pp. 100-106.

Volino, R. J., and Hultgren L. S., 2001, "Measurements in Separated and Transitional Boundary Layers Under Low-Pressure Turbine Airfoil Conditions," ASME, J. of Turbomachinery, Vol. 123, pp. 189-197.

Wright, L., Schobeiri, M. T., 1999, "The Effect of Periodic Unsteady Flow on Boundary Layer and Heat Transfer on a Curved Surface," ASME Transactions, Journal of Heat Transfer, November 1998, Vol. 120, pp. 22-33.

APPENDIX-A

A.1 Data Reduction Programs

1) Data reduction program for obtaining time-averaged parameter for steady measurement

```
*-------------------------------------------------------------------------------------------
*   ENSEMBLE- This program calculates the time averaged velocity,
*                     turbulence intensity, and fluctuation rms velocity

*                     for single wire probes and applies ANGLE CORRECTION

*   FILES: filp         : data file containing the the information on
*         (input)          the number of data points and the names of
*                          document file, data file and output file.
*                          .dat -data files      (input)
*                          .doc -document filles.(input)
*                           ...a.out - output files.  (output)
*   CTA.CAL           : velocity calibration file  (input)
          *  Signal connection:
*  Ch1 : Trigger                  Ch3: Differential pressure transducer

*  Ch2 : Thermocouple          Ch4: Hot wire
          *-------------------------------------------------------------------------------------------
---
      program ENSEMBLE
      parameter (max=2000000)
      integer nsamp,sampfreq,i,nb,j
      integer theta,theta1
      real tsens,fcorr,vcorr,vcorr1
      real hwvel(4),sum,v
      real gamma,tcal
      real trig,temp,pres,hw,kin_visc
      real ctc(5),acal(3),t(2)
      real u(max),du(max),tur1(max),Re_ex(max)
      real dt(max),dx(max)
      character*115 fil
      character*115 inputfile
c     open the file containing velocity calibration constants for hot wire
      open(unit=8,file='cta.cal')
      read(8,*)(ctc(i), i=5,1,-1)
      write(*,*) ctc(5),ctc(4),ctc(3),ctc(2),ctc(1)
      close(8)
```

```
      open the file containing angle calibration coefficients
      open(unit=9,file='angcal.cof')
      read(9,*)(acal(i), i=1,3)
      close(unit=9)
c     open the master file
      open(unit=10,file='BUSPROAC.PAR')
      read(10,*) tsens
      read(10,*) theta
      read(10,*) tcal
      close(10)
      open(unit=13,file='caltherm.cof')
      read(13,*)(t(i), i=1,2)
      write(*,*) t(2),t(1)
      close(unit=13)
      open(unit=7,file='master.fil')
      read(7,*)nfile
      vcorr=acal(1)+(acal(2)*theta)+(acal(3)*theta*theta)
      vcorr1=acal(1)+(acal(2)*theta1)+(acal(3)*theta1*theta1)
      fcorr=vcorr/vcorr1
      write(*,*)'V_correction factor is,',fcorr
      nsamp=20000
      sampfreq=20000
      do j=1,nfile
         read(7,200)inputfile
         do i=1,max
            u(i)=0.0
         enddo
         open(unit=11,file=inputfile,status='old')
         sum=0.0
         do 510 i=1,nsamp
                  read(11,*)temp,hw
                  temp=t(2)*temp+t(1)
                  hw=hw*sqrt((tsens-tcal)/abs(tsens -temp))
                  hw=hw*(hw*(hw*(hw*ctc(5)+ctc(4))+
     $            ctc(3))+ctc(2))+ctc(1)
                  hw=hw*fcorr
                  hw=hw/vcorr
c     Calculate the sum for the ensemble average of the U velocity
                  u(i)=hw+u(i)
                  sum=sum+u(i)
510      continue
```

```
      close(11)
      v=sum/nsamp
      do i=1,nsamp
         u(i)=u(i)
      enddo
c     Calculate the ensemble RMS and turbulence calculation
      do i=1,max
         du(i)=0.0
      enddo
      open(unit=11,file=inputfile,status='old')
      do 600 i=1,nsamp
            read(11,*)temp,hw
            temp=t(2)*temp+t(1)
            hw=hw*sqrt((tsens-tcal)/abs(tsens -temp))
            hw=hw*(hw*(hw*(hw*ctc(5)+ctc(4))+
     $      ctc(3))+ctc(2))+ctc(1)
            hw=hw*fcorr
            hwvel=hw/vcorr
            du(i)=(hw-v)**2
600   continue
      close(11)
      delt=20.0/float(nsamp)
      d=0.2715
      do i=1,nsamp
         du(i)=sqrt(du(i))
         tur1(i)=du(i)*100./u(i)
         dt(i)=(i)*delt*1000
      enddo
      ip=index(inputfile,'.')
      fil=inputfile(:(ip-1))//'.out'
c     Write to the output file
      open(unit=12,file=fil,status='new')
      write(12,74)
      do i=1,nsamp
         write(12,75)dt(i),u(i),du(i),tur1(i)
      enddo
      close(12)
    enddo
c   Formats
5   format(a26,f9.3)
74  format('    dt[ms]     u[m/s]     du[m/s]    Tu[%]')
```

```
75  format(4(1x,f16.10))
200format(a115)
      stop
      end
```

2) Data reduction program for obtaining ensemble-averaged parameter for unsteady measurement

```
*-------------------------------------------------------------------------------------------------
*   ENSEMBLE- This program calculates the ensemble averaged velocity,
*                    turbulence intensity, and fluctuation rms velocity
*                    for single wire probes and applies ANGLE CORRECTION
*   FILES: filp         : data file containing the the information on
*         (input)          the number of data points and the names of
*                          document file, data file and output file.
*                          .dat -data files      (input)
*                          .doc -document filles.(input)
*                           ...a.out - output files.  (output)
*   CTA.CAL          : velocity calibration file              (input)
          *  Signal connection:
*  Ch1 : Trigger                  Ch3: Differential pressure transducer

*  Ch2 : Thermocouple          Ch4: Hot wire
           *-------------------------------------------------------------------------------------------------
----
      program ENSEMBLE
      parameter (max=2500000)
      integer sampfreq,nsamp,i,nb,j
      integer nsamperevol,nrev
      integer ntext(6)
      real rps,rpm,vcorr,vcorr1,fcorr
      real hwvel(4)
      real gamma,tsens,tcal
      real trig,temp,pres,hw,hwfil
      real ctc(5),acal(3),t(2)
      real u(max),du(max),tur(max),ufil(max),dufil(max)
      real dt(max),dx(max),turfil(max)
      character*50 fil
      character*50 inputfile
c     open the file containing velocity calibration constants for hot wire
```

```
      open(unit=8,file='cta.cal')
      read(8,*)(ctc(i), i=5,1,-1)
      write(*,*) ctc(5),ctc(4),ctc(3),ctc(2),ctc(1)
      close(8)
c     open the file containing angle calibration coefficients
      open(unit=9,file='angcal.cof')
      read(9,*)(acal(i), i=1,3)
      close(unit=9)
c     open the master file
      open(unit=10,file='BUSPROAC.PAR')
      read(10,*) tsens
      read(10,*) theta
      read(10,*) tcal
      close(10)
      open(unit=13,file='caltherm.cof')
      read(13,*)(t(i), i=1,2)
      write(*,*) t(2),t(1)
      close(unit=13)
      open(unit=7,file='master.fil')
      read(7,*)nfile

      vcorr=acal(1)+(acal(2)*theta)+(acal(3)*theta*theta)
      vcorr1=1.6372625
      fcorr=vcorr/vcorr1
      write(*,*)'V_correction factor is = ',fcorr
c     write(*,*)acal(3),acal(2), acal(1)
      sampfreq=20000
      rps=1
      nrev=100
      nsamperevol=float(sampfreq)/rps
      nsamp=int(float(nrev)*nsamperevol)
      rpm=rps*60
      do j=1,nfile
         read(7,200)inputfile
         do i=1,max
            ufil(i)=0.0
            u(i)=0.0
         enddo
         open(unit=11,file=inputfile,status='old')
         do 800 nb = 1,nrev
                  do 510 i=1,nsamperevol
```

```
c                       read(11,*)temp,pres,hwfil,hw
                        read(11,*)trig,temp,pres,hwfil,hw
                        temp=t(2)*temp+t(1)
                        hwfil=hwfil*sqrt((tsens-tcal)/(tsens -temp))
                        hwfil=hwfil*(hwfil*(hwfil*(hwfil*ctc(5)+ctc(4))+
   $                    ctc(3))+ctc(2))+ctc(1)
                        hw=hw*sqrt((tsens-tcal)/(tsens -temp))
                        hw=hw*(hw*(hw*(hw*ctc(5)+ctc(4))+
   $                    ctc(3))+ctc(2))+ctc(1)
                        hw=hw/fcorr
c                       hw=hw/vcorr
*   Calculate the sum for the ensemble average of the U velocity
                        ufil(i)=ufil(i)+hwfil
                        u(i)=u(i)+hw
510             continue
800     continue
        close(11)
        do i=1,nsamperevol
           ufil(i)=ufil(i)/nrev
           u(i)=u(i)/nrev
        enddo
c   Calculate the ensemble RMS and turbulence calculation
        do i=1,max
           du(i)=0.0
           dufil(i)=0.0
        enddo
        open(unit=11,file=inputfile,status='old')
        do 900 nb=1,nrev
        do 600 i=1,nsamperevol
                read(11,*)temp,pres,hwfil,hw
                read(11,*)trig,temp,pres,hwfil,hw
                temp=t(2)*temp+t(1)
                hwfil=hwfil*sqrt((tsens-tcal)/(tsens -temp))
                hwfil=hwfil*(hwfil*(hwfil*(hwfil*ctc(5)+ctc(4))+
   $            ctc(3))+ctc(2))+ctc(1)
                hw=hw*sqrt((tsens-tcal)/(tsens -temp))
                hw=hw*(hw*(hw*(hw*ctc(5)+ctc(4))+
   $            ctc(3))+ctc(2))+ctc(1)
                hw=hw/fcorr
c               hw=hw/vcorr
                dufil(i)=(hwfil-ufil(i))**2+dufil(i)
```

```
                du(i)=(hw-u(i))**2+du(i)
600     continue
900     continue
        close(11)
        delt=1.0/float(sampfreq)
        vbelt = 5.0*rpm/60.0
        delx = vbelt*delt
        do i=1,nsamperevol
            dufil(i)=sqrt(dufil(i)/nrev)
            turfil(i)=dufil(i)*100./ufil(i)
            du(i)=sqrt(du(i)/nrev)
            tur(i)=du(i)*100./u(i)
            dt(i)=(i-1)*delt*1000
            dx(i)=(i-1)*delx*1000
        enddo
        ip=index(inputfile,'.')
        fil=inputfile(:(ip-1))//'.out'
c   Write to the output file
        open(unit=12,file=fil,status='new')
        write(12,74)
        write(12,76)
        do i=1,nsamperevol
            write(12,75)dt(i),dx(i),ufil(i),dufil(i),turfil(i),u(i),du(i),
    &       tur(i)
c           write(12,75)dt(i),ufil(i),dufil(i),turfil(i),u(i),du(i),tur(i)
        enddo
        close(12)
    enddo
c   Formats
5    format(a26,f9.6)
74  format('VARIABLES="dt(msec)", "dx(mm)", "ufil(m/s)", "dufil(m/s)",
    & "Tufil(%)", "u(m/s)", "du(m/s)", "Tu(%)"')
76  format('ZONE I=20000, F=POINT')
75  format(8(1x,f15.10)
200   format(a50)
    stop
    end
```

3) Data reduction program for separating the data into three segments and each

corresponding to one wake passing frequency

```
*-------------------------------------------------------------------------------------
*     SEP_DATA - This program reads the data and separates
*                        data into three separate segments, each corresponding
*                        to one wake passing frequency
*     Files - Reads in LIMIT.TXT which specifies the starting and ending
*              length for each wake passing frequency.
*     Variables
*     nsamp=number of samples
*     s1=starting point  (steady)
*     s2=starting point for the  wake passing frequency zone (160 mm)
*     s3=starting point for the wake passing frequency zone (80 mm)
*     e1=end point for the steady zone
*     e2=end point for the  wake frequency zone (160 mm)
*     e3=end point for the  wake frequency zone (80 mm)
*-------------------------------------------------------------------------------------

      program sep_data
      implicit none
      integer max,ncount,nst,ip
      parameter(max=60000)
      integer nsamp,i,sampfreq,nfile,j
      real s1,s2,s3,s4,e1,e2,e3,e4
      real dt(max),dx(max),u(max),du(max),tur(max)
      real ufil(max),dufil(max),turfil(max)
      real dtm,delt
      character*135 label
      character*60 fil1,fil2,fil3
      character*60 inputfile
      open(unit=1,file='limit.txt',status='old')
      read(1,*)nsamp
      read(1,*)sampfreq    !Hz
      read(1,*)s1,e1
      read(1,*)s2,e2
      read(1,*)s3,e3
c     read(1,*)s4,e4
      close(1)
      open(unit=7,file='master1.fil')
      read(7,*)nfile
```

```
      do j=1,nfile
         read(7,'(a)')inputfile
         delt=1./float(sampfreq)
         ncount = 1
         ip=index(inputfile,'.')
         fil1=inputfile(:(ip-1))//'a.out'
         fil2=inputfile(:(ip-1))//'b.out'
         fil3=inputfile(:(ip-1))//'c.out'
         open(unit=2,file=inputfile,status='old')
         open(unit=3,file=fil1)
         open(unit=4,file=fil2)
         open(unit=5,file=fil3)
         read(2,'(a)')label
         read(2,'(a)')label
         do i=1,nsamp
            read(2,24)dt(i),dx(i),ufil(i),dufil(i),turfil(i),u(i),du(i),tur(i)
c     selecting the first wake passing frequency zone (steady)
            if((dx(i).ge.s1).and.(dx(i).le.e1)) then
               if(ncount.eq.1) then
               nst = i
               ncount = 2
               endif
            dtm = (i-nst)*delt*1000+75
            write(3,24)dtm,dx(i),ufil(i),dufil(i),turfil(i),u(i),du(i),tur(i)
            endif
c     selecting the second wake passing frequency zone (160 mm)
            if((dx(i).ge.s2).and.(dx(i).le.e2)) then
               if(ncount.eq.2) then
               nst = i
               ncount = 3
               endif
            dtm = (i-nst)*delt*1000+400
            write(4,24)dtm,dx(i),ufil(i),dufil(i),turfil(i),u(i),du(i),tur(i)
            endif
c     selecting the third wake passing frequency zone (80 mm)
            if((dx(i).ge.s3).and.(dx(i).le.e3)) then
               if(ncount.eq.3) then
               nst = i
               ncount = 4
               endif
            dtm = (i-nst)*delt*1000+700
```

```
c           dtm = (i-nst)*delt*1000+700
            write(5,24)dtm,dx(i),ufil(i),dufil(i),turfil(i),u(i),du(i),tur(i)
            endif
         end do
         close(2)
         close(3)
         close(4)
         close(5)
      enddo
24    format(8(1x,f15.10))
      end
```

4) Data reduction program for obtaining time-averaged quantities

```
      program average
      implicit none
      character*85 outfile
      character*65 inputfile
      real dt,dx,u,du,Tu,m_dt,m_dx,m_u
      real m_du,m_Tu
      integer i,j,k,nfile,counter
      open(1,file='media2.inf ',status='old')
      read(1,*)nfile
      read(1,'(a)')outfile
      open(3,file=outfile,status='unknown')
      do i=1,nfile
         m_u=0.0
         m_du=0.0
         m_Tu=0.0
         read(1,'(a)')inputfile
         open(2,file=inputfile,status='old')
         read(2,*)
         counter=0
         do while (.not.eof(2))
            read(2,*)dt,u,du,Tu
            counter=counter+1
            m_u=u+m_u
            m_du=du+m_du
            m_Tu=Tu+m_Tu
         end do
```

```
        m_u=m_u/float(counter)
        m_du=m_du/float(counter)
        m_Tu=m_Tu/float(counter)
        write(3,100)m_u,m_du,m_Tu
        close(2)
      enddo
100format(3(1x,f18.10))
      end
```

5) Data reduction program for obtaining time-averaged boundary layer parameters

```
-----------------------------------------------------------------------------------------------------
c     This program generates the ensemble averaged boundary layer parameters,
c     delta,delta1,delta2,delta3,H12,H23, etc. as a function of time (t/T : 0-3)
-----------------------------------------------------------------------------------------------------
      program ENSBL2
      implicit none
      integer i,j,n,k,counter
      integer npol,start,ns,ks
      character*65 inputfile,fo1
      real y,srod,ycoord,itime
      real dt,dx,ufil,dufil,tufil,t,tau,u1,du,tu
      real a,g,u,f1,f2,f3
      real yintpol,uintpol,upot,ypot
      real break0,cscoef0,break1,cscoef1
      real break2,cscoef2,break3,cscoef3
      real low,high,ue,delta,delta1,delta2,delta3
      real H12,H23,xt
      real*8 acoeff(20),var(20),coeff(20)
      real csitg,csval
      real Udelta,S1,y1,y2,Udelta1
      dimension dt(100),ufil(100),dufil(100)
      dimension tufil(100)
      dimension u1(100),du(100),tu(100)
      dimension ypot(50),upot(50)
      dimension a(100),g(100),y(100),u(100),f1(100),f2(100),f3(100)
      dimension yintpol(500),uintpol(500)
      dimension break0(100),cscoef0(4,100),break1(100),cscoef1(4,100)
      dimension break2(100),cscoef2(4,100),break3(100),cscoef3(4,100)
c     csakm    Gives spline coefficients of the data points
```

```
c    csitg    Uses the spline coefficients to calculate the integral
c    iwkin    Assigns larger workspace for the program
c    csval    Gives the interpolated values using the spline coeffs
c    lsfit    Fits the potential flow with a first order polynomial

     external csakm,csitg,iwkin,csval,lsfit
     call iwkin(43338)
     write(*,*)'Enter the approximate BL thickness in mm. '
     read(*,*)ycoord
     ycoord=ycoord/1000.
     open(unit=2,file='master.fil',status='old')
     read(2,25) fo1
     read(2,25) inputfile
25   format(a65)
     close(unit=2)
c    Input of the data
     open(unit=8,file=inputfile,status='old')
     read(8,*)
     read(8,*)
     i=0

    do while(.not.eof(8))
       i=i+1
       read(8,*) a(i),ufil(i),dufil(i),tufil(i),u1(i),du(i),tu(i)
       a(i)=a(i)/1000.0
       g(i)=u1(i)
     enddo
     close(unit=8)
     open(unit=14,file=fo1,status='new')
     write(14,74)
c    Calculation of the potential flow fit
c    Initializing the parameters
     n=i-1
     start=0
     i=1
     do while(a(i).le.ycoord)
        if(a(i).lt.ycoord) then
        start=i+1
        elseif(a(i).eq.ycoord) then
        start=i
        endif
```

```
          i=i+1
      enddo
c     Assigning the data to fit for potential flow
      do i=start,n
          ypot(i-start+1)=a(i)
          upot(i-start+1)=g(i)
      enddo
c     Fitting the potential flow
      npol=1
      ns=n-start+1

      call LSFIT(ns,ypot,upot,npol,acoeff,var,coeff,ks)
c     Calculating Ue and u(i) where u-inviscid=a(i)*coeff(2)+coeff(1)
c      f1(i)    function to be integrated for displacement thickness
c      f2(i)    function to be integrated for momentum thickness
c      f3(i)    function to be integrated for energy thickness
      Ue=coeff(1)
      do i=1,n
          y(i)=a(i)
          u(i)=g(i) - (a(i)*coeff(2)+coeff(1)) + Ue
          f1(i)=1-u(i)/Ue
          f2(i)=u(i)/Ue*(1.0-u(i)/Ue)
          f3(i)=u(i)/Ue*(1.0-u(i)*u(i)/Ue/Ue)
      enddo
c     Calculation of the boundary layer thickness, delta using the
c     calculated velocity "u".
c     The boundary layer thickness is located using interpolated values
c     of the calculated velocity "u".
      xt=0.0
      call csakm(n,y,u,break0,cscoef0)
      do i=1,500
          xt=xt+y(n)/500
          yintpol(i)=xt
          uintpol(i)=csval(xt,n-1,break0,cscoef0)
      enddo
      i=1
      do while((abs(Ue-uintpol(i)).ge.0.01*Ue).and.(i.le.500))
          i=i+1
      enddo
      k=i-1
      delta=yintpol(k)
```

```
c    Limits of integration
     low=0.0
     high=delta
     call csakm(n,y,f1,break1,cscoef1)
     delta1=csitg(low,high,n-1,break1,cscoef1)
     call csakm(n,y,f2,break2,cscoef2)
     delta2=csitg(low,high,n-1,break2,cscoef2)
     call csakm(n,y,f3,break3,cscoef3)
     delta3=csitg(low,high,n-1,break3,cscoef3)
     H12=delta1/delta2
     H23=delta2/delta3
     delta=delta*1000.
     delta1=delta1*1000.
     delta2=delta2*1000.
     delta3=delta3*1000.
**********************************************************************
c    S1 is the slope of the potential core of u vs y
c    write(*,*)coeff(1),coeff(2),coeff(3),Ue
     S1=coeff(2)
c    Find delta and Udel at y/delta=1.0
c    Up(i)=S1*a(i)+Ue
     do i=1,n
        y1=a(i)*1000.0
        y2=a(i+1)*1000.0            if((y1.lt.delta).and.(y2.gt.delta))then
c          Udelta1=S1*delta/1000+Ue
        Udelta=(delta-y1)*(g(i+1)-g(i))/(y2-y1)+g(i)
        endif
        enddo
c    write(*,*)Udelta,Udelta1
c    Output data to the file "bounlay.par" to be read by the program law of the wall
     write(14,34)delta/1000,delta1/1000,delta2/1000,delta3/1000,Udelta, S1,Ue
34   format(7(1x,f15.10))
74   format('     delta         delta1         delta2         delt
    &a3        Udelta            S1          Ue')
     stop
     end

     SUBROUTINE LSFIT(N,X,Y,NPOL,A,VAR,Coeff,KS)
C  NOTE: This file contains LSFIT, LSGET, and SIMQ
C  LSFIT IS A LEAST-SQUARES POLYNOMIAL FIT OF Y VS. X.  THE
POLYNOMIAL
```

```
C  IS OF ORDER NPOL.
C  N=NUMBER OF DATA POINTS
C  X=INDEPENDENT VARIABLE
C  Y=DEPENDENT VARIABLE
C  NPOL=ORDER OF POLYNOMIAL TO BE FIT
C  A IS THE COEFFICIENT MATRIX WHICH MUST BE DIMENSIONED TO AT
LEAST
C  (NPOL+1)*(NPOL+1) IN THE CALLING PROGRAM
C  VAR IS A DUMMY ARRAY WHICH MUST BE DIMENSIONED TO AT LEAST
C  NPOL+NPOL+1 IN THE CALLING PROGRAM.
C  Coeff=ANSWER VECTOR, I.E. THE COEFFICIENTS OF THE POLYNOMIAL.
Coeff
C  MUST BE DIMENSIONED TO AT LEAST NPOL+NPOL+1 IN THE CALLING
PROGRAM
      IMPLICIT REAL*8 (A-H,O-Z)
      REAL*8 A(1),Coeff(1),VAR(1)
      REAL*4 X(1),Y(1)
      NPOLP1=NPOL+1
      NPOL2=NPOL+NPOL
      DO 60 I=0,NPOL2
            IP=I+1
            XAV=0.d0
            XYAV=0.d0
            DO 50 J=1,N
                  XINC=1.d0
                  if(i.ne.0) then
                  DO 40 K=1,I
                        XINC=XINC*X(J)
40                CONTINUE
                  end if
                  XAV=XAV+XINC
                  XYAV=XYAV+XINC*Y(J)
50          CONTINUE
            VAR(IP)=XAV/N
            Coeff(IP)=XYAV/N
60    CONTINUE
      ICOUNT=0
      DO 80 I=1,NPOLP1
            DO 70 J=1,NPOLP1
                  ICOUNT=ICOUNT+1
                  INDEX=I+J-1
```

```
                    A(ICOUNT)=VAR(INDEX)
70          CONTINUE
80  CONTINUE
    CALL SIMQ(A,Coeff,NPOLP1,KS)
    RETURN
    END
C-------------------------------------------------------------------------------------------------------
--
    SUBROUTINE LSGET(NPOL,Coeff,XINPUT,YOUT)
C   LSGET IS THE LEAST-SQUARES 'GET' SUBROUTINE TO BE USED IN
C   CONJUNCTION WITH LSFIT.
C   NPOL = ORDER OF POLYNOMIAL
C   XINPUT = X POINT WHERE Y IS WANTED
C   YOUT = FITTED VALUE OF THE POLYNOMIAL AT X
    REAL*8 Coeff(1)
    REAL*4  XINPUT,YOUT
    NPOLP1=NPOL+1
    YOUT=0.
    XINC=1.
    DO 10 I=1,NPOLP1
          IF (I.GT.1) XINC=XINC*XINPUT
          YOUT=YOUT+XINC*Coeff(I)
10  CONTINUE
    RETURN
    END

C    -------------------------------------------------------------------------------------------------
--
C   SUBROUTINE SIMQ
C   PURPOSE
C   OBTAIN SOLUTION OF A SET OF SIMULTANEOUS LINEAR EQUATIONS,
C   AX=B
C   USAGE
C   CALL SIMQ(A,B,N,KS)
C   DESCRIPTION OF PARAMETERS
C   A - MATRIX OF COEFFICIENTS STORED COLUMNWISE.  THESE ARE
C   DESTROYED IN THE COMPUTATION.  THE SIZE OF MATRIX A IS
C   N BY N.
C   B - VECTOR OF ORIGINAL CONSTANTS (LENGTH N). THESE ARE
C   REPLACED BY FINAL SOLUTION VALUES, VECTOR X.
C   N - NUMBER OF EQUATIONS AND VARIABLES. N MUST BE .GT. ONE.
```

```
C   KS - OUTPUT DIGIT
C   0 FOR A NORMAL SOLUTION
C   1 FOR A SINGULAR SET OF EQUATIONS
C   REMARKS
C   MATRIX A MUST BE GENERAL.
C   IF MATRIX IS SINGULAR , SOLUTION VALUES ARE MEANINGLESS.
C   AN ALTERNATIVE SOLUTION MAY BE OBTAINED BY USING MATRIX
C   INVERSION (MINV) AND MATRIX PRODUCT (GMPRD).
C   SUBROUTINES AND FUNCTION SUBPROGRAMS REQUIRED
C   NONE
C   METHOD
C   METHOD OF SOLUTION IS BY ELIMINATION USING LARGEST PIVOTAL
C   DIVISOR. EACH STAGE OF ELIMINATION CONSISTS OF INTERCHANGING
C   ROWS WHEN NECESSARY TO AVOID DIVISION BY ZERO OR SMALL
C   ELEMENTS.
C   THE FORWARD SOLUTION TO OBTAIN VARIABLE N IS DONE IN
C   N STAGES. THE BACK SOLUTION FOR THE OTHER VARIABLES IS
C   CALCULATED BY SUCCESSIVE SUBSTITUTIONS. FINAL SOLUTION
C   VALUES ARE DEVELOPED IN VECTOR B, WITH VARIABLE 1 IN B(1),
C   VARIABLE 2 IN B(2),....., VARIABLE N IN B(N).
C   IF NO PIVOT CAN BE FOUND EXCEEDING A TOLERANCE OF 0.0,
C   THE MATRIX IS CONSIDERED SINGULAR AND KS IS SET TO 1. THIS
C   TOLERANCE CAN BE MODIFIED BY REPLACING THE FIRST STATEMENT.
C    ----------------------------------------------------------------------------------------------------
--
      SUBROUTINE SIMQ(A,B,N,KS)
      IMPLICIT REAL*8 (A-H,O-Z)
      DIMENSION A(1),B(1)
C   FORWARD SOLUTION
      TOL=0.0d0
      KS=0
      JJ=-N
      DO 65 J=1,N
           JY=J+1
           JJ=JJ+N+1
           BIGA=0
           IT=JJ-J
           DO 30 I=J,N
C   SEARCH FOR MAXIMUM COEFFICIENT IN COLUMN
                IJ=IT+I
                IF(ABS(BIGA)-ABS(A(IJ))) 20,30,30
```

```
  20              BIGA=A(IJ)
                  IMAX=I
  30      CONTINUE
C   TEST FOR PIVOT LESS THAN TOLERANCE (SINGULAR MATRIX)
          IF(ABS(BIGA)-TOL) 35,35,40
  35      KS=1
      RETURN
C   INTERCHANGE ROWS IF NECESSARY
  40 I1=J+N*(J-2)
      IT=IMAX-J
      DO 50 K=J,N
      I1=I1+N
      I2=I1+IT
      SAVE=A(I1)
      A(I1)=A(I2)
      A(I2)=SAVE
C   DIVIDE EQUATION BY LEADING COEFFICIENT
  50A(I1)=A(I1)/BIGA
      SAVE=B(IMAX)
      B(IMAX)=B(J)
      B(J)=SAVE/BIGA
C   ELIMINATE NEXT VARIABLE
      IF(J-N) 55,70,55
  55IQS=N*(J-1)
      DO 65 IX=JY,N
      IXJ=IQS+IX
      IT=J-IX
      DO 60 JX=JY,N
      IXJX=N*(JX-1)+IX
      JJX=IXJX+IT
  60A(IXJX)=A(IXJX)-(A(IXJ)*A(JJX))
  65B(IX)=B(IX)-(B(J)*A(IXJ))
C   BACK SOLUTION
  70NY=N-1
      IT=N*N
      DO 80 J=1,NY
      IA=IT-J
      IB=N-J
      IC=N
      DO 80 K=1,J
      B(IB)=B(IB)-A(IA)*B(IC)
```

```
      IA=IA-N
   80 IC=IC-1
      RETURN
      END
```

6) Data reduction program for obtaining equally distributed profile along the y axis by using Akima interpolation

```
      Program int
      implicit none
      integer i,nfils,ip,j,counter,k,nintv,n
      real srod,dt,dx,coord,uintpol
      real ufilintpol,duintpol,tuintpol,dufilintpol,tufilintpol
      real ufil,dufil,tufil,u1,du,tu
      real xt,newcoord
      real break0,cscoef0,xdat,fdat
      real csval
      character*45 inputfile
      character*85 outputfile
      dimension inputfile(50),outputfile(50)
      dimension dx(50,20000)
      dimension dt(50,20000),ufil(50,20000),dufil(50,20000)
      dimension tufil(50,20000),coord(50),xt(50)
      dimension u1(50,20000),du(50,20000),tu(50,20000)
      dimension ufilintpol(50,20000),newcoord(50),xdat(50),fdat(50)
      dimension dufilintpol(50,20000),uintpol(50,20000),duintpol(50,20000),
     &          tuintpol(50,20000),tufilintpol(50,20000)
      dimension break0(50),cscoef0(4,50)
c     csakm    Gives spline coefficients of the data points
c     iwkin    Assigns larger workspace for the program
c     csval    Gives the interpolated values using the spline coefficients
      external csakm,csval
      call iwkin(43338)
      open(unit=2,file='master.fil',status='old')
      read(2,*)nfils
      do i=1,nfils
         read(2,25) inputfile(i)
25       format(a45)
```

```
      enddo
      close(2)
      open(unit=10,file='11_234coord.dat',status='old')
      do i=1,nfils
         read(10,*) coord(i)
      enddo
      close(10)
      do i=1,nfils
         open(unit=8,file=inputfile(i),status='old')
         j=0
        do while(.not.eof(8))
         j=j+1
         read(8,*) dt(i,j),dx(i,j),ufil(i,j),dufil(i,j),
     &                 tufil(i,j),u1(i,j),du(i,j),tu(i,j)
         enddo
         counter=j
      enddo
      close(unit=8)
      n=nfils
      open(unit=20,file='10_56coord.dat',status='old')
      do i=1,nfils
         read(20,*) newcoord(i)
      enddo
      close(20)
      nintv=n-1
c     Interpolation of the filtered velocity
      do j=1,counter
         do i=1,nfils
            fdat(i)=ufil(i,j)
            xdat(i)=coord(i)
         enddo
         call csakm(n,xdat,fdat,break0,cscoef0)
         do i=1,nfils
            xt=newcoord(i)
            ufilintpol(i,j)=csval(xt,nintv,break0,cscoef0)
         enddo
      enddo
c     Interpolation of the filtered rms velocity
      do j=1,counter
         do i=1,nfils
            fdat(i)=dufil(i,j)
```

```
            xdat(i)=coord(i)
          enddo
          call csakm(n,xdat,fdat,break0,cscoef0)
          do i=1,nfils

            xt=newcoord(i)
            dufilintpol(i,j)=csval(xt,nintv,break0,cscoef0)
          enddo
        enddo
c       Interpolation of the filtered turbulence intensity
        do j=1,counter
          do i=1,nfils
            fdat(i)=tufil(i,j)
            xdat(i)=coord(i)
          enddo
          call csakm(n,xdat,fdat,break0,cscoef0)
          do i=1,nfils
            xt=newcoord(i)
            tufilintpol(i,j)=csval(xt,nintv,break0,cscoef0)
          enddo
        enddo
c       Interpolation of the raw velocity
        do j=1,counter
          do i=1,nfils
            fdat(i)=u1(i,j)
            xdat(i)=coord(i)
          enddo
          call csakm(n,xdat,fdat,break0,cscoef0)
          do i=1,nfils
            xt=newcoord(i)
            uintpol(i,j)=csval(xt,nintv,break0,cscoef0)
          enddo
        enddo
c       Interpolation of the raw rms velocity
        do j=1,counter
          do i=1,nfils
            fdat(i)=du(i,j)
            xdat(i)=coord(i)
          enddo
          call csakm(n,xdat,fdat,break0,cscoef0)
          do i=1,nfils
```

```
            xt=newcoord(i)
            duintpol(i,j)=csval(xt,nintv,break0,cscoef0)
        enddo
    enddo
c   Interpolation of the raw velocity
    do j=1,counter
        do i=1,nfils
            fdat(i)=tu(i,j)
            xdat(i)=coord(i)
        enddo
        call csakm(n,xdat,fdat,break0,cscoef0)
        do i=1,nfils
            xt=newcoord(i)
            tuintpol(i,j)=csval(xt,nintv,break0,cscoef0)
        enddo
    enddo
    open(unit=22,file='masterout.fil',status='old')
    do i=1,nfils
        read(22,45) outputfile(i)
45      format(a85)
    enddo
    close(22)
    do i=1,nfils
        open(unit=30,file=outputfile(i),status='new')
        do j=1,counter
            write(30,24) dt(i,j),dx(i,j),ufilintpol(i,j),dufilintpol(i,j),
   &                     tufilintpol(i,j),uintpol(i,j),duintpol(i,j),tuintpol(i,j)
24          format(8(1x,f15.10))
        enddo
    enddo
    end
```

7) Data reduction program for obtaining equally distributed values along y axis for time-averaged values

```
ccccccccccccccccccccccccccccccccccccccccccccccccccccccccccccccccccccccccccccccccccccccc
cThis program generates the interpolated time-averaged values along the boundary layer
c
```

```
ccccccccccccccccccccccccccccccccccccccccccccccccccccccccccccccccccccccccccccccccccccc
      program interpolation
      integer ndata,npoint
      parameter(ndata=50)
      parameter(npoint=28)
      integer i,nintv
      real break(ndata),cscoef(4,ndata),csval,f,xnew(ndata),fdata(npoint),xdata(npoint)
      real uintpol(ndata),tuintpol(ndata)
      real y(npoint),ufil(npoint),tufil(npoint),u1(npoint)
      real du(npoint),tu(npoint),dufil(npoint)
      character*40 inputfile
      character*30 outputfile
      external csakm,csval
      open(unit=2,file='master.fil',status='old')
      read(2,25) inputfile
      read(2,35) outputfile
25    format(a40)
35    format(a30)
      close(unit=2)
      open(unit=8,file=inputfile,status='old')
      do i=1,npoint
         read(8,*) y(i),u1(i),tu(i)
      enddo
      close(unit=8)
      open(unit=9,file='newpoints.txt',status='old')
      do i=1,ndata
         read(9,*) xnew(i)
      enddo
c     Interpolation of the velocity
      do 10 i=1,npoint
            xdata(i)=y(i)
            fdata(i)=u1(i)
10    continue
      call csakm(ndata,xdata,fdata,break,cscoef)
      nintv=ndata-1
      do 20 i=1, ndata
            x=xnew(i)
            uintpol(i)=csval(x,nintv,break,cscoef)
20    continue
c     Interpolation of the turbulence intensity
      do 30 i=1,npoint
```

```
            xdata(i)=y(i)
            fdata(i)=tu(i)
30  continue
    call csakm(ndata,xdata,fdata,break,cscoef)
    nintv=ndata-1
    do 40 i=1, ndata
            x=xnew(i)
            tuintpol(i)=csval(x,nintv,break,cscoef)
40  continue
    open(unit=10,file=outputfile,status='new')
    do i=1, ndata
       write(10,75) xnew(i),uintpol(i),tuintpol(i)
    enddo
75  format(3(1x,f15.10))
    end
```

8) Data reduction program for obtaining contour plots from ensemble-averaged results

```
c-------------------------------------------------------------------------------------
c     Used for data analysis for unsteady boundary layer (UBL-series)
c     development study.
c     This is a processing program that converts s series of ensemble
c     averaged xxxxxxxa,b.OUT files to plots in the distance/time
c     domain.
c-------------------------------------------------------------------------------------
      program CONT
      implicit none
      integer nfils,i,j,n
      real ufil,dufil,Tufil
      real dt,dx,u(50),du,Tu(50),y(50)
      real ratio
      character*30 inputfile
      character*35 outfile
      nfils=30
      outfile='D:\results\cfd\contourcfd.out'
      open(3,file=outfile,status='unknown')
      write(3,74)
      write(3,76)
```

```
      do i=1,50
         open(unit=11,file='ratio.inf',status='old')
         do j=1,nfils
            open(unit=10,file='contour.fil',status='old')
            read(11,*)ratio
            read(10,'(a)')inputfile
            open(2,file=inputfile,status='old')
            do n=1,50
               read(2,*)y(n),u(n),Tu(n)
            enddo
            write(3,93)ratio,y(i),u(i),Tu(i)
         enddo
         close(10)
         close(11)
      enddo
      close(3)
93    format(4(1x,f15.10))
74    format('VARIABLES="s/s_o","y(mm)","u(m/s)","Tu(%)"')
76    format('ZONE I=1500, F=POINT')
      stop
      end
```

9) Data reduction program for obtaining contour plots from time-averaged results

```
c-------------------------------------------------------------------------------------
c     Used for data analysis for unsteady boundary layer (UBL-series)
c     development study.
c     This is a processing program that converts s series of ensemble
c     averaged xxxxxxxa,b.OUT files to plots in the distance/time
c     domain.
c-------------------------------------------------------------------------------------
      program CONT
      implicit none
      integer nfils,i,j
      real ufil,dufil,Tufil,m_Tufil,m_dufil,m_ufil
      real dt,dx,u,du,Tu,m_dt,m_dx,m_u
      real ratio,srod,period,wallnormal
      character*75 inputfile,outfile
      write(*,*)'Enter rod spacing in mm.'
      read(*,*) srod
```

```
      period=srod/5
      open(unit=10,file='contour.fil',status='old')
      read(10,*)nfils
      read(10,'(a)')outfile
      open(3,file=outfile,status='unknown')
      write(3,74)
      write(3,76)
      open(unit=11,file='ratio.inf',status='old')
c     open(unit=11,file='11_7coord.dat',status='old')
      do i=1,nfils
         read(11,*)ratio
c        read(11,*)wallnormal
         read(10,'(a)')inputfile
         open(2,file=inputfile,status='old')
         do while (.not.eof(2))
            read(2,*)dt,dx,ufil,dufil,Tufil,u,du,Tu
c           if(dt.ge.400)then
            if(dt.ge.700)then
c           dt=dt-400.0
            dt=dt-700.0
            if(dt/period.gt.3.0)then
            go to 22
            endif
            write(3,93)ratio,dt/period,ufil,dufil,Tufil,u,du,Tu
c           write(3,93)dt/period,wallnormal,ufil,dufil,Tufil,u,du,Tu
            endif
         enddo
22       close(2)
      enddo
      close(3)
93  format(8(1x,f15.10))
74  format('VARIABLES="s/so","t/tau","ufil(m/s)", "dufil(m/s)", "Tufil
   &(%)","u(m/s)","du(m/s)","Tu(%)"')
c74format('VARIABLES="t/tau","y/l","ufil(m/s)", "dufil(m/s)", "Tufil
c &(%)","u(m/s)","du(m/s)","Tu(%)"')
76  format('ZONE I=29791, F=POINT')
      stop
      end
```

APPENDIX-B

B.1 Uncertainty Analysis for Single Hot-Wire Measurements

Kline-McKlintock Uncertainty Analysis for Single Hot-Wire Probe Calibration

I) Calibration

$Tair := (22.7 + 273.15)K$ $\omega Tair := 0.5K$ Free-stream air temperature

$Pamb := \left(\frac{753.8}{25.4}\right)in\_Hg$ $\omega Pamb := \left(\frac{0.5}{25.4}\right)in\_Hg$ Atmospheric pressure

$R := 287\frac{joule}{kg \cdot K}$ Gas constant, uncertainty assumed to be zero

$Ea := 0.33$ $\omega Ea := 0.002$ Voltage of Anemometer

$D1 := 38.1mm$ $\omega D1 := 0.5mm$ Outer diameter of calibration nozzle

$D2 := 152.9mm$ $\omega D2 := 0.5mm$ Inner diameter of calibration nozzle

$Ptrans := \left(\frac{0.04}{25.4}\right)in\_Hg$ $\omega Ptrans := 0.6Pa$ Pressure read from pressure transducer

1) Determine uncertainty for air density

$\rho := \frac{Pamb}{R \cdot Tair}$ $\rho = 1.18\frac{kg}{m^3}$

Note: DrhoDTair=Partial derivative of rho with respect to Tair

$D\rho DTair := \frac{-Pamb}{R \cdot Tair^2}$ $D\rho DTair = -3.989 \times 10^{-3}\frac{kg}{m^3 K}$

$D\rho DPamb := \frac{1}{R \cdot Tair}$ $D\rho DPamb = 1.178 \times 10^{-5}\frac{s^2}{m^2}$

$$\omega\rho := \left[\left(D\rho DTair \cdot \omega Tair \right)^2 + \left(D\rho DPamb \cdot \omega Pamb \right)^2 \right]^{0.5} \qquad \omega\rho = 2.143 \times 10^{-3} \frac{kg}{m^3}$$

$$\%\rho := \left(\frac{\omega\rho}{\rho} \right) \cdot 100 \qquad \%\rho = 0.182$$

$$V := \left[\frac{(2 \cdot Ptrans)}{\rho \cdot \left(1 - \frac{D1^4}{D2^4} \right)} \right]^{0.5} \qquad V = 3.008 \frac{m}{s}$$

$$DVDD2 := -2.8284271247461 \cdot \left[\frac{Ptrans^{0.5}}{\rho^{0.5} \cdot \left(1 - \frac{D1^4}{D2^4} \right)^{1.5}} \right] \cdot \frac{D1^4}{D2^5} \qquad DVDD2 = -0.152 \text{ Hz}$$

$$DVDD1 := 2.8284271247461 \cdot \left[\frac{Ptrans^{0.5}}{\rho^{0.5} \cdot \left(1 - \frac{D1^4}{D2^4} \right)^{1.5}} \right] \cdot \frac{D1^3}{D2^4} \qquad DVDD1 = 0.611 \text{ Hz}$$

$$DVD\rho := -0.707106781186 \cdot \frac{Ptrans^{0.5}}{\rho^{1.5} \cdot \left(1 - \frac{D1^4}{D2^4} \right)^{0.5}} \qquad DVD\rho = -1.274 \frac{m^4}{kg\ s}$$

$$DVDPtrans = \frac{0.7071067811865475244}{\left[\rho^{0.5} \cdot \left(1 - \frac{D1^4}{D2^4} \right)^{0.5} \right] \cdot Ptrans^{0.5}} \qquad DVDPtrans = 0.283 \frac{m^2 s}{kg}$$

2) Determine uncertainty for velocity

$$\omega V := \left[(DVDD1 \cdot \omega D1)^2 + (DVDD2 \cdot \omega D2)^2 + (DVDp \cdot \omega \rho)^2 + (DVDPtrans \cdot \omega Ptrans)^2 \right]^{0.5}$$

$$\omega V = 0.17 \frac{m}{s}$$

$$\%V := \left(\frac{\omega V}{V} \right) \cdot 100 \qquad \%V = 5.642$$

The percentage of uncertainty for other velocities

$$V := 15 \frac{m}{s} \qquad \%V := 0.284$$

$$V := 10 \frac{m}{s} \qquad \%V := 0.529$$

$$V := 5 \frac{m}{s} \qquad \%V := 2.053$$

$$\%Vn := \left[\left(\omega V \cdot \frac{100}{V} \right)^2 + 1.2^2 \right]^{0.5} \qquad \%Vn = 5.768$$

The uncertainty of the curve fit according to S. Yavuzkurt (1984) is 1.2%. Thus the new velocity uncertainty is given by;

The curve fit uncertainty is calculated as follows:

1. The measured velocity is curved fit against anemometry voltage
2. The residuals of the curve fit are calculated
3. The residuals are divided by measured velocity at which they occur
4. The quantity in 3 is squared and summed for all velocities
5. The sum of the squares is divided by the number of data points and the square root is taken

6. The percentage uncertainty in the curve fit is called beta and the equation is given by

Determine uncertainty of velocity due to error in anemometer voltage

$$Vn1 := \left(1.374268 + 4.3283137Ea + 1.4779551Ea^2 - 0.24928452Ea^3 + 0.1867769Ea^4\right)\frac{m}{s}$$

$$DVn1DEa := 4.3283137 + 2.9559102Ea - 0.74785356Ea^2 + 0.7471076Ea^3 \qquad DVn1DEa = 5.249$$

$$\omega Vn1 := DVn1DEa\,\omega Ea\cdot\frac{m}{s} \qquad Vn1 = 2.957\frac{m}{s} \qquad \omega Vn1 = 0.01\frac{m}{s}$$

Total calibration uncertainty for velocity due to velocity reading, curve fit, and voltage error

$$\%Vtotalc := \left[\%Vn^2 + \left(100\cdot\frac{\omega Vn1}{Vn1}\right)^2\right]^{0.5} \qquad \%Vtotalc = 5.779$$

S. Yavuzkurt is below

II) Determine uncertainty of the velocity after data reduction

$E := 0.33$	$\omega E := 0.002$	Anemometer voltage
$Tsen := 250$	$\omega Tsen := 0.5$	Temperature of hot-wire sensor (C)
$T := 24$	$\omega T := 1$	Temperature of air during measurements (
$Tcal := 22.7$	$\omega Tcal := 1$	Temperature of air during calibration (C)

En is the anemometer voltage that has been corrected for temperature

$$En := E\cdot\left[\frac{(Tsen - T)}{(Tsen - Tcal)}\right]^{0.5} \qquad En = 0.329$$

$$DEnDTcal := 0.5\cdot E\cdot\left[\frac{(Tsen - T)^{0.5}}{(Tsen - Tcal)^{1.5}}\right] \qquad DEnDTcal = 7.238\times 10^{-4}$$

$$DEnDT := -0.5\cdot\frac{E}{\left[(Tsen - T)^{0.5}\cdot(Tsen - Tcal)^{0.5}\right]} \qquad DEnDT = -7.28\times 10^{-4}$$

$$DEnDE := \frac{(Tsen - T)^{0.5}}{(Tsen - Tcal)^{0.5}} \qquad DEnDE = 0.997$$

$$\omega En := \left[(DEnDTcal\cdot\omega Tcal)^2 + (DEnDT\cdot\omega T)^2 + (DEnDE\cdot\omega E)^2\right]^{0.5} \qquad \omega En = 2.243\times 10^{-3}$$

$$\%En := 100\cdot\frac{\omega En}{En} \qquad \%En = 0.682$$

Determine uncertainty of effective velocity due to error in corrected voltage

$$Vn := \left(1.374268 + 4.3283137En + 1.4779551En^2 - 0.24928452En^3 + 0.1867769En^4\right)\frac{m}{s}$$

$$Vn = 2.952\frac{m}{s}$$

$$DVnDEn := 4.3283137 + 2.9559102En - 0.74785356En^2 + 0.7471076En^3 \qquad DVnDEn = 5.247$$

$$\omega Vdata := DVnDEn\cdot\omega En\cdot\frac{m}{s} \qquad \omega Vdata = 0.012\frac{m}{s}$$

Total velocity uncertainty for calibration and data reduction

$$\%Vtotal := \left[\left(100\cdot\frac{\omega Vdata}{Vn}\right)^2 + \%Vtotalc^2\right]^{0.5} \qquad \%Vtotal = 5.792$$

REPORT DOCUMENTATION PAGE		Form Approved OMB No. 0704-0188

1. REPORT DATE *(DD-MM-YYYY)*	2. REPORT TYPE	3. DATES COVERED *(From - To)*
01-03-2009	Final Contractor Report	2000-2003

4. TITLE AND SUBTITLE
Experimental Study of the Effects of Periodic Unsteady Wakes on Flow Separation in Low Pressure Turbines

5a. CONTRACT NUMBER

5b. GRANT NUMBER

5c. PROGRAM ELEMENT NUMBER

6. AUTHOR(S)
Ozturk, Burak; Schobeiri, Meinhard, T.

5d. PROJECT NUMBER
NCC3-793

5e. TASK NUMBER

5f. WORK UNIT NUMBER
WBS 561581.02.08.03.21.02

7. PERFORMING ORGANIZATION NAME(S) AND ADDRESS(ES)
Texas A&M University
College Station, Texas 77843

8. PERFORMING ORGANIZATION REPORT NUMBER
E-16040

9. SPONSORING/MONITORING AGENCY NAME(S) AND ADDRESS(ES)
National Aeronautics and Space Administration
Washington, DC 20546-0001

10. SPONSORING/MONITORS ACRONYM(S)
NASA

11. SPONSORING/MONITORING REPORT NUMBER
NASA/CR-2009-214831

12. DISTRIBUTION/AVAILABILITY STATEMENT
Unclassified-Unlimited
Subject Categories: 02, 07, and 34
Available electronically at http://gltrs.grc.nasa.gov
This publication is available from the NASA Center for AeroSpace Information, 301-621-0390

13. SUPPLEMENTARY NOTES
This report is based on the M.S. Thesis of Burak Ozturk. Cooperative Agreement Technical Officer, David E. Ashpis, Organization code RTT, e-mail: ashpis@nasa.gov, 216-433-8317.

14. ABSTRACT
The present study, which is the first of a series of investigations of low pressure turbine (LPT) boundary layer aerodynamics, is aimed at providing detailed unsteady boundary layer flow information to understand the underlying physics of the inception, onset, and extent of the separation zone. A detailed experimental study on the behavior of the separation zone on the suction surface of a highly loaded LPT-blade under periodic unsteady wake flow is presented. Experimental investigations were performed on a large-scale, high-subsonic unsteady turbine cascade research facility with an integrated wake generator and test section unit. Blade Pak B geometry was used in the cascade. The wakes were generated by continuously moving cylindrical bars device. Boundary layer investigations were performed using hot wire anemometry at Reynolds number of 110,000, based on the blade suction surface length and the exit velocity, for one steady and two unsteady inlet flow conditions, with the corresponding passing frequencies, wake velocities, and turbulence intensities. The reduced frequencies cover the entire operation range of LP-turbines. In addition to the unsteady boundary layer measurements, blade surface pressure measurements were performed at Re = 50,000, 75,000, 100,000, 110,000, and 125,000. For each Reynolds number, surface pressure measurements are carried out at one steady and two periodic unsteady inlet flow conditions. Detailed unsteady boundary layer measurement identifies the onset and extension of the separation zone as well as its behavior under unsteady wake flow. The results, presented in ensemble-averaged and contour plot forms, help to understand the physics of the separation phenomenon under periodic unsteady wake flow.

15. SUBJECT TERMS
Turbomachinery; Transition; Turbulence; Wakes; Boundary layers; Separation; Turbulent spots; Intermittency; Unsteady flow; Turbines; Low pressure turbine; Anemometry; Hot wire; Turbulence grid; Scales

16. SECURITY CLASSIFICATION OF:			17. LIMITATION OF ABSTRACT	18. NUMBER OF PAGES	19a. NAME OF RESPONSIBLE PERSON
a. REPORT	b. ABSTRACT	c. THIS PAGE			STI Help Desk (email:help@sti.nasa.gov)
U	U	U	UU	152	19b. TELEPHONE NUMBER *(include area code)* 301-621-0390